3-28-2018

Higher Energy Gap Control of Fluorescence in Conjugated Polymers

Chien-Hung Chiang
Louisiana State University and Agricultural and Mechanical College

HIGHER ENERGY GAP CONTROL OF FLUORESCENCE IN CONJUGATED POLYMERS

A Dissertation

Submitted to the Graduate Faculty of the
Louisiana State University and
Agricultural and Mechanical College
in partial fulfillment of the
requirements for the degree of
Doctor of Philosophy

in

The Department of Chemistry

by
Chien-Hung Chiang
B.S., Tamkang University, Taiwan, 2007
M.S., Tamkang University, Taiwan, 2009
May 2018

In memory of

Kao, Liao Pi-Shuang

1929-2017

ACKNOWLEDGMENTS

I would like to acknowledge Professor Evgueni E. Nesterov, whom I learnt the most from at Louisiana State University, for his leadership, counseling, and inspiration. I valued him as an excellent mentor and friend who has great patient and constantly challenges me while at LSU.

Also, I would like to thank my committee: Prof. David Spivak, Jayne Garno, and Krishnaswamy Nadakumar for their kindness, humor, and encouragement.

To group members, past and present: Brian Imsick, Deepa Pangeni, Carlos Chaves, Sourav Chatterjee, Sang Gil Youm, Chun-Han Wang, Peter Kei and Gerard Ducharme. Thank you for making Annex 460 a great place to work.

Special acknowledgement goes to Drs. Xin Li, Thomas Weldeghiorghis, Susan Verberne-Sutton, Lu Lu, Ang Li, Rafael Cueto, Arturo Carranza, Mirza Ardella Saputra, and the late Dale Treleaven for their expertise and helpful insight.

Foremost among, I sincerely appreciate my wife, Sih-Ting Chen, and my family for their unconditional love and support, and my son, Ethan Yichi Chiang, for the infinite joy he brings to my life.

TABLE OF CONTENTS

ABBREVIATIONS AND ACRONYMS

AFM	Atomic Force Microscopy
CP	Conjugated Polymer
CV	Cyclic Voltammogram
Cys	Cysteine
DCM	Dichloromethane
DFT	Density Functional Theory
DIPA	Diisopropylamine
DMF	*N,N*-dimethylformamide
DMSO	Dimethylsulfoxide
DNA	Deoxyribonucleic Acid
ET	Energy Transfer
FRET	Fluorescence Resonance Energy Transfer
F	Fluorescence Intensity
GPC	Gel-permeation Chromatography
GSH	Glutathione
Hcy	Homocysteine
HEPES	(4-(2-hydroxyethyl)-1-piperazineethanesulfonic acid)
HOMO	Highest Occupied Molecular Orbital
ICT	Intramolecular Charge Transfer
ITO	Indium-tin Oxide
PET	Photoinduced Electron Transfer
LUMO	Lowest Unoccupied Molecular Orbital
MS	Mass Spectroscopy
NMR	Nuclear Magnetic Resonance
NO	Nitric Oxide
OFET	Organic Field Effect Transistor
OLED	Organic Light-emitting Diode
OPV	Organic Photovotaic
OPE	Oligo(*para*-phenylene ethynylene)
P3HT	Poly(3-hexylthiophene)
PAc	Polyacetylene
PAE	Poly(arylene ethynylene)
PANI	Polyaniline
PAV	Poly(arylene vinylene)
PBS	Phosphate-Buffered Silane
PDI	Polydispersity Index
PEDOT	Poly(3,4-ethylenedioxythiophene)
PFO	Polyfluorene
PMMA	Poly(methyl-methacrylate)
PPE	Poly(*para*-phenylene ethenylene)
PPETE	Poly[*para*-(phenylene ethylene)-*alt*-(thienylene ethynylene)]
ppm	Parts-per-million
PPP	Poly(*para*-phenylene)

PPV	Poly(*para*-phenylene vinylene)
PPy	Polypyrrole
PT	Polythiophene
PTV	Poly(thienylene vinylene)
RMS	Root Mean Square
TBAF	Tetrabutylammonium Fluoride (Bu_4NF)
TEG	Triethylene Glycol
THF	Tetrahydrofuran
tmeda	*N,N,N'*-trimethylethylenediamine
UV-vis	Ultraviolet-visible

ABSTRACT

Chemo- and biosensors based on fluorescent conjugated polymer benefit from greater detection sensitivity due to amplification of the electronic perturbations produced by analyte binding. This amplification stems from the exciton-transporting properties of conjugated polymers. A conventional design paradigm relies on the analyte binding events which generate sites of lower energy relative to the polymer energy: either fluorescence quenching sites (*turn-off* sensors) or bathochromically shifted fluorophores (*turn-on* sensors). In both type sensors, the excitons migrate to the lower-energy site created by analyte binding.

This dissertation primarily focused the investigation of an alternative paradigm when analyte binding creates higher energy gap sites in the polymer backbone. Such higher-energy gap sites act as "roadblocks" for excitons to reduce their migration length. Decreasing exciton migration length is accompanied by increasing fluorescence intensity, thus generating an amplified turn-on fluorescent response. The new paradigm expands the generality and universality of the signal amplification concept in conjugated polymers, and can be used to design amplifying turn-on fluorescent sensors for various practically useful analytes such as hydrogen sulfide and cysteine.

In the last part of this dissertation, we present a series of poly(*p*-phenylene ethynylene) thin films prepared by stepwise surface-initiated polymerization. In addition to experimental simplicity and reproducibility of the preparation, and broad variety of compatible building blocks, this method requires low material consumption and no purification for the final bulk thin films. The stepwise surface-initiated polymerization yields dense films of covalently immobilized polymer chains with precisely controlled molecular structure and organization.

CHAPTER 1. INTRODUCTION TO CONJUGATED POLYMERS AS CHEMOSENSORY MATERIALS

1.1 Overview of Conjugated Polymers

Conjugated polymers (CPs) are organic macromolecules with π–conjugation delocalized over a large number of repeating units.[1] The field of conjugated polymers became popular since finding of metallic electrical conductivity in oxidatively doped polyacetylene (PAc) films by Shirakawa, Heeger, and MacDiarmid in 1977 (in 2000 they received Nobel Prize in Chemistry for that discovery).[2–4] They found that the conductivity of polyacetylene increased nearly ten orders of magnitude upon exposure of the polymer film to iodine.[5,6] Since that initial studies, extensive research on the photophysical, electrochemical, and magnetic properties of conjugated polymers has been a popular target in academic community.[7] In addition to fundamental research significance, the tunable electronic and optical properties, flexibility, and solution processability made conjugated polymers a promising class of materials for the next generation electronics such as organic light-emitting diodes (OLEDs),[8] organic field-effect transistors (OFETs),[9] photorefractive devices,[10] organic photovoltaic cells (OPVs),[11] and chemosensory materials.[12–16]

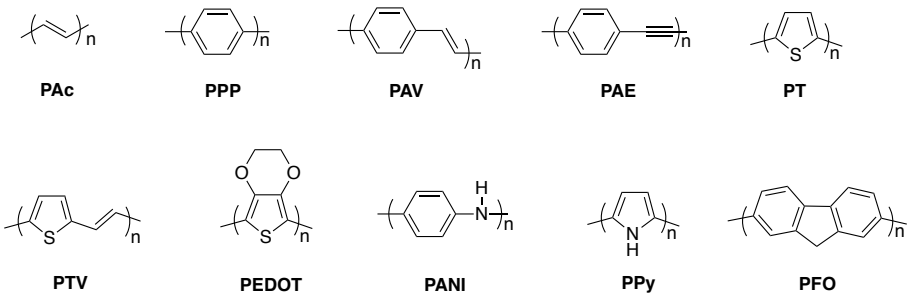

Figure 1.1. Representative chemical structures and abbreviated names of common conjugated polymers.

These properties mainly stem from (1) the extended π–electron delocalization over entire conjugated polymer backbone which reduces the energy gap between the valence and the conduction bands down to 1.5~3.0 eV; and (2) the efficiency of inter- and intramolecular excitation

energy (exciton) migration, especially in the condensed and solid state. Figure 1.1 shows common conjugated polymers such as poly(*para*-phenylene) (PPP), poly(*para*-phenylene vinylene)s(PPV), poly(*para*-phenylene ethynylene) (PPE), polythiophene (PT), poly(thienylene vinylene) (PTVs), poly(3,4-ethylenedioxythiophene) (PEDOT), polyaniline (PANI), polypyrrole (PPy), and polyfluorene (PFO).[17]

1.2 Inter- and Intramolecular Excitation Energy Transfer

It is important to understand how the electronic excitation energy (exciton) transfers in/between conjugated polymer chains prior to designing OLED, OFET, solar cells, and chemo-/biosensory devices.[18] A quasi-particle exciton is generally referred to the excitation energy and the surrounding environment changes in bond length and angles along the π-conjugated system in response to the formation of the excited state.[19]

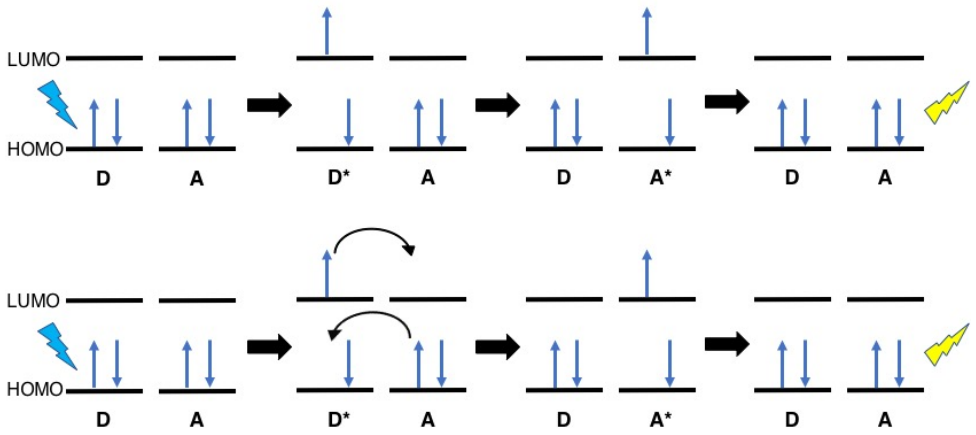

Figure 1.2. Schematic diagrams showing mechanisms of Förster (top) and Dexter (bottom) energy transfer processes.

Generally, excitation energy can migrate intermolecularly and/or intramolecularly, in which the former occurs via dipole–induced dipole through-space interactions (Förster-type)[20] and the latter happens by the combination of through-space mechanism and via the through-bond mechanism occurring through strong orbital overlap between chromophores (Dexter-type) (Figure

1.2).[21] Nevertheless, whether the Förster-type or Dexter-type mechanism dominates the excitation energy transfer in conjugated polymers still remains a point of debates in research literature owing to the difficulty of quantitative differentiating one from the other.[22,23] In an ideal scenario of strong intrachain electronic coupling where through-bond Dexter-type mechanism dominates, excitons one-dimensionally walk along the isolated polymer chains whose structure is hypothesized to be a defect-free planar conformation with complete electron delocalization along the backbone. In reality, however, the disordered nature of conjugated polymers tends to form abundance of structural defects such as kinking, coiling, twisting, etc., whereby these inherently defects can greatly inhibit Dexter energy migration since the orbital coherence between segmented chromophores is discontinuous (Figure 1.3).[24]

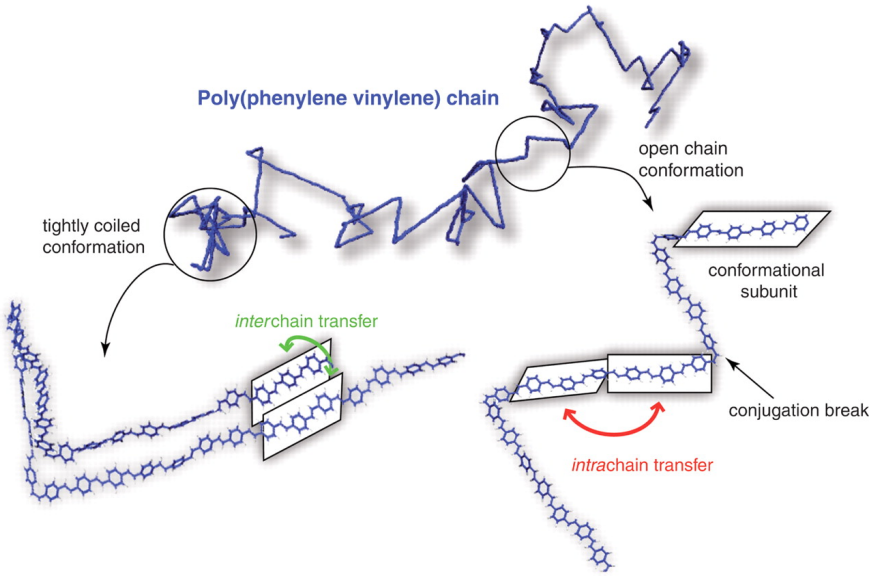

Figure 1.3. Example of single-chain conformation of a poly(phenylene vinlyene) conjugated polymer, referred to as the defect cylinder conformation. Conformational disorder produces a chain of linked chromophores (or conformational subunits) outlined conceptually by the boxes. The intramolecular excitation energy transfer (migration along the backbone) is the predominant mechanism when the polymer chain assumes an open, extended conformation, typical for solutions in good solvents such as chloroform; on the other hand, intermolecular interactions (hopping between segments in close proximity) are dominant for tightly coiled configurations, typically found in polymer nanoparticles, or thin films. Reproduced with permission from Ref. 24. Copyright © 2009 The American Association for the Advancement of Science.

The luminescence signature of intermolecular migration usually combines bathochromic emission, longer lifetime, and lower quantum yield, since delocalization between segments reduces the excited state energy relative to the isolated chain exciton. A detailed elucidation of these two mechanisms was presented by Schwartz *et al.*[25] In that work, isolated extended alkoxy-PPV macromolecular chains were incorporated into long cylindrical pores of an extended silica matrix in order to eliminate any intermolecular interactions, and the polarized luminescence spectroscopy showed that the excitation energy diffusion along the isolated polymer backbone was a slower process ($10^{-11} \sim 10^{-10}$ s) due to weak dipole coupling along the extended polymer chain. At the same time, intermolecular energy migration was found to be much faster ($10^{-12} \sim 10^{-11}$ s).

Although intramolecular energy transfer is generally considered less efficient than its intermolecular counterpart, some recent studies have shown that the intramolecular migration in isolated polymers may be actually efficient. Swager *et al.* found that intramolecular energy transfer indeed was the major pathway for excitation migration in conjugated polymers in anisotropic Langmuir-Blodgett films of monolayered PPE.[26–28] The substantial contribution of through-bond Dexter-type mechanism of excitation energy transfer along the conjugated polymer backbone was found in chain-extended conformations of uniformly aligned PPEs in nematic liquid crystalline media (Figure 1.4).[29] Unlike through-space hopping by Förster-type route, excitation energy transfer by orbital overlap is dramatically affected by structural defects and molecular alignments. This significance was elegantly addressed by dissolving PPE derivatives in nematic liquid crystals, allowing finely manipulation of the chain-extension lengths and molecular alignments of the PPE backbone. The end-capped low-energy gap fluorophores was introduced to accept intramolecular excitations and therefore the efficiency of energy migration could be evaluated via site-selective emission of the termini. When the temperature was increased above the nematic-isotropic

transition of the liquid crystal, the dramatically diminished fluorescence from the terminal fluorophores, along with simultaneous increase in the backbone PPE emission strongly indicated the disrupting of conjugated length and related diminishing of the energy migration by Dexter-type mechanism.

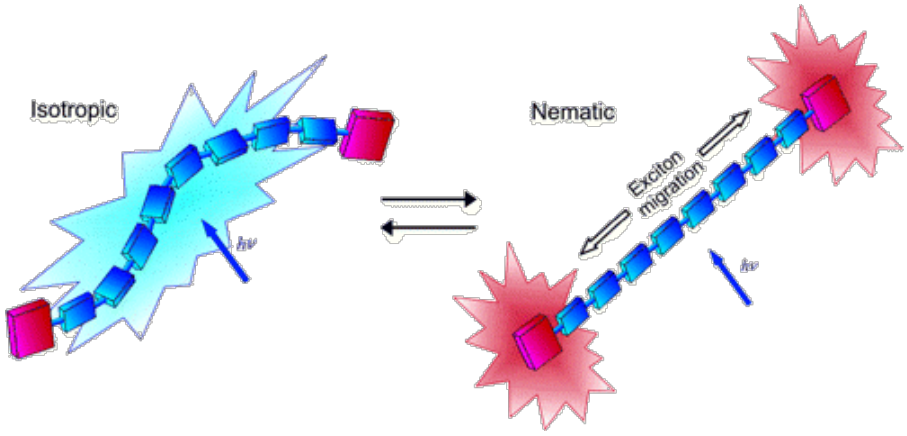

Figure 1.4. Simplified representation of conjugated polymer PPE in isotropic and liquid crystalline solutions. In isotropic solution, the conformational disorder in the polymer backbone prevents efficient intramolecular exciton migration, thus resulting in predominant emission from the PPE backbone. In nematic liquid crystalline solution, the increased electronic conjugation in the straightened and planarized polymer chains is higher, which leads to the enhanced intramolecular migration toward the terminal groups with a concomitant increase in the termini's emission. Reproduced with permission from Ref. 29. Copyright © 2005 American Chemical Society.

Quantitative differentiation of the contribution from intermolecular and intramolecular energy transfer pathways can be performed by subensemble analytical methods such as cryogenic single molecular spectroscopy.[30] This analytical method is based on the measuring zero-phonon transition line accompanying distinct vibrionic band of individual chromophores within a polymer chain, and thereby can differentiate between intermolecular, intramolecular, and dynamic modes of disorder. Lupton *et al.* recently investigated poly(3-hexylthiophene) (P3HT) in Zeonex480 and poly(methyl methacrylate) (PMMA) matrices, to simulate isolated and aggregated polymer chains, respectively. They found that single chromophore in the conjugated chain was flexible and could adopt wide range of subtly varying conformations (e.g. bending of backbone, chain torsion, and

changes in bond alternation) that affect the adjacent chromophore in a single chain through coherent oscillation, which is also responsible for intermolecular energy transfer.

Förster and Dexter mechanisms both contribute greatly to energy transfer in conjugated polymers. Although the Förster mechanism is considered to play a major role in high concentration solutions and aggregates states due to close interchain distance, Dexter energy transfer, which is based on orbital overlap along π-electron delocalized conjugated backbone, is efficient in more dilute solutions.

1.3 Signal Amplification in Conjugated Polymer Sensors

A photon absorption generates a strongly bound electron-hole pair (exciton) that can randomly walk along the conjugated system as well as hop from one conjugated system to another before a photophysical and/or photochemical process occurs. By using site-selective fluorescence technique, it was found that inherent Stokes shift in conjugated polymers is smaller than that induced by exciton migration. Therefore, the photoluminescence occurring from the lower energy gap segments gives conjugated polymer a larger Stokes shift and inhomogeneous featureless luminescence spectrum. In case of an isolated polymer chain, excitation energy migration happens intramolecularly in a slow process relying on orbital overlap,[31] and the diffusion length of exciton ranges from 5 to 14 nm.[32,33] Swager *et al.* demonstrated, by end-capping poly(*para*-phenylene ethynylene)s with a lower energy gap anthracene end groups, that the exciton effectively migrates to the lowest energy gap site (Figure 1.5).[34]

On the other hand, conjugated polymer photoluminescence can be efficiently quenched via a photoinduced electron transfer (PET) process, where excited state electron on the conduction band is brought back to the valence band by passing through the LUMO of an electron-deficient analyte bound to the polymer backbone. Combined with an efficient exciton migration (especially

when it becomes a three-dimensional process in solid and condensed states), this process is known as *"turn-off"* amplification mechanism. Swager *et al.* and Whitten *et al.* independently demonstrated that electron-deficient molecules such as nitro-aromatic explosives can effectively bind to electron-reach conjugated polymers (Figure 1.6).[35,36,37] They showed that a single chemical binding or unbinding event can trigger electronic perturbations along the entire π-electron conjugated backbone, thereby the collective response can be measured optically or electrochemically. It is important to note that such a response is dominated by static quenching.

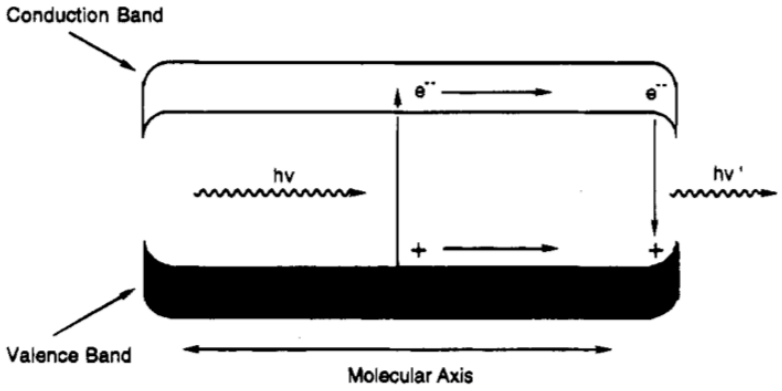

Figure 1.5. Representation of energy migration in a conjugated polymer molecular wire with a decrease in band gap at the termini. Reproduced with permission from Ref. 34. Copyright © 1995 American Chemical Society.

In contrast to the *"turn-off"* mechanism where the metal-ligand coordination or van der Waals interactions between the polymers and the electron-deficient quenchers are responsible for the photoluminescence quenching, Kim and Swager demonstrated an example of an unprecedented *"turn-on"* fluorescence amplifying conjugated polymer for fluoride anion detection.[38] In Figure 1.7, a non-emissive pendant fluoride-reactive group, electronically coupled with the conjugated polymer backbone, lactonizes to form a lower-energy coumarin fluorophore after treating with analytical amount of fluoride anion. This forces the excitons produced in the polymer backbone to migrate to the lower-energy coumarin site with accompanying increase in the coumarin fluorescence. The resulting fluorescence amplification is approximately 100 times with respect to

a small molecule analog. However, there are only a limited number of suitable analytical reactions that can form a lower-energy highly fluorescent fluorophore where its absorption and emission are bathochromically shifted relative to the CP backbone. This indeed intrinsically limits the generality and application potential of this approach.

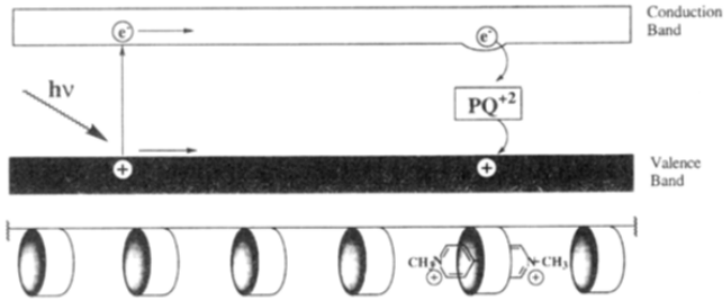

Figure 1.6. Conceptual illustration of energy migration to a receptor site occupied by PET quencher methyl viologen (paraquat, PQ^{2+}). When the excited electron encounters a receptor site with a bound PQ^{2+} group, electron transfer quenching occurs. Reproduced with permission from Ref. 37. Copyright © 1995 American Chemical Society.

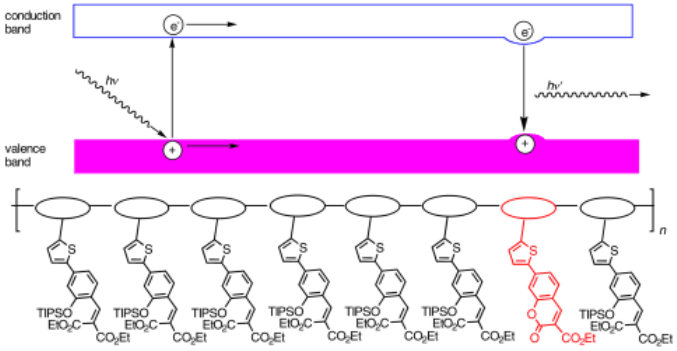

Figure 1.7. Schematic band diagram illustrating the mechanism by which a semiconducting polymer can produce an enhanced *turn-on* fluorescence chemosensory response. The horizontal dimension represents the position along the polymer backbone shown schematically at the bottom. Excitons are created by absorption of a photon ($h\upsilon$) and they migrate along the polymer backbone. Fluoride-induced lactonization of the electronically coupled receptor groups produces an exciton trapping site with a smaller band gap (E_g) and recombination of excitons at that site results in a new amplified emission. Reproduced with permission from Ref. 38. Copyright © 2003 Wiley-VCH.

To address this challenge, Nesterov *et al.* introduced an alternative "higher energy gap" paradigm — where instead of relying on the formation of a smaller energy gap emissive site where

excitation energy from the conjugated polymer backbone is funneled, the generation of a local higher energy gap site in the π-conjugated backbone is able to restrict the energy migration along the isolated π-electron conjugated system.[39] Importantly, this concept relies on the small changes at the analyte-reactive site rather than on drastic changes in the π-electron conjugated backbone Poly(*p*-arylene vinylene)s (PAVs) emerged as an excellent conjugated polymer choice for this mechanism due to its extraordinary emissive nature and low energy band gap (λ_{em} > 500 nm), as well as a better feasibility to functionalize with analyte-specific receptor groups compared to other classes of conjugated polymers. In the initial study, diethyl chlorophosphate (DCP), a commonly used mimics of organophosphorus warfare agents, was chosen as an analytical detection target. The PAV polymer sensor incorporated naphthalene based hydroxy oxime reactive group that can facilely convert to the corresponding isoxazole upon reacting with DCP. The formation of isoxazole unit, which possesses a noticeable higher HOMO-LUMO gap relative to the unreacted hydroxy oxime, resulted in an amplified *turn-on* fluorescent response. Since the *turn-on* response in the higher energy gap mechanism is based on modulation of the intramolecular exciton migration in CPs, it produces an amplification effect similar to that observed in cases of *turn-off* sensors for electron deficient analytes.

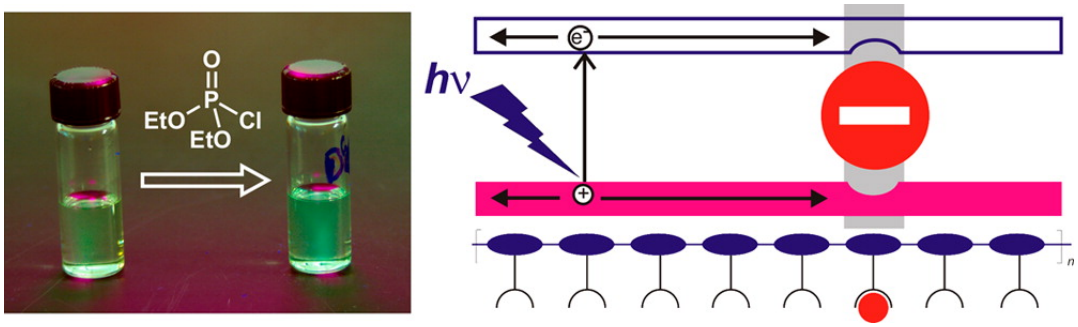

Figure 1.8. Schematic diagram illustrating the higher energy gap control of CP fluorescence: an analyte (red circle) binding creates a local higher energy gap site in the CP backbone which acts as a "roadblock" and decreases the length of the excitation/exciton migration along the π-conjugated system, resulting in the increase of fluorescent intensity of the conjugated polymer. Reproduced with permission from Ref. 39. Copyright © 2013 American Chemical Society.

1.4 *Turn-On* Sensory Systems Based on Fluorescent Conjugated Polymers

1.4.1 Sensing Metal Ions

In contrast to *turn-off*, quenching-based conjugated polymer fluorescent sensors, research literature describes rather limited number of *turn-on* conjugated polymer based fluorescent sensors. This is probably related to the difficulties with general design principles of such sensors. Below, we provide an overview of known *turn-on* sensors based on conjugated polymers. Many of such sensors are based on binding metal cations by chelating ligands which results in diminishing PET quenching process. Jones *et al.* reported sensor **1** based on poly[*p*-(phenylene ethylene)-*alt*-(thienylene ethynylene)] containing *N,N,N'*-trimethylethylenediamine (tmeda-PPETE) pendant units that showed *turn-on* selective fluorescent response on Hg^{2+} over Ca^{2+}, Zn^{2+} and H^{+} at the submicromolar concentrations.[40] The low quantum yield of the pristine polymer (ϕ_{FL} = 0.09) was attributed to PET from the conjugated backbone to the amino group of the uncomplexed receptor tmeda. Upon binding with Hg^{2+}, a stable tmeda/Hg^{2+} complex was formed which lowered the HOMO of the receptor and inhibited the PET process, resulting in the increase of the fluorescence intensity. Fan and Jones also prepared an inorganic/organic hybrid complex, tmeda-PPETE/Cu^{2+}, which showed selective response on detection of Fe^{2+} cations.[41] In the initial state, the pre-coordinating with Cu^{2+} completely quenched the polymer fluorescence.

Upon the addition of Fe^{2+}, tmeda-PPETE/Cu^{2+} hybrid system showed a gradual enhancement in fluorescence up to 150-fold, and was highly selective toward Fe^{2+} over Ca^{2+}, Hg^{2+}, Zn^{2+}, Ni^{2+}, Co^{2+}, Mn^{2+}, and H^{+} ions. The authors proposed that the amplified fluorescent response not only simply resulted from the difference in association constants between tmeda and various metal ions, but was due to the competitive binding between Cu^{2+} and other metal ions.

Zhu and co-workers reported a poly(*p*-phenylene ethynylene) derivative **2** incorporating a single diastereomer *(R,R)*-salen unit as a Zn^{2+} receptor that showed a 7.8-fold increase in fluorescence upon gradual addition of Zn^{2+}.[42] The formation of Zn^{2+} metallopolymer significantly suppressed PET quenching process as well as resulted in planarization of the polymer backbone to increase the π-electron conjugation. Noteworthy, **2** exhibited a good selectivity for Zn^{2+} over Cd^{2+} and Hg^{2+} despite all three ions being in the same group of the periodic table and having closed-shell configurations.

Li and co-workers also investigated Hg^{2+} detection by the rhodamine incorporating poly[*p*-(phenylene ethylene)-*alt*-(thienylene ethynylene) sensor polymer **3**.[43] Changes that were observed upon addition of Hg^{2+} in both absorption and fluorescence spectra could be attributed to FRET from the conjugated backbone to the ring-opened isomer of rhodamine. It was found that the fluorescence intensity ratio of conjugated backbone to rhodamine emission bands increased by a factor of 18.6. Sensor **3** showed good selectivity toward Hg^{2+}, even over the background of 20 equiv. of metal ions including Li^{+}, Na^{+}, K^{+}, Ca^{2+}, Ba^{2+}, Mg^{2+}, Al^{3+}, Ag^{+}, Cu^{2+}, Co^{2+}, Ni^{2+}, Mn^{2+}, Pb^{2+}, Zn^{2+}, and Cd^{2+}.

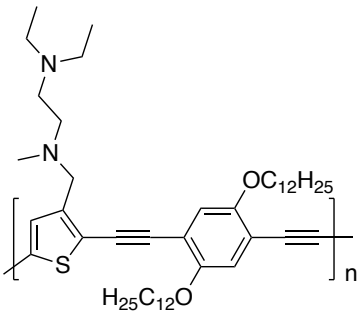

1

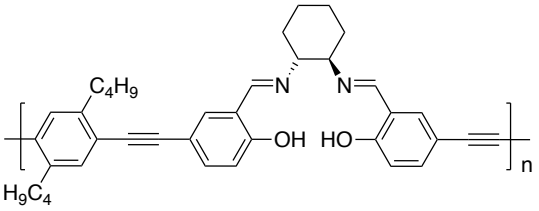

2

Recently, Hua and co-workers have prepared poly(fluorene-*co*-thiocarbonyl quinacridone) Hg^{2+} fluorescence turn-on probe **4**, which demonstrated excellent sensitivity and 32-fold fluorescent intensity increase upon analyte binding.[44] The fluorescent emission of **4** was initially

suppressed by the presence of thiocarbonyl moiety in the conjugated backbone. Addition of mercury ion resulted in conversion of thiocarbonyl to carbonyl functional group bringing about the absorbance change and turn-on intensity increase in fluorescence. Furthermore, Hua also demonstrated that the nanoparticles of **4** expressed good sensitivity and selectivity toward Hg^{2+} in PBS solution and in the presence of HeLa cells.

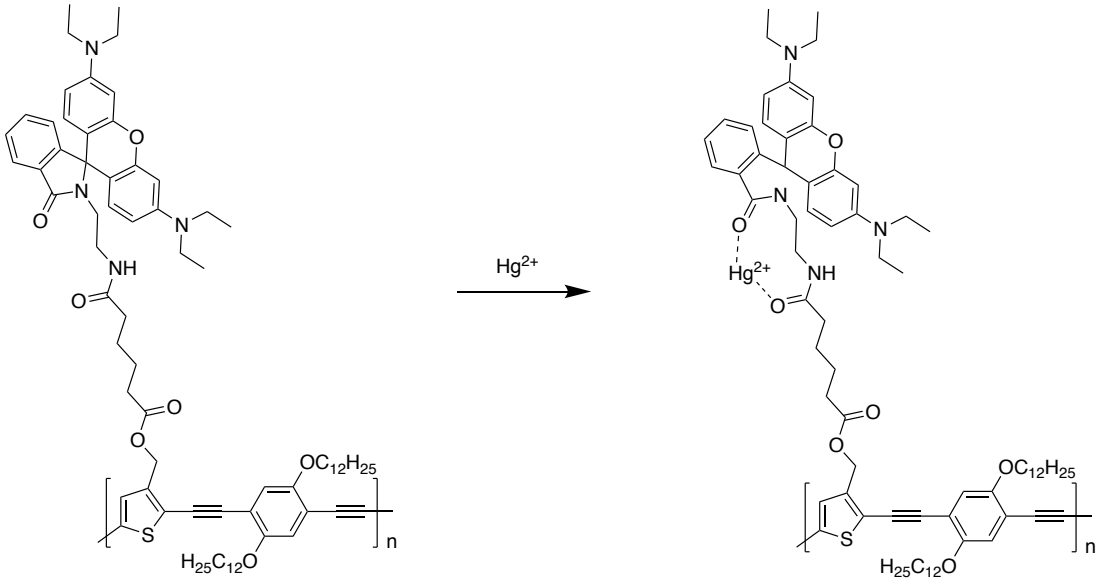

3

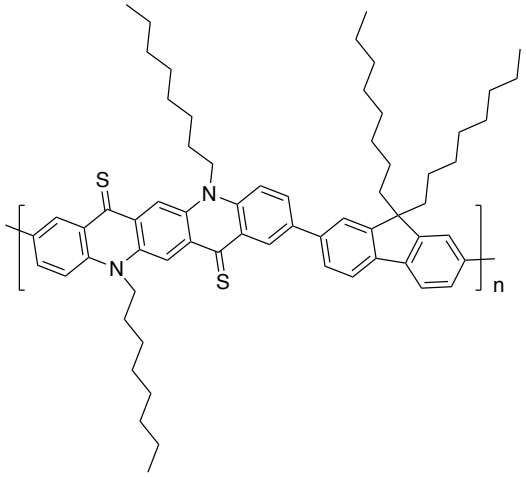

4

Wang *et al.* reported a K^+ sensor based on excitation energy transfer from water-soluble polyfluorene **5** to the fluorescein labelled G-rich single-strained DNA.[45] With quaternary

ammonium cations in the side chains, **5** can electrostatically attract to the negatively charged G-rich ssDNA and form a 1:1 complex with it. The loose complex of **5** and random coiled ssDNA showed a predominant fluorescence band from **5** at 422 nm and a low-intensity band at 527 nm due to an inefficient FRET from polymer **5** to fluorescein chromophore. Addition of the complex of **5** and fluorescein-labeled ssDNA to an aqueous solution of K^+ resulted in the significant turn-on increase of the fluorescein fluorescence band, which was due to shortening the distance between **5** and G-quadruplex forming in the presence of K^+. The FRET ratio (I_{527}/I_{422}) of the polyfluorene to fluorescein emission bands increased about 2, 3.4, and 16 times in the presence of 8.5, 30, and 50 mM KCl, respectively. Selectivity examination showed a much weaker response on the addition of Mg^{2+} and Ca^{2+}; and negligible response on Na^+, NH_4^+, and Li^+ due to the inability of these ions to facilitate formation of the G-quadruplex secondary structure.

Smith *et al.* exploited benzo-15-crown-5-ether based poly(*p*-phenylene vinylene)s derivative (CE-OPV) **6** as an Eu^{3+} chemosensor.[46] Sensor **6** represented a rare case when a crown-ether based conjugated polymer exhibited turn-on fluorescence enhancement since ion-enhanced aggregation typically effectively traps and non-radiatively dissipates the emissive energy.[47] The authors argued that the fluorescence enhancement could be caused by suppression of ICT.

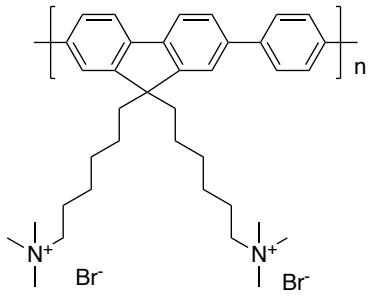

5

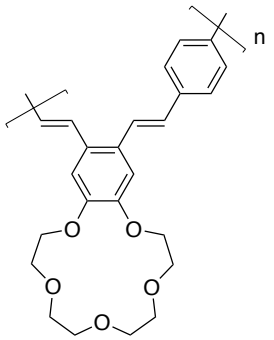

6

Zhu *et al.* have prepared a chiral conjugated polymer by joining a (*R,R*)-salen ligand with a perylenetetracarboxylic acid derivative.[48] Conjugated polymer sensor **7** exhibited only a weak

fluorescent band at 635 nm prior to coordinating with added Hg^{2+}, and the authors proposed that it was attributed to an efficient intramolecular charge transfer (ICT) between the salen and perylenetetracarboxylate units along the polymer backbone. They observed a significant (up to 26 times) increase of fluorescence intensity upon addition of Hg^{2+} with an excellent selectivity.

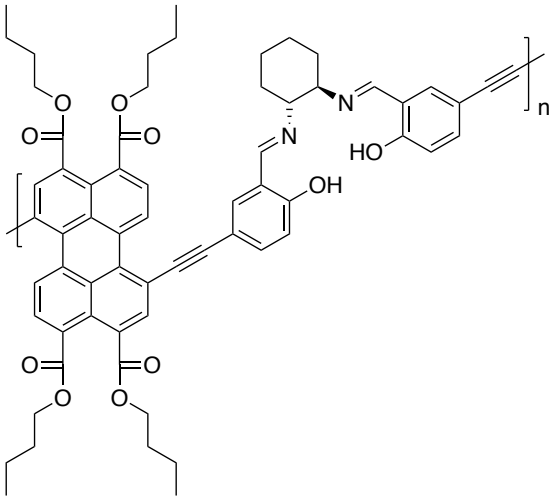

7

1.4.2 Small Organic Molecules and Bioanalytes

Lippard and co-workers reported a bipyridyl-incorporating poly(*p*-phenylene vinylene) conjugated polymer sensor **8** to detect NO gaseous molecule with nanomolar sensitivity.[49] **8**/Cu^{2+} complex showed a moderate fluorescence quenching, whereas the introduction of 300 eq. of NO increased the polymer emission by 2.8-fold. The authors proposed that in alcohol solution, the NO can reduce paramagnetic Cu^{2+} cation to diamagnetic Cu^{1+} cation; the paramagnetic properties of Cu^{2+} were mainly responsible for the initial fluorescence quenching.

Li and co-workers prepared a polyfluorene derivative **9** containing imidazole pendant side groups that are chelating toward Cu^{2+} to be used as a cyanide turn-on sensor.[50] Excitation energy transfer from the conjugated polymer backbone to imidazole-bound Cu^{2+} lead to dramatic reduction in fluorescence emission at 402 nm while the replacement of imidazole with other

nitrogen-containing heterocyclic units would not be sufficient to diminish the emission. **9**/Cu^{2+} complex showed a significant fluorescence response upon the addition of CN^-.

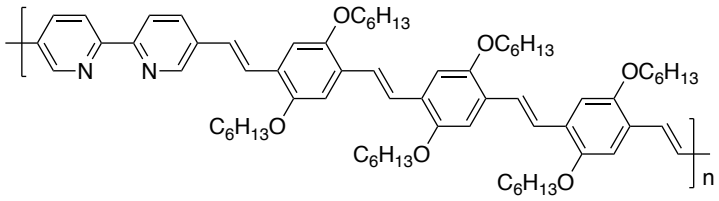

8

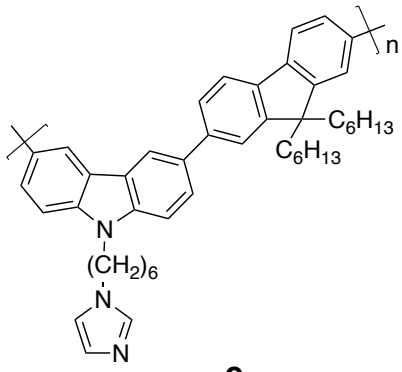

9

Zhu *et al.* demonstrated that a chiral imine-based conjugated polymer **10** incorporating both (*S*)-2,2′-binaphthol (BINOL) and (*S*)-2,2′-binaphthyldiamine (BINAM) units can selectively recognize (*D*)-phenylalaninol over its enantiomer (*L*)-phenylalaninol.[51] The binding of (*D*)-phenylalaninol to the chiral polymer backbone inhibited PET process and therefore triggered the fluorescence turn-on response. The enantioselective response of **10** can be attributed to the formation of a more stable **10**/(*D*)-phenylalaninol diastereomer complex stemming from the interactions of hydroxy and imine functional groups on BINOL and a target amino alcohol. Noteworthy, reduction of imine units upon the treatment with $NaBH_4$ converted **10** in a non-conjugated polymer which showed a much lower fluorescence response. The polymer **10** showed an enantiomeric fluorescence difference ratio (*ef*) of 6.85-fold for (*D*)-phenylalaninol with respect to its enantiomer. The authors unveiled good analyte selectivity of **10** since no significant fluorescence enhancement was noticed upon addition of (*D*)/(*L*)-mandelic acid, (*R*)/(*S*)-

phenylethylamine, and (*D*)/(*L*)-phenylglycinol. The authors further extended the concept of enantioselective recognition for the sensing chiral (*L*)-α-hydroxycarboxylic acids.[52] (*R,R*)-salen incorporating poly(*p*-phenylene ethynylene) **11** showed only a weak fluorescence since the strong intramolecular hydrogen bonding between the hydroxy and imine groups on the salen moiety quenched the fluorescence of **11**, whereas the fluorescent emission could be subsequently restored by binding of target (*L*)-α-hydroxycarboxylic acids. The sensor **11** showed *ef* of 8.41 for (*L*)-mandelic acid over (*D*)-mandelic acid, and 6.55 for (*L*)-lactic acid over (*D*)-lactic acid. Reduction of the imine group to saturated amine resulted in a disordered and flexible polymer with a strong intrinsic fluorescence. In contrast to polymer sensor **11**, the reduced disordered polymer showed formation of an unstable complex with mandelic acid which was acting as a site for nonradiative relaxation, leading to fluorescence quenching (turn-off response).

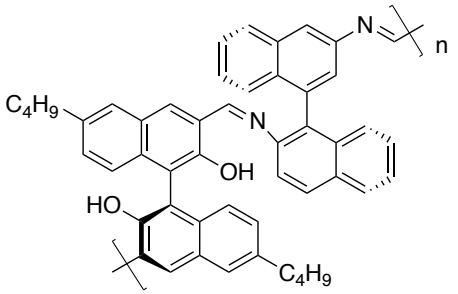

10

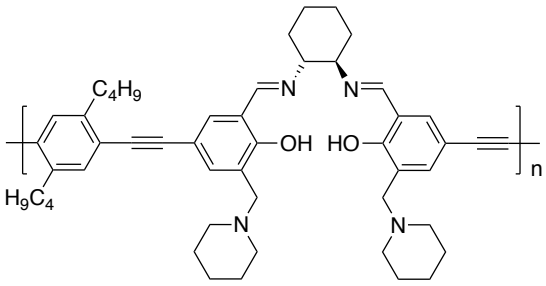

11

Recently, Pu and co-workers reported a chiral 1,1′-bis-2-naphthol based conjugated polymer **12** whose fluorescence was initially quenched by the aldehyde groups.[53] Treating the enantiomeric polymer (*S*)-**12**/Zn^{2+} complex with (*R*)-leucinol yielded a large increase in fluorescence emission at 535 nm, whereas a weaker fluorescence increase was observed for (*L*)-leucinol. In addition, good selectivity over various 2-aminoalcohols was observed. The authors hypothesized that the most sterically bulky substituent adjacent to the chiral amine center gave the highest *ef* value. The importance of having conjugated polymer entity was demonstrated by the

fact that a small molecule counterpart of the polymer **12** showed only a negligible difference in the enantioselective fluorescent response.

Wang *et al.* designed conjugated hydroxy-functionalized polyquinoline polymer **13** as a fluoride anion sensor, which operated based on the formation of hydrogen bonding between F^- and the hydroxy group.[54] Addition of F^- resulted in the appearance of a new absorption peak at around 500 nm, as well as significantly increased the fluorescence band at 620 nm up to 147-fold. In contrast, a small molecule counterpart of the polymer **13** exhibited only a much smaller 14.7 times fluorescent enhancement. The authors proposed that the turn-on sensing effect involved two mechanisms: the formation of phenolate induced by F^- and the ICT between quinolone and the phenolate moieties. The former was investigated by ^1H NMR using a small molecule analog which showed diminishing of the hydroxy peak. The role of the second mechanism was clearly indicated by the long range bathochromic shift in absorption and emission spectra. Additionally, no obvious change occurred upon addition of Cl^-, Br^-, and $H_2PO_4^-$.

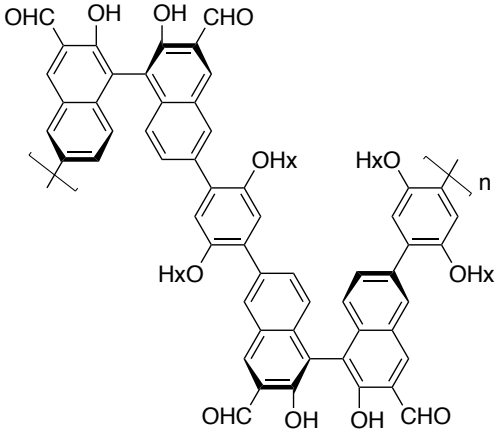

12

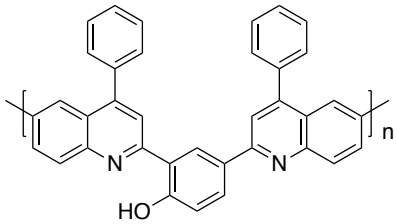

13

Thomas and Swager reported an amino-functionalized poly(*p*-phenylene) **14** whose fluorescence could be increased by adding trace amounts of a reducing agent hydrazine.[55] Although **14** showed such an enhancement only in thin films, the observed hydrazine detection

limit was 100 ppb. It was likely due to the presence of inherently oxidized defect sites in the bulk materials as well as the much greater exciton migration in conjugated polymers in solid state relative to an isolated chain in dilute solution. It is noteworthy that less electron-rich **15** and **16** showed lower response compared to **14**, indicating that most readily oxidized polymer gave the largest fluorescence enhancement.

Tian *et al.* prepared naphthalimide-functionalized poly(phenylacetylene) **17** which exhibited both fluorescent ratiometric and colorimetric responses on addition of F^-.[56] In the presence of F^-, ICT could be facilitated by the conversion of amide (electron donor) to imine (electron acceptor) moiety,[57] resulting in a large electron density redistribution and showing charge transfer peaks in the UV-vis and emission spectra. **17** demonstrated good selectivity for fluoride over other halogen anions such as Br^-, Cl^-, and I^-.

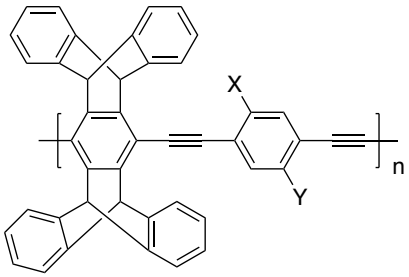

14: X=Y=O(*n*-$C_{10}H_{21}$)
15: X=N(*n*-C_8H_{17})$_2$; Y=H
16: X=Y=N(*n*-C_8H_{17})$_2$

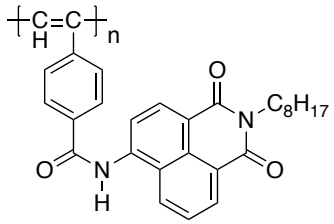

17

Kakuchi and co-workers introduced a concept of anion/urea halogen bonding promoted deaggregation that unquenched the fluorescence of conjugated polymers.[58] Urea-functionalized poly(phenylenebutadiynylene) **18** intrinsically favors interchain aggregation since the abundant urea units tend to form multiple intermolecular hydrogen bonds, which resulted in the aggregation-induced quenched polymer emission band at 460 nm. Upon addition of F^-, the stronger association between F^- anion and urea resulted in disassembly of the aggregated state of **18** thereby producing

a new fluorescence band at 493 nm originating from the isolated polymer. Polymer sensor **18** showed a good response on F^-; however, it also showed a relatively low selectivity and lacked discrimination against other anions such as AcO^-, BzO^-, and N_3^-.

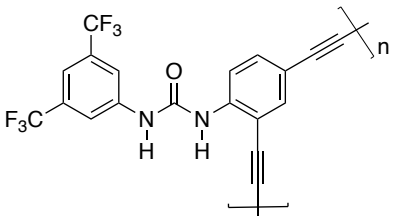

18

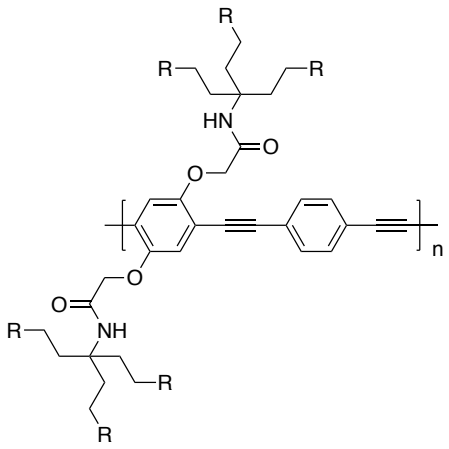

19: $NH_3^+Cl^-$

In a sharp contrast to the above-described work, Zhao and Schanze developed a conjugated polymer sensor where anion-enhanced aggregation resulted in a turn-on ratiometric fluorescent response.[59] The cationic polyelectrolyte poly(*p*-phenylene ethynylene) **19** bearing ammonium-functionalized side chains showed excellent water solubility and intense blue fluorescence at 432 nm with well resolved vibronic structure. The intensity of the emission band at 432 nm decreased upon increasing concentration of added pyrophosphate which was accompanied by enhancement of a red-shifted broad emission band at 520 nm. The latter was due to the pyrophosphate-induced aggregation of conjugated polymer **19** and resulting intermolecular exciton coupling. On the other hand, phosphate anion chelated **19** showed no change in absorption and fluorescence spectra. The authors hypothesized that pyrophosphate bearing two anionic units could efficiently crosslink the polycationic chains of **19** thereby resulting in aggregation and aggregation-related observed spectroscopic changes.

Bai *et al.* prepared a 2,2′-bisimidazole incorporating conjugated polymer **20** whose fluorescence was effectively quenched upon formation of a complex with Cu^{2+} through PET between the polymer backbone and Cu^{2+} as the electron acceptor.[60] The **20**/Cu^{2+} complex demonstrated good fluorescence enhancement upon titration with pyrophosphate anion due to the formation of a more stable complex of pyrophosphate/Cu^{2+} thereby inhibiting the PET process. Of many common hard and soft anions, only pyrophosphate was found to trigger fluorescence enhancement of up to 9-fold within three minutes and the pyrophosphate detection limit was found to be 0.17 ppm.

The same authors also utilized poly[2,2′-bisimidazole-*co*-carbazole] conjugated polymer **21** as a platform for sensing cysteine.[61] Upon addition of Ag^{+} to the polymer, the complex **21**/Ag^{+} showed decreasing intensity of fluorescence emission at 416 nm and a simultaneous red shift of 40 nm. Two possible mechanisms were proposed to rationalize this observation: the first was PET from the polymer **21** to Ag^{+} and the second was Ag^{+}-induced interchain aggregation resulting in an efficient FRET.[62] The complex **21**/Ag^{+} was then used to detect cysteine since Ag^{+} possesses strong association constant towards cysteine. The fluorescence ratio (F_{416nm}/F_{456nm}) increased 4 times upon addition of cysteine, and the detection limit was established at 90 nM. **21**/Ag^{+} complex showed good selectivity towards cysteine among 15 other amino acids, yet glutathione showed a similar fluorescence response.

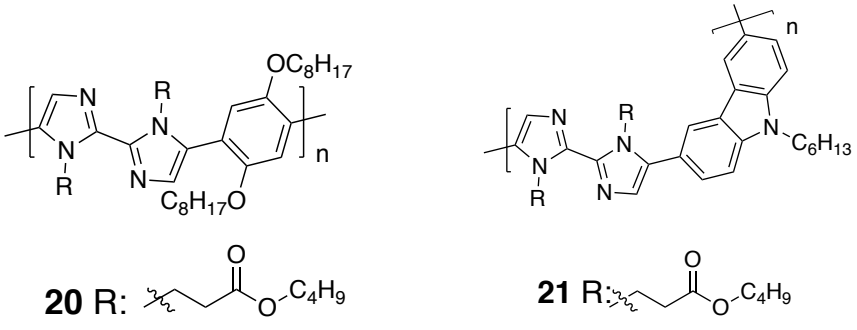

Swager *et al.* demonstrated that a nonemissive thioether-containing poly(*p*-phenylene ethynylene) **22** displayed amplified turn-on fluorescence when exposed to hydrogen peroxide.[63] Pristine **22** showed a low fluorescence quantum yield (λ_{FL} 457 nm, Φ_{FL} 0.01), but it was increased by more than 49-fold upon the addition of an oxidizing agent H_2O_2. Low concentration of H_2O_2 (100 nM) was sufficient to trigger the fluorescence response from **22** in three hours, however excess amount of H_2O_2 lead to oxidizing the ethynyl linker thereby interrupting the π-electron conjugated system. Fluorescence lifetime studies of **22** showed that the increased k_{FL} was due to the greater spatial overlap of the frontier molecular orbitals due to delocalization of the HOMO along the conjugated backbone and the increased τ_{FL} was due to the decrease in the rate if intersystem crossing.

Thomas and co-workers reported diaryltetracene-functionalized poly(fluorene-*co*-phenylene) **23** as a ratiometric fluorescent singlet oxygen ($^1O_2$) sensor.[64] The pendant diaryltetracene can undergo [4+2] cycloaddition with $^1O_2$ to form endoperoxide species. Formation of these species can suppress excitation energy migration from the polymer backbone to diaryltetracene chromophore and therefore restore fluorescence of the polymer backbone. This resulted in drastic changes in the emission spectra, where a tetracene emission band at 512 nm steadily decreased whereas the polymer backbone emission band at 417 nm increased.

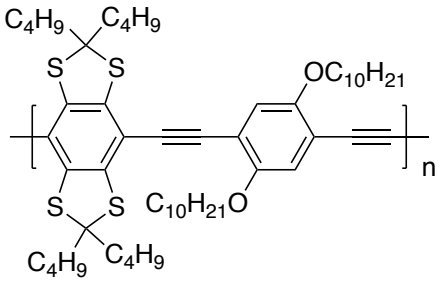

22

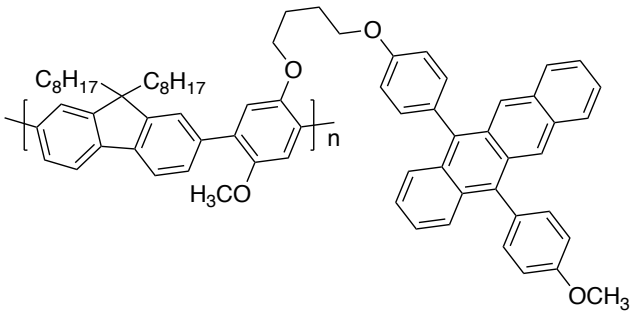

23

The authors also showcased an alternative route of the excitation energy migration interruption. In conjugated polymer **24**, the $^1O_2$ acceptor diethynyltetracene unit was electronically coupled to the excitation energy donor poly(*p*-phenylene ethynylene).[65] Upon exposure to reactive singlet oxygen, fluorescence of the conjugated polymer backbone at 469 nm greatly increased. This was due to the oxidized tetracene chromophore no longer accepting excitation energy. Time-resolved fluorescence spectroscopy and excited-state lifetime studies found that the lifetime of **24** gradually increased with an increasing fraction of the oxidized tetracene.

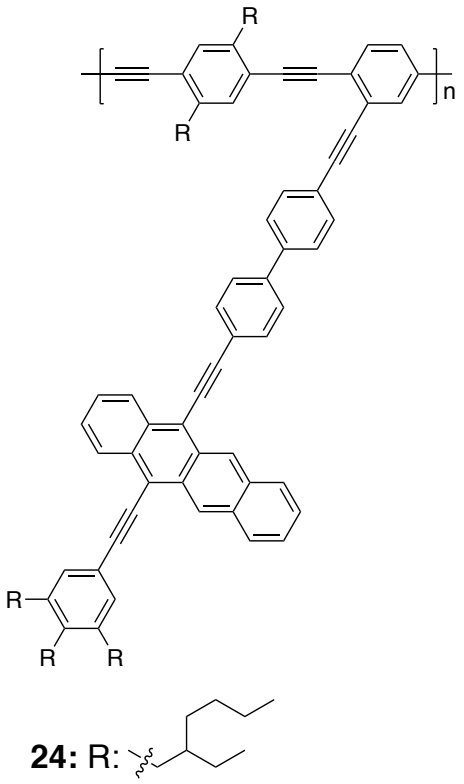

24: R:

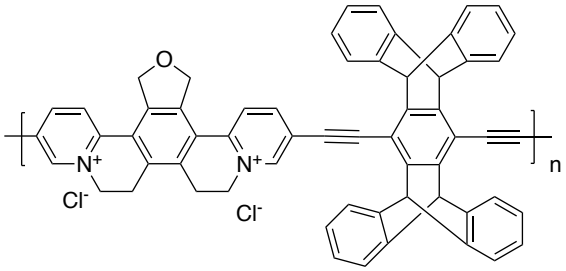

25

Rochat and Swager reported an n-type conjugated polymer poly(pyridinium *p*-phenylene) **25** that was designed as a sensor for electron rich bioanalytes.[66] This sensor could detect concentration of caffeine as low as 25 ppm. Reduction of 48% in fluorescence intensity with electron rich indole units could be attributed to the quenching due to electron transfer from indole to the high ionization potential conjugated polymer. This was evaluated in Stern-Volmer

quenching experiments and fluorescence lifetime studies.[67,68] Unexpectedly, other analytes resulted in an increase in emission intensity, thus suggesting a more complex fluorescence amplification mechanism. With its large hydrophobic pentiptycene unit, **25** could display some intermolecular hydrophobic interactions which could be interrupted by added aromatic analytes.

Swager and coworkers also demonstrated a pseudoratiometric polymer-on/dye-off mechanism for sensing cyclic ketone vapors.[69] The loading of 0.5 wt. % of a squaraine dye in the thin film of poly(*p*-phenylene ethynylene) **26** facilitated excitation energy transfer from the polymer to the squaraine chromophore. The insignificant spectral overlap between emission of **26** and squaraine absorption indicated domination of the Dexter-type mechanism of energy migration and therefore the excitation energy transfer was extremely sensitive to the intermolecular distance and orientation. Introduction of cyclohexanone upon exposure of the thin film to the analyte vapor sterically disturbed and changed mutual positions of the conjugated polymer and squaraine thereby resulting in decreasing energy migration to the squarane chromophore, with overall decrease of squaraine fluorescence band and concomitant increase of the fluorescence emission from **26**.

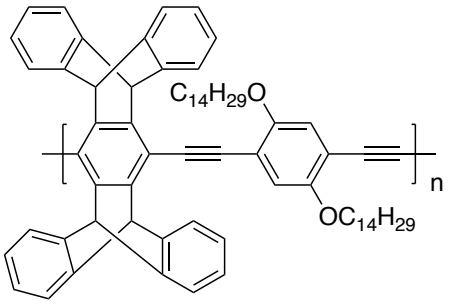

26

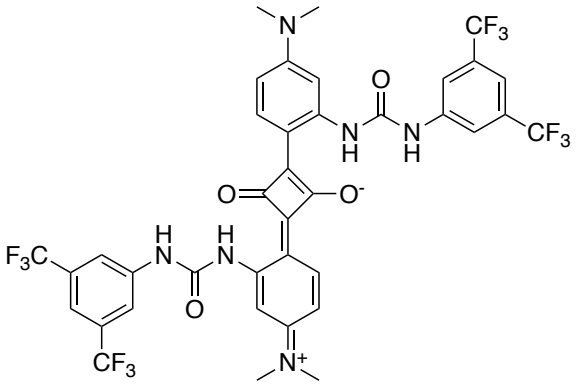

squaraine

A wide variety of analytes ranging from metal ions, small organic nucleophiles to large biomolecules can be categorized into four main fluorescence turn-on mechanisms, such as FRET, aggregation/deaggregation, suppression of ICT, and suppression of PET. FRET requires

sophisticated chromophore design to allow spectral overlap between energy donors and acceptors. Aggregation/deaggregation is highly dependent on the surrounding solvent molecules resulting in ratiometric fluorescence response. On the other hand, suppression of ICT/PET is usually operated through direct removal/neutralization of electron deficient quenchers from the polymer chains leading to fluorescent reminiscence of conjugated polymers without causing emission shift. While there is a continuous ongoing expansion of the research on chemosensor design based on the four conventional strategies, this dissertation will focus on a new concept towards the design of *turn-on* fluorescent sensors.

1.5 Research Focus

This dissertation focuses on the developing and studies of the higher energy gap paradigm as a general principle in designing *turn-on* amplifying fluorescent conjugated polymer sensors, as the previous developments of *turn-on* fluorescent conjugated polymer sensors were impeded due to the need for excessively sophisticated design in terms of energy level matching and the practical difficulty in materials synthesis. To demonstrate the practical utility of the higher energy gap paradigm, chapter 2 describes the development of an efficient *turn-on* amplifying fluorescent sensor for hydrogen sulfide — an important industrial and biomedical analytical target. From a fundamental standpoint, the higher energy gap paradigm demonstrated the importance of the through-bond (Dexter-type) mechanism for intramolecular energy transfer in conjugated polymers — still a widely debated issue.

In chapter 3, to further generalize and study in detail the higher energy gap paradigm, a conjugated polymer based amplifying *turn-on* fluorescence sensor for cysteine detection is described. In particular, it illustrated sensitivity of the higher energy gap mechanism even to very

small (about 0.1 eV) changes in HOMO-LUMO gap at the receptor side, which makes it a concept of choice for designing a broad variety of practically useful chemosensors.

Chapter 4 describes the development of a new concept towards preparation of precision conjugated polymer thin films via stepwise alternating polymerization. A series of immobilized alternating donor-acceptor poly(*p*-arylene ethynylene)s (PAEs) ultrathin films was prepared via *grafted-from* stepwise Sonogashira polymerization. This chapter exemplified stepwise metal-catalyzed polymerization as an efficient and economical approach to precision conjugated polymer films. The properties, structure and morphology of the thin films have been investigated using atomic force microscopy (AFM), grazing incidence X-ray scattering and neutron reflectometry, as well as optical spectroscopy and electrochemical methods.

1.6 References

(1) Epstein, A. J. Transition and Metallic State in Conducting Polymers. In *Handbook of conducting polymers. Conjugated polymers: theory, synthesis, properties, and characterization*, 3rd ed.; Skotheim, T. A., Reynolds, J. R., Eds.; CRC Press: Boca Raton, 2007, 3-5.

(2) Shirakawa, H. The Discovery of Polyacetylene Film: The Dawning of an Era of Conducting Polymers (Nobel Lecture). *Angew. Chem. Int. Ed.* **2001**, *40*, 2574–2580.

(3) MacDiarmid, A. G. "Synthetic Metals": A Novel Role for Organic Polymers (Nobel Lecture). *Angew. Chem. Int. Ed.* **2001**, *40*, 2581–2590.

(4) Heeger, A. J. Semiconducting and Metallic Polymers: The Fourth Generation of Polymeric Materials (Nobel Lecture). *Angew. Chem. Int. Ed.* **2001**, *40*, 2591–2611.

(5) Chiang, C. K.; Druy, M. A.; Gau, S. C.; Heeger, A. J.; Louis, E. J.; MacDiarmid, A. G.; Park, Y. W.; Shirakawa, H. Synthesis of Highly Conducting Films of Derivatives of Polyacetylene, (CH)X. *J. Am. Chem. Soc.* **1978**, *100*, 1013–1015.

(6) Shirakawa, H.; Louis, E. J.; MacDiarmid, A. G.; Chiang, C. K.; Heeger, A. J. Synthesis of Electrically Conducting Organic Polymers: Halogen Derivatives of Polyacetylene, (CH) X. *J. Chem. Soc. Chem. Commun.* **1977**, *16*, 578.

(7) Swager, T. M. *50th Anniversary Perspective*: Conducting/Semiconducting Conjugated Polymers. A Personal Perspective on the Past and the Future. *Macromolecules* **2017**, *50*, 4867–4886.

(8) Perepichka, I. F.; Perepichka, D. F.; Meng, H.; Wudl, F. Light-Emitting Polythiophenes. *Adv. Mater.* **2005**, *17*, 2281–2305.

(9) Sirringhaus, H. 25th Anniversary Article: Organic Field-Effect Transistors: The Path Beyond Amorphous Silicon. *Adv. Mater.* **2014**, *26*, 1319–1335.

(10) Tsutsumi, N. Molecular Design of Photorefractive Polymers. *Polym. J.* **2016**, *48*, 571–588.

(11) Cheng, Y.-J.; Yang, S.-H.; Hsu, C.-S. Synthesis of Conjugated Polymers for Organic Solar Cell Applications. *Chem. Rev.* **2009**, *109*, 5868–5923.

(12) Thomas, S. W.; Joly, G. D.; Swager, T. M. Chemical Sensors Based on Amplifying Fluorescent Conjugated Polymers. *Chem. Rev.* **2007**, *107*, 1339–1386.

(13) Rochat, S.; Swager, T. M. Conjugated Amplifying Polymers for Optical Sensing Applications. *ACS Appl. Mater. Interfaces* **2013**, *5*, 4488–4502.

(14) McQuade, D. T.; Pullen, A. E.; Swager, T. M. Conjugated Polymer-Based Chemical Sensors. *Chem. Rev.* **2000**, *100*, 2537–2574.

(15) Bunz, U. H. F.; Seehafer, K.; Bender, M.; Porz, M. Poly(Aryleneethynylene)s (PAE) as Paradigmatic Sensor Cores. *Chem Soc Rev* **2015**, *44*, 4322–4336.

(16) Swager, T. M. The Molecular Wire Approach to Sensory Signal Amplification. *Acc. Chem. Res.* **1998**, *31*, 201–207.

(17) *Conjugated Polymers: A Practical Guide to Synthesis*; Müllen, K., Reynolds, J. R., Masuda, T., Eds.; RSC polymer chemistry series; RSC Publishing: Cambridge, 2014.

(18) *Photochemistry and Photophysics of Polymer Materials*; Allen, N. S., Ed.; J. Wiley: Hoboken, N.J, 2010.

(19) Schwartz, B. J. CONJUGATED POLYMERS AS MOLECULAR MATERIALS: How Chain Conformation and Film Morphology Influence Energy Transfer and Interchain Interactions. *Annu. Rev. Phys. Chem.* **2003**, *54*, 141–172.

(20) Förster, T. Zwischenmolekulare Energiewanderung und Fluoreszenz. *Ann. Phys.* **1948**, *437*, 55–75.

(21) Dexter, D. L. A Theory of Sensitized Luminescence in Solids. *J. Chem. Phys.* **1953**, *21*, 836–850.

(22) Brédas, J.-L.; Beljonne, D.; Coropceanu, V.; Cornil, J. Charge-Transfer and Energy-Transfer Processes in π-Conjugated Oligomers and Polymers: A Molecular Picture. *Chem. Rev.* **2004**, *104*, 4971–5004.

(23) Scholes, G. D.; Rumbles, G. Excitons in Nanoscale Systems. *Nat. Mater.* **2006**, *5*, 683–696.

(24) Collini, E.; Scholes, G. D. Coherent Intrachain Energy Migration in a Conjugated Polymer at Room Temperature. *Science* **2009**, *323*, 369–373.

(25) Nguyen, T.; Wu, J.; Doan, V.; Schwartz, B. J.; Tolbert, S. H. Control of Energy Transfer in Oriented Conjugated Polymer-Mesoporous Silica Composites. *Science* **2000**, *288*, 652–656.

(26) Levitsky, I. A.; Kim, J.; Swager, T. M. Mass and Energy Transport in Conjugated Polymer Langmuir−Blodgett Films: Conductivity, Fluorescence, and UV−Vis Studies. *Macromolecules* **2001**, *34*, 2315–2319.

(27) Levitsky, I. A.; Kim, J.; Swager, T. M. Energy Migration in a Poly(Phenylene Ethynylene): Determination of Interpolymer Transport in Anisotropic Langmuir−Blodgett Films. *J. Am. Chem. Soc.* **1999**, *121*, 1466–1472.

(28) Kim, J.; Swager, T. M. Control of Conformational and Interpolymer Effects in Conjugated Polymers. *Nature* **2001**, *411*, 1030–1034.

(29) Nesterov, E. E.; Zhu, Z.; Swager, T. M. Conjugation Enhancement of Intramolecular Exciton Migration in Poly(*p* -Phenylene Ethynylene)S. *J. Am. Chem. Soc.* **2005**, *127*, 10083–10088.

(30) Thiessen, A.; Vogelsang, J.; Adachi, T.; Steiner, F.; Vanden Bout, D.; Lupton, J. M. Unraveling the Chromophoric Disorder of Poly(3-Hexylthiophene). *Proc. Natl. Acad. Sci.* **2013**, *110*, E3550–E3556.

(31) Schwartz, B. J.; Hide, F.; Andersson, M. R.; Heeger, A. J. Ultrafast Studies of Stimulated Emission and Gain in Solid Films of Conjugated Polymers. *Chem. Phys. Lett.* **1997**, *265*, 327–333.

(32) Haugeneder, A.; Neges, M.; Kallinger, C.; Spirkl, W.; Lemmer, U.; Feldmann, J.; Scherf, U.; Harth, E.; Gügel, A.; Müllen, K. Exciton Diffusion and Dissociation in Conjugated Polymer/Fullerene Blends and Heterostructures. *Phys. Rev. B* **1999**, *59*, 15346–15351.

(33) Theander, M.; Yartsev, A.; Zigmantas, D.; Sundström, V.; Mammo, W.; Andersson, M. R.; Inganäs, O. Photoluminescence Quenching at a Polythiophene / C60 Heterojunction. *Phys. Rev. B* **2000**, *61*, 12957–12963.

(34) Swager, T. M.; Gil, C. J.; Wrighton, M. S. Fluorescence Studies of Poly(p-Phenyleneethynylene)s: The Effect of Anthracene Substitution. *J. Phys. Chem.* **1995**, *99*, 4886–4893.

(35) Zhou, Q.; Swager, T. M. Fluorescent Chemosensors Based on Energy Migration in Conjugated Polymers: The Molecular Wire Approach to Increased Sensitivity. *J. Am. Chem. Soc.* **1995**, *117*, 12593–12602.

(36) Zhou, Q.; Swager, T. M. Method for Enhancing the Sensitivity of Fluorescent Chemosensors: Energy Migration in Conjugated Polymers. *J. Am. Chem. Soc.* **1995**, *117*, 7017–7018.

(37) Chen, L.; McBranch, D. W.; Wang, H.-L.; Helgeson, R.; Wudl, F.; Whitten, D. G. Highly Sensitive Biological and Chemical Sensors Based on Reversible Fluorescence Quenching in a Conjugated Polymer. *Proc. Natl. Acad. Sci.* **1999**, *96*, 12287–12292.

(38) Kim, T.-H.; Swager, T. M. A Fluorescent Self-Amplifying Wavelength-Responsive Sensory Polymer for Fluoride Ions. *Angew. Chem. Int. Ed.* **2003**, *42*, 4803–4806.

(39) Pangeni, D.; Nesterov, E. E. "Higher Energy Gap" Control in Fluorescent Conjugated Polymers: Turn-On Amplified Detection of Organophosphorous Agents. *Macromolecules* **2013**, *46*, 7266–7273.

(40) Fan, L.-J.; Zhang, Y.; Jones, W. E. Design and Synthesis of Fluorescence "Turn-on" Chemosensors Based on Photoinduced Electron Transfer in Conjugated Polymers. *Macromolecules* **2005**, *38*, 2844–2849.

(41) Fan, L.-J.; Jones, W. E. A Highly Selective and Sensitive Inorganic/Organic Hybrid Polymer Fluorescence "Turn-on" Chemosensory System for Iron Cations. *J. Am. Chem. Soc.* **2006**, *128*, 6784–6785.

(42) Xu, Y.; Meng, J.; Meng, L.; Dong, Y.; Cheng, Y.; Zhu, C. A Highly Selective Fluorescence-Based Polymer Sensor Incorporating an (R,R)-Salen Moiety for Zn2+ Detection. *Chem. - Eur. J.* **2010**, *16*, 12898–12903.

(43) Zhu, M.; Zhou, C.; Zhao, Y.; Li, Y.; Liu, H.; Li, Y. Synthesis of a Fluorescent Polymer Bearing Covalently Linked Thienylene Moieties and Rhodamine for Efficient Sensing. *Macromol. Rapid Commun.* **2009**, *30*, 1339–1344.

(44) Qu, Y.; Zhang, X.; Wu, Y.; Li, F.; Hua, J. Fluorescent Conjugated Polymers Based on Thiocarbonyl Quinacridone for Sensing Mercury Ion and Bioimaging. *Polym Chem* **2014**, *5*, 3396–3403.

(45) He, F.; Tang, Y.; Wang, S.; Li, Y.; Zhu, D. Fluorescent Amplifying Recognition for DNA G-Quadruplex Folding with a Cationic Conjugated Polymer: A Platform for Homogeneous Potassium Detection. *J. Am. Chem. Soc.* **2005**, *127*, 12343–12346.

(46) Ramachandran, G.; Simon, G.; Cheng, Y.; Smith, T. A.; Dai, L. The Dependence of Benzo-15-Crown-5 Ether-Containing Oligo Paraphenylene Vinylene (CE-OPV) Emission Upon Complexation with Metal Ions in Solution. *J. Fluoresc.* **2003**, *13*, 427–436.

(47) Kim, J.; McQuade, D. T.; McHugh, S. K.; Swager, T. M. Ion-Specific Aggregation in Conjugated Polymers: Highly Sensitive and Selective Fluorescent Ion Chemosensors. *Angew. Chem.* **2000**, *39*, 3868–3872.

(48) Li, J.; Wu, Y.; Song, F.; Wei, G.; Cheng, Y.; Zhu, C. A Highly Selective and Sensitive Polymer-Based OFF-ON Fluorescent Sensor for Hg $^{2+}$ Detection Incorporating Salen and Perylenyl Moieties. *J Mater Chem* **2012**, *22*, 478–482.

(49) Smith, R. C.; Tennyson, A. G.; Lim, M. H.; Lippard, S. J. Conjugated Polymer-Based Fluorescence Turn-On Sensor for Nitric Oxide. *Org. Lett.* **2005**, *7*, 3573–3575.

(50) Li, Z.; Lou, X.; Yu, H.; Li, Z.; Qin, J. An Imidazole-Functionalized Polyfluorene Derivative as Sensitive Fluorescent Probe for Metal Ions and Cyanide. *Macromolecules* **2008**, *41*, 7433–7439.

(51) Meng, J.; Wei, G.; Huang, X.; Dong, Y.; Cheng, Y.; Zhu, C. A Fluorescence Sensor Based on Chiral Polymer for Highly Enantioselective Recognition of Phenylalaninol. *Polymer* **2011**, *52*, 363–367.

(52) Song, F.; Wei, G.; Wang, L.; Jiao, J.; Cheng, Y.; Zhu, C. Salen-Based Chiral Fluorescence Polymer Sensor for Enantioselective Recognition of α-Hydroxyl Carboxylic Acids. *J. Org. Chem.* **2012**, *77*, 4759–4764.

(53) Zhang, X.; Wang, C.; Wang, P.; Du, J.; Zhang, G.; Pu, L. Conjugated Polymer-Enhanced Enantioselectivity in Fluorescent Sensing. *Chem Sci* **2016**, *7*, 3614–3620.

(54) Tong, H.; Wang, L.; Jing, X.; Wang, F. "Turn-On" Conjugated Polymer Fluorescent Chemosensor for Fluoride Ion. *Macromolecules* **2003**, *36*, 2584–2586.

(55) Thomas, S. W.; Swager, T. M. Trace Hydrazine Detection with Fluorescent Conjugated Polymers: A Turn-On Sensory Mechanism. *Adv. Mater.* **2006**, *18*, 1047–1050.

(56) Qu, Y.; Hua, J.; Jiang, Y.; Tian, H. Novel Side-Chain Naphthalimide Polyphenylacetylene as a Ratiometric Fluorescent Chemosensor for Fluoride Ion. *J. Polym. Sci. Part Polym. Chem.* **2009**, *47*, 1544–1552.

(57) Boiocchi, M.; Del Boca, L.; Gómez, D. E.; Fabbrizzi, L.; Licchelli, M.; Monzani, E. Nature of Urea−Fluoride Interaction: Incipient and Definitive Proton Transfer. *J. Am. Chem. Soc.* **2004**, *126*, 16507–16514.

(58) Sakai, R.; Nagai, A.; Tago, Y.; Sato, S.; Nishimura, Y.; Arai, T.; Satoh, T.; Kakuchi, T. Fluorescence Turn-On Sensing of Anions Based on Disassembly Process of Urea-Functionalized Poly(Phenylenebutadiynylene) Aggregates. *Macromolecules* **2012**, *45*, 4122–4127.

(59) Zhao, X.; Schanze, K. S. Fluorescent Ratiometric Sensing of Pyrophosphate via Induced Aggregation of a Conjugated Polyelectrolyte. *Chem. Commun.* **2010**, *46*, 6075.

(60) Bao, Y.; Wang, H.; Li, Q.; Liu, B.; Li, Q.; Bai, W.; Jin, B.; Bai, R. 2,2′-Biimidazole-Based Conjugated Polymers as a Novel Fluorescent Sensing Platform for Pyrophosphate Anion. *Macromolecules* **2012**, *45*, 3394–3401.

(61) Bao, Y.; Li, Q.; Liu, B.; Du, F.; Tian, J.; Wang, H.; Wang, Y.; Bai, R. Conjugated Polymers Containing a 2,2′-Biimidazole Moiety—a Novel Fluorescent Sensing Platform. *Chem Commun* **2012**, *48*, 118–120.

(62) Bao, B.; Yuwen, L.; Zheng, X.; Weng, L.; Zhu, X.; Zhan, X.; Wang, L. A Fluorescent Conjugated Polymer for Trace Detection of Diamines and Biogenic Polyamines. *J. Mater. Chem.* **2010**, *20*, 9628.

(63) Dane, E. L.; King, S. B.; Swager, T. M. Conjugated Polymers That Respond to Oxidation with Increased Emission. *J. Am. Chem. Soc.* **2010**, *132*, 7758–7768.

(64) Zhang, J.; Sarrafpour, S.; Pawle, R. H.; Thomas III, S. W. Acene-Linked Conjugated Polymers with Ratiometric Fluorescent Response to 1O2. *Chem. Commun.* **2011**, *47*, 3445.

(65) Altınok, E.; Smith, Z. C.; Thomas, S. W. Two-Dimensional, Acene-Containing Conjugated Polymers That Show Ratiometric Fluorescent Response to Singlet Oxygen. *Macromolecules* **2015**, *48*, 6825–6831.

(66) Rochat, S.; Swager, T. M. Water-Soluble Cationic Conjugated Polymers: Response to Electron-Rich Bioanalytes. *J. Am. Chem. Soc.* **2013**, *135*, 17703–17706.

(67) Kim, Y.; Whitten, J. E.; Swager, T. M. High Ionization Potential Conjugated Polymers. *J. Am. Chem. Soc.* **2005**, *127*, 12122–12130.

(68) Kim, Y.; Swager, T. M. Sensory Polymers for Electron-Rich Analytes of Biological Interest. *Macromolecules* **2006**, *39*, 5177–5179.

(69) Cox, J. R.; Müller, P.; Swager, T. M. Interrupted Energy Transfer: Highly Selective Detection of Cyclic Ketones in the Vapor Phase. *J. Am. Chem. Soc.* **2011**, *133*, 12910–12913.

CHAPTER 2. HIGHER ENERGY GAP CONTROL OF FLUORESCENCE IN CONJUGATED POLYMERS: *TURN-ON* AMPLIFYING CHEMOSENSORS FOR HYDROGEN SULFIDE*

2.1 Introduction

Signal amplification through photoexcitation energy (exciton) migration is a characteristic feature of conjugated polymer (CP) fluorescent sensory materials.[1–3] Amplifying CP-based fluorescent chemo- and biosensors are attractive for sensing a broad variety of analytes including environmental hazards, explosives, and chemical warfare agents and biological species.[4–9] Compared to small-molecule based sensors, they provide higher sensitivity, broader analyte detection range, and tenability of spectroscopic response characteristic. The large majority of the conventional amplifying CP-based fluorescent sensors utilize the effect of CP fluorescence quenching by electrodeficient anayltes via photoinduced electron transfer mechanism and therefore display a *turn-off* response.[10–15] On the other hand, sensors displaying *turn-on* fluorescent response (i.e., increasing their fluorescent emission upon interacting with an analyte) are more desirable from a practical standpoint but are much more difficult to design. A typical scheme that allows achieving an amplified *turn-on* response utilizes reversal of the CP fluorescence quenching phenomenon. In such a scheme, the CP fluorescence is initially diminished through the reversible coordination of a quenching moiety to the polymer conjugated backbone. A selective interaction of a target analyte with the quenching moiety shifts the equilibrium toward the anaylte-quencher complex, therefore restoring the CP fluorescence.[16–18]

---

* "Reproduced in part with permission from Chiang, C.-H.; Pangeni, D.; Nesterov, E. E. *Macromolecules* **2017**, *50*, 6961-6966, DOI: 10.1021/acs.macromol.7b01706, Copyright 2017 American Chemical Society."

A related scheme utilizing fluorescent resonance energy transfer (FRET) effect for *turn-on* sensing of various non-quenching analytes (such as DNA and other biomolecules) has been also developed.[19–21] Although useful and efficient, these approaches possess intrinsic limitation such as relative complexity of the sensing scheme, the need to employ chromophores with spectral characteristics matching the FRET requirements, and the necessity to functionalized one of the components of the sensor (or the CP itself) with a FRET acceptor fluorophore. An alternative (but less commonly used) approach to achieve amplified *turn-on* response is to incorporate an analyte-specific unit/chromophore as part of the polymer π-conjugated backbone.[22] In dilute solution of CP sensors, the intramolecular excitation energy (exciton) transfer process occurs by the combination of through-space dipole-induced dipole (Förster-type) mechanism and through-bond electron exchange (Dexter-type) mechanism.[23–25] Although the relative contribution of through-bond mechanism is often debated to be inessential compared to the contribution of the through-space mechanism,[26,27] its major role has been demonstrated in some specific cases.[28,29] Indeed, when the sensing unit is electronically coupled to the polymer π-electron system, the fluorescent behavior is controlled by the through-bond energy transfer (which does not depend on the spectral overlap which determines the efficiency of the FRET-based sensors) and therefore could provide a powerful general mechanism to achieve an amplified fluorescent response. On the basis of this consideration, we recently proposed a "higher energy gap" paradigm, where a *turn-on* amplification can be achieved via restricting exciton migration in the π-conjugated polymer backbone through generating a higher energy gap site upon reaction with an analyte.[30] In this scheme, the receptor site is part of the CP π-conjugated system (Figure 2.1). Reaction with a target analyte results in a local increase in the energy (HOMO-LUMO) gap at that site, which creates a local "roadblock" that randomly migrating excitons in the polymer backbone cannot pass through

via the through-bond mechanism. Although the intramolecularly migrating excitons can still pass through the "roadblock" sites via the through-space (Förster-type) mechanism, the major reduction in the efficiency of the through-bond contribution is expected to substantially shorten the exciton diffusion length. Such a restriction of the exciton diffusion length should reduce the probability of exciton nonradiative quenching due to decreasing its chance to encounter with intrinsically present quenching sites in the CP chain, such as conformational or structural defects, as well as transient defects such as triplet states, photogenerated free charge carriers, or charge-separated states, etc.[31,32] Therefore, by the design, this is expected to result in an increasing intensity of the CP fluorescent emission, i.e., a pronounced turn-on effect. Importantly, the fluorescent intensity enhancement in this case originates in the CP π-electron system and therefore does not depend on whether the reaction with analyte produces a fluorescent or nonfluorescent chromophore—a major and universal advantage of the current approach over all the other previously developed schemes. Since the fluorescence enhancement via the "higher energy gap" mechanism directly related to the exciton migration in CP, it should produce a similar kind of signal amplification as with utilizing quenching-based *turn-off* fluorescent sensing schemes. In the present work, we demonstrate how the general "higher energy gap" principle can be employed to rationally design an efficient amplifying turn-on fluorescent sensor for H_2S detection.

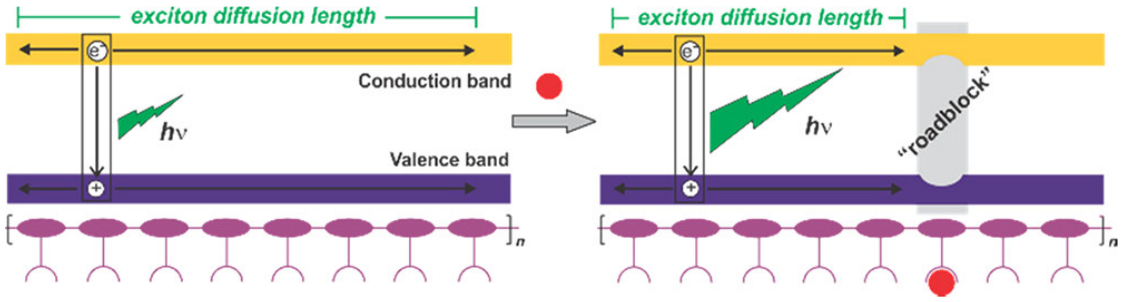

Figure 2.1. Schematic diagram of the "higher energy gap" control of CP fluorescence: reaction with an analyte (red circle) creates a local higher energy gap site in the CP backbone which shortens the exciton diffusion length in the polymer, therefore causing an increase in the intensity of fluorescent emission.

Hydrogen sulfide (H_2S) is an attractive target for the development of different types of sensors owing its significance in industrial toxicology, human physiology, pathology, and biomedicine.[33–36] In particular, its presence at low (from nanomolar to micromolar) concentration in biological media has made it a popular target for the development of fluorescent chemosensors.[37–43] However, none of the described H_2S-responsive chemosensors were amplifying, whereas, due to the low concentration in physiological media, its detection would benefit from signal amplification provided by using the CP platform. Therefore, to demonstrate the power of the "higher energy gap" paradigm, we decided to apply it toward designing an amplifying fluorescent *turn-on* sensor for H_2S. We also demonstrated the role of various structural factors in the design of the "higher energy gap" sensors and how the sensing performance of such systems can be rationally optimized.

2.2 Molecular Design and Synthesis Routes

In order to design an amplifying *turn-on* sensor based on the "higher energy gap" principle, one needs to choose a relatively low energy fluorescent polymer and functionalize it with an analyte-specific unit in such a way that the reaction with the analyte would generate a local increase in the CP backbone energy gap. Typically, for each analyte of interest there are a few reactions that satisfy this requirement. For H_2S detection, we decided to use nucleophilic addition of hydrosulfide anion HS^- (form of H_2S in the physiological conditions) to an electron-deficient double bond as such a reaction.[44,45] Therefore, we proposed a CP sensor **2-P1** which includes an H_2S receptor unit that is a fusion between cyanine and naphthalene moieties (Scheme 1a). The naphthalene fragment of the receptor is part of the polymer's poly(arylene vinlyene) π-conjugated backbone. The specific selection of poly(arylene vinlyene) conjugated polymer was dictated by the requirement to have a fluorescent CP with a relatively low energy gap as a main prerequisite

for the "higher energy gap" design. Reaction of hydrosulfide anion with the cyanine moiety in **2-P1** results in an effective electronic "isolation" of this π-delocalized unit from the naphthalene moiety, therefore resulting in a substantial increase in the HOMO-LUMO gap at this local site, but without disrupting the overall π-conjugation in the polymer. Preliminary DFT computations (at the B3LYP/6-31G* level of theory) confirmed that the HOMO-LUMO gap of the receptor chromophore would increase from 2.84 to 4.12 eV after the reaction with HS^- due to the effective electronic isolation of the cyanine unit from the CP π-conjugated system (Figure 2.2). Therefore, this shall create a local higher energy gap site – an effective "roadblock" for excitons randomly migrating in the polymer π-conjugated backbone. Restricting the intramolecular exciton migration would result in an amplified *turn-on* fluorescent response.

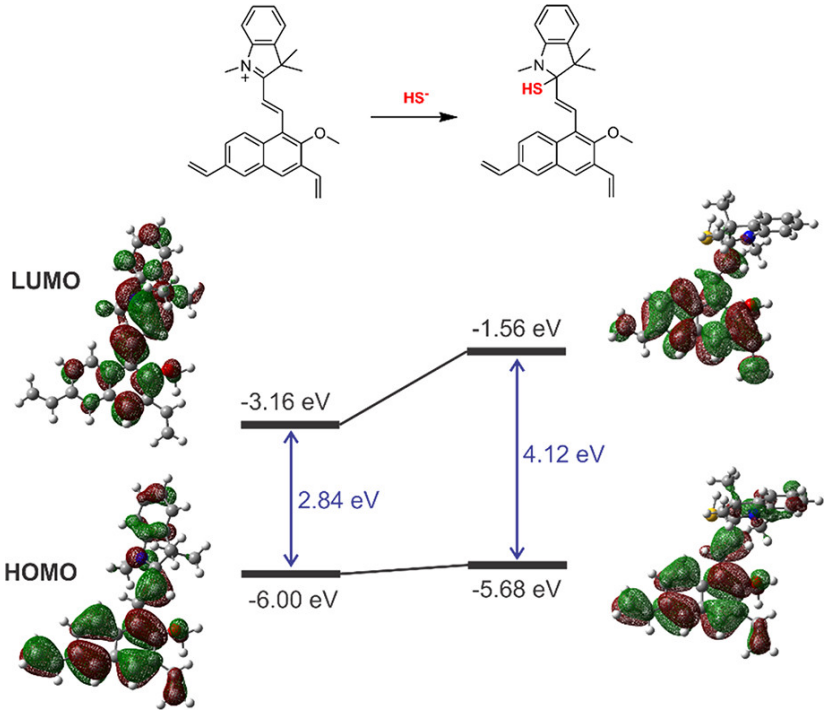

Figure 2.2. DFT computational studies (B3LYP/6-31G*) of the HOMO-LUMO gap change in the cyanine receptor upon reaction with H_2S. The molecule was truncated for better computational efficiency. Computed HOMO and LUMO surfaces of the initial receptor indicate complete electronic delocalization over the entire molecule. Reaction with HS^- effectively electronically isolates the former cyanine unit resulting in the increasing energy gap of the π-conjugated moiety from 2.84 to 4.12 eV.

The polymer **2-P1** was functionalized with tri(ethylene glycol) (TEG) substituents in order to increase the polymer's solubility in aqueous media (as H_2S detection is normally carried out in aqueous system). It was prepared using Suzuki coupling polymerization of the two properly functionalized monomers followed by postpolymerization installation of the cyanine moiety via Knoevenagel condensation and subsequent purification via reprecipitation and dialysis. Determination of the extent of fluorescent amplification in the polymer sensor **2-P1** required comparison with a corresponding small-molecules sensor analogue **2-M1** (Scheme 1b) which was also prepared using Suzuki coupling. Since the "higher energy gap" mechanism is based on blocking the intramolecular exciton migration in the CP π-conjugated backbone, it was expected to be significantly affect by the polymer conjugation length. In order to test this, through varying the polymerization conditions, we prepared two polymer **2-P1a** and **2-P1b** with different molecular weights–polymer **2-P1a** with a number-average molecular weight M_n 27.7 kDa and a shorter polymer **2-P1b** with M_n 15.5 kDa. We anticipated a much stronger response with the polymer sensor **2-P1a** due to its higher conjugation length.

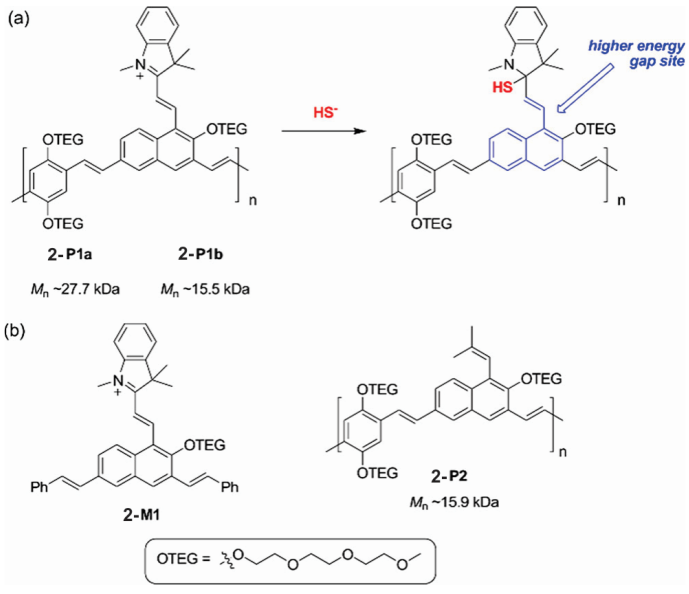

Scheme 2.1. (a) Mechanism of H_2S sensing through the formation of the higher energy gap site in the backbone of CP **2-P1**; (b) structure of the small-molecule sensor **2-M1** and control CP **2-P2**.

To further confirm the action of the "higher energy gap" mechanism in polymer **2-P1**, we prepared a reference conjugated polymer **2-P2** (*M*n 15.9 kDa) without the cyanine H_2S sensing moiety to test that the poly(arylene vinlyene) conjugated backbone itself would not produce spectroscopic response on H_2S addition (Scheme 2.1b).

2.3 Photophysical Properties and Fluorescent Amplification

The UV/vis absorption spectrum of the small-molecule sensor **2-M1** displayed an intense band at 324 nm and a smaller band at 447 nm, the latter possible due to the presence of the cyanine moiety (Figure 2.2, left). In contrast, the polymer **2-P1a** displayed the main absorption band at 416 nm (bathochromic shift of 92 nm compared to the main band of **2-M1**) which reflected substantial electronic delocalization in the polymer. No separate longer wavelength cyanine chromophore band was noticeable, although it could be overshadowed by the intense main CP band. Polymer **2-P1b** (with a lower degree of polymerization) expectedly displayed a less bathochromically shifted absorption band, which reflected its apparently lower conjugation length (Figure 2.2, left). A noticeable shoulder at approximately 450 nm was indicative of the presence of the cyanine moiety chromophore. Similar to absorption spectra, fluorescence spectra also indicated a significant electronic delocalization in the cased of CP sensor **2-P1a** and **2-P1b**, which displayed broad band with a maximum at approximately 510 nm and a shoulder at 680 nm, possible due to the energy transfer to the lower energy cyanine chromophore (Figure 2.2, right). The overall fluorescent intensity of the polymers **2-P1a** and **2-P1b** was quite low, possible due to strong exciton quenching with the electron–deficient cyanine moieties.

We first tested the response of the small-molecule sensor **2-M1**. Addition of 200 nM aqueous HS^- to a dilute 13.3 μM solution of **2-M1** in acetonitrile produced no detectable change in absorption spectrum and an approximately 2.5-fold enhancement in the integrated fluorescent

intensity F/F_0 (expressed as a ration of integrated intensities with and without added analyte). Further increasing of the added HS^- concentration up to 10 μM produced no change in the absorption spectra and resulted in the unexpected decrease of the fluorescent intensity (Figure 2.5). Overall, the small-molecule sensor **2-M1** demonstrated a rather insignificant *turn-on* fluorescent response and a narrow analyte detection range, therefore indicating its poor ability to act as an H_2S fluorescent sensor.

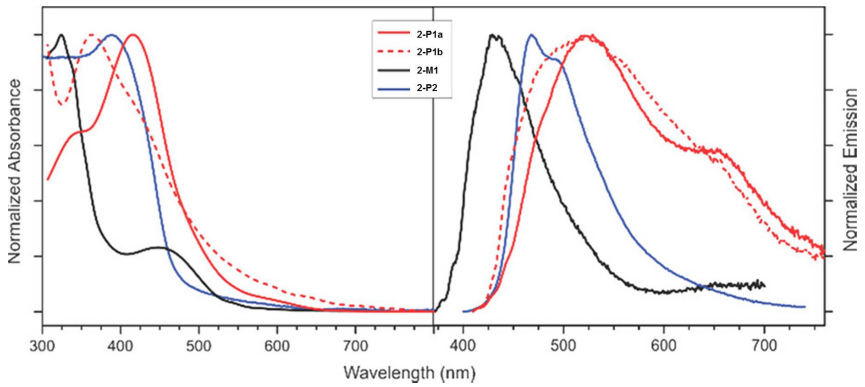

Figure 2.3. Normalized UV/vis absorption (left) and normalized fluorescence (right) spectra of CP sensor **2-P1a** and **2-P1b** and related compounds in acetonitrile solutions. Concentrations: 10.8 μM (**2-P1a** and **2-P1b**), 13.3 μM (**2-M1**), and 10.0 μM (**2-P2**). Extinction coefficient ($M^{-1}cm^{-1}$): 32600 (**2-P1a**), 14800 (**2-P1b**), 46400 (**2-M1**), and 5500 (**2-P2**).

We then proceeded with studying the CP sensor **2-P1a** designed using the "higher energy gap" principle. Adding increasing concentrations (from 200 nM to 0.1 mM) of aqueous HS^- to a dilute 10.8 μM solution of **2-P1a** in acetonitrile produced a substantial gradual increase of the fluorescent emission, up to 74-fold as an integrated intensity ration F/F_0 (Figure 2.4). The lack of a significant change in the absorption spectra as well as no substantial wavelength shift accompanying the fluorescence enhancement indicated only minor electronic perturbations in the extended π-electron conjugated system of **2-P1a** upon reaction with HS^-, in agreement with our design based on the higher energy gap mechanism. Indeed, creating exciton "roadblocks" in the CP **2-P1a** backbone via reaction of the cyanine receptor with HS^- diminished exciton

intramolecular migration length and resulted in increasing fluorescent emission from the polymer. Overall, the polymer **2-P1a** sensor demonstrated a significant turn-on response, with approximately 10 times higher detection sensitivity and a broad analyte detection range, all in a dramatic contrast with the poor sensing performance of the small-molecules analogue **2-M1** (Figure 2.5). Also in a good agreement with the "higher energy gap" mechanism, CP sensor **2-P1b**, with a smaller degree of polymerization, displayed a much diminished *turn-on* sensing performance, with only a 30-fold maximal increase in F/F_0 and approximately 20 times lower sensitivity than the polymer **2-P1a** (Figure 2.5). Indeed, the overall short conjugation length in **2-P1b** was responsible for a more limited intramolecular exciton migration and thus a smaller fluorescent enhancement upon creating higher energy gap "roadblocks" in the CP backbone. That the "roadblocks" responsible for the turn-on fluorescence enhancement were created via the reaction of HS^- with the cyanine moiety was clearly illustrated by the control polymer **2-P2** which showed absolutely no response on HS^- addition (Figure 2.5).

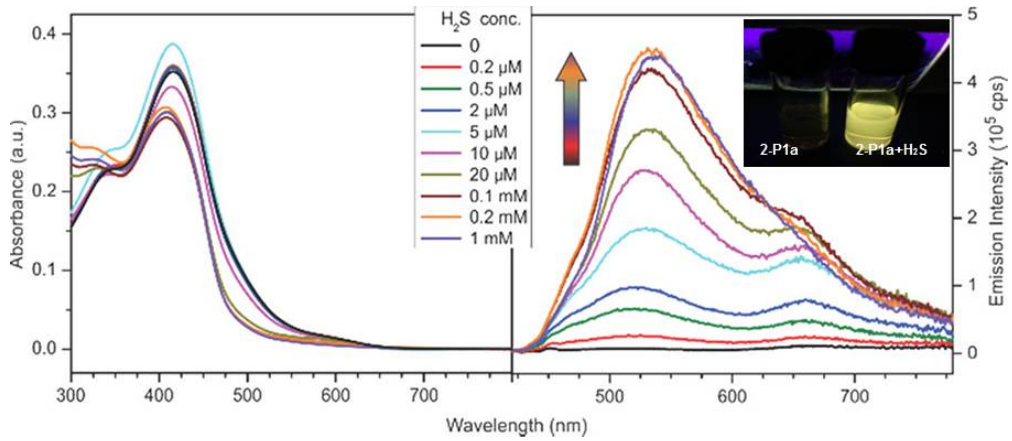

Figure 2.4. Change in absorption (left) and fluorescence (right) spectra of a 10.8 μM solution of **2-P1a** in acetonitrile upon addition of increasing concentration of H_2S (the spectra were acquired in 6 min after H_2S addition). The inset shows a photograph of the solution before and after addition of 100 μM HS^- upon irradiation with a hand-held UV lamps.

When evaluating the role of the "higher energy gap" mechanism in controlling the *turn-on* fluorescent response in the present case, it is important also to discuss possible contribution of an

alternative mechanism based on fluorescence quenching by electron-deficient cyanine moiety in the CP sensors **2-P1a** and **2-P1b**. In principle, the cyanine unites can potentially play the role of quencher of the polymer fluorescence, and the subsequent reaction with HS^- can essentially convert these electron-deficient quenchers to nonquenchers. A similar mechanism for the fluorescence control of a small-molecules organic fluorophores has been previously demonstrated.[46–48] It is possible that such a quenching might be responsible for the initially low fluorescent intensity of the polymer **2-P1a,b**, and reduction of this quenching via reaction with HS^- could be part of the mechanism for the observed fluorescence enhancement. However, the dominant role of this alternative mechanism in our case is hardly possible. Indeed, considering the high density of the "quenching" cyanine sites in the CPs (one cyanine group per repeating unit), and taking into account the "superquenching" mechanism based on intramolecular exciton migration to the quenching sites,[1,4,16] reaction even of a large fraction of cyanine units with HS^- would still leave enough quenching sites on the CP chain to keep overall fluorescence low.

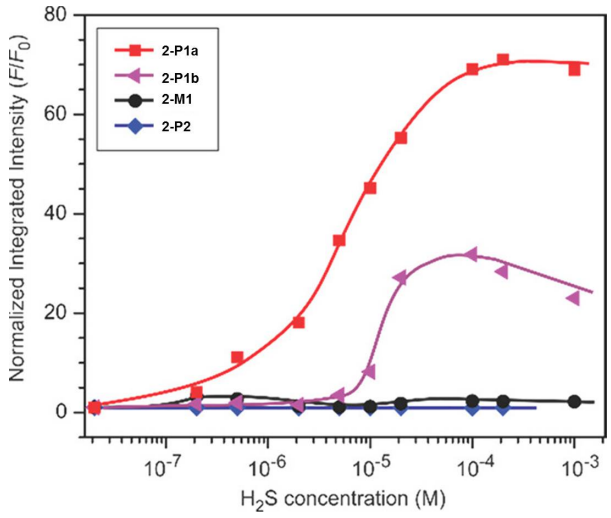

Figure 2.5. Change in integrated fluorescence intensity of acetonitrile solution of polymer **2-P1a**, **2-P1b**, and **2-P2**, and monomer compound **2-M1** upon addition of increasing concentration H_2S. The intensity is expressed as a ration of integrated area of a fluorescence band at each H_2S concentration divided by the area of the fluorescent band in the absence of analyte (F/F_0). THe plot uses logarithmic scale for the H_2S concentration axis to illustrate the broad range (from nanomolar to millimolar) of detectable anaylte concentrations in the case of polymer sensor **2-P1a**.

Only when most cyanine sites have reacted with HS^- (i.e., at the very high H_2S concentrations) could one expect the fluorescence turn-on response, if this mechanism played any significant role. Thus, if the alternative mechanism dominated, the turn-on response at the very low H_2S concentration would not be observed. This directly contradicts our experimental observation of the broad detection range starting with nanomolar H2S concentrations and demonstrates the dominant role of the "higher energy gap" mechanism. Quantitative estimation of the relative contribution of the two mechanism is difficult and is beyond the scope of this work.

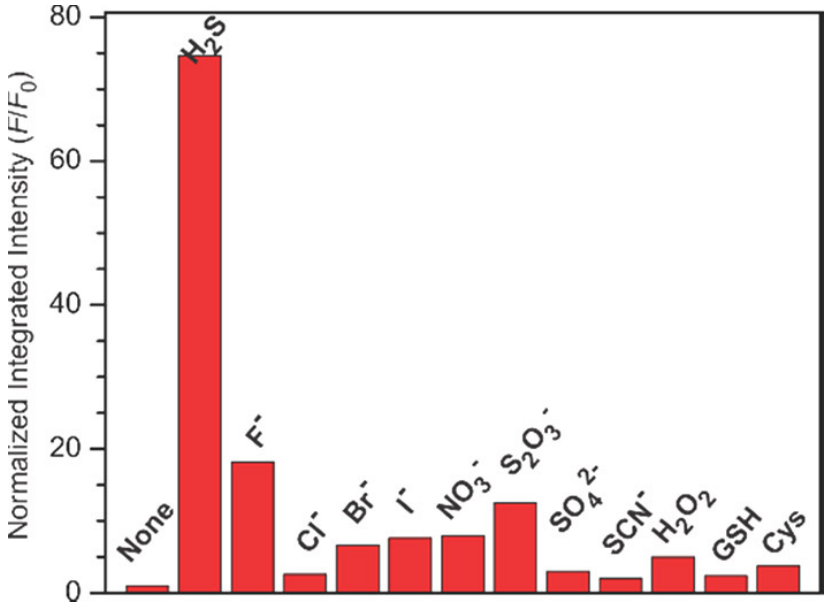

Figure 2.6. Normalized integrated fluorescence intensity (as a ratio of integrated areas of fluorescent bands after and before addition of the analyte) of a 10.8 μM solution of polymer **2-P1a** in acetonitrile upon addition of various analytes.

For the practical applications of the sensor polymer **2-P1a**, it should display not only high sensitivity but also high selectivity toward the target analyte. Figure 2.6 shows fluorescent response of **2-P1a** to various potentially competing nucleophiles, including a model for reactive oxygen species (H_2O_2) and ubiquitous biological thiols (glutathione (GSH) and cysteine (Cys)). Although F^- and $S_2O_3^-$ anions did cause a small increase of fluorescence, only H_2S stimulated a significant fluorescent response. Therefore, excellent selectivity of **2-P1a** coupled with its high

response sensitivity and broad analyte concentration detection range could make it an excellent H_2S detector.

2.4 Conclusions

We have developed a novel general principle for desiging efficient amplifying turn-on fluorescent sensors based on the "higher energy gap" paradigm. The "higher energy gap" mechanism is based on the restricting intramolecular exciton migration in CPs by creating high-energy sites in the conjugated polymer backbone upon reaction with analyte. Fundamentally, the success of this paradigm illustrates the importance of the through-bond (Dexter-type) mechanism for intramolecular energy transfer in conjugated polymers–a point of controversial debates in the literature. From the broader materials design standpoint, this means that in order to achieve the best efficiency of the "higher energy gap" mechanism, one needs to use CPs with smaller energy gap, potentially even smaller than that provided by the poly(arylene vinylene) backbone used in the present work. From a general practical standpoint, the new concept described herein will enable simple design of a wide range of highly efficient amplifying turn-on fluorescent sensors and indicators, based on conventional analyte-selective reactions.

2.5 References

(1) Swager, T. M. The Molecular Wire Approach to Sensory Signal Amplification. *Acc. Chem. Res.* **1998**, *31*, 201–207.

(2) Liu, Y.; Ogawa, K.; Schanze, K. S. Conjugated Polyelectrolytes as Fluorescent Sensors. *J. Photochem. Photobiol. C Photochem. Rev.* **2009**, *10*, 173–190.

(3) Feng, X.; Liu, L.; Wang, S.; Zhu, D. Water-Soluble Fluorescent Conjugated Polymers and Their Interactions with Biomacromolecules for Sensitive Biosensors. *Chem. Soc. Rev.* **2010**, *39*, 2411.

(4) McQuade, D. T.; Pullen, A. E.; Swager, T. M. Conjugated Polymer-Based Chemical Sensors. *Chem. Rev.* **2000**, *100*, 2537–2574.

(5) Thomas, S. W.; Joly, G. D.; Swager, T. M. Chemical Sensors Based on Amplifying Fluorescent Conjugated Polymers. *Chem. Rev.* **2007**, *107*, 1339–1386.

(6) Rochat, S.; Swager, T. M. Conjugated Amplifying Polymers for Optical Sensing Applications. *ACS Appl. Mater. Interfaces* **2013**, *5*, 4488–4502.

(7) Sun, X.; Wang, Y.; Lei, Y. Fluorescence Based Explosive Detection: From Mechanisms to Sensory Materials. *Chem Soc Rev* **2015**, *44*, 8019–8061.

(8) Jiang, H.; Taranekar, P.; Reynolds, J. R.; Schanze, K. S. Conjugated Polyelectrolytes: Synthesis, Photophysics, and Applications. *Angew. Chem. Int. Ed.* **2009**, *48*, 4300–4316.

(9) Kim, H. N.; Guo, Z.; Zhu, W.; Yoon, J.; Tian, H. Recent Progress on Polymer-Based Fluorescent and Colorimetric Chemosensors. *Chem Soc Rev* **2011**, *40*, 79–93.

(10) Yang, J.-S.; Swager, T. M. Fluorescent Porous Polymer Films as TNT Chemosensors: Electronic and Structural Effects. *J. Am. Chem. Soc.* **1998**, *120*, 11864–11873.

(11) Rose, A.; Zhu, Z.; Madigan, C. F.; Swager, T. M.; Bulović, V. Sensitivity Gains in Chemosensing by Lasing Action in Organic Polymers. *Nature* **2005**, *434*, 876–879.

(12) Li, J.; Kendig, C. E.; Nesterov, E. E. Chemosensory Performance of Molecularly Imprinted Fluorescent Conjugated Polymer Materials. *J. Am. Chem. Soc.* **2007**, *129*, 15911–15918.

(13) Fan, C.; Wang, S.; Hong, J. W.; Bazan, G. C.; Plaxco, K. W.; Heeger, A. J. Beyond Superquenching: Hyper-Efficient Energy Transfer from Conjugated Polymers to Gold Nanoparticles. *Proc. Natl. Acad. Sci.* **2003**, *100*, 6297–6301.

(14) Kim, I.-B.; Erdogan, B.; Wilson, J. N.; Bunz, U. H. F. Sugar-Poly(Para-Phenylene Ethynylene) Conjugates as Sensory Materials: Efficient Quenching by Hg2+ and Pb2+ Ions. *Chem. - Eur. J.* **2004**, *10*, 6247–6254.

(15) Xie, D.; Parthasarathy, A.; Schanze, K. S. Aggregation-Induced Amplified Quenching in Conjugated Polyelectrolytes with Interrupted Conjugation. *Langmuir* **2011**, *27*, 11732–11736.

(16) Chen, L.; McBranch, D. W.; Wang, H.-L.; Helgeson, R.; Wudl, F.; Whitten, D. G. Highly Sensitive Biological and Chemical Sensors Based on Reversible Fluorescence Quenching in a Conjugated Polymer. *Proc. Natl. Acad. Sci.* **1999**, *96*, 12287–12292.

(17) Pinto, M. R.; Schanze, K. S. Amplified Fluorescence Sensing of Protease Activity with Conjugated Polyelectrolytes. *Proc. Natl. Acad. Sci.* **2004**, *101*, 7505–7510.

(18) Wosnick, J. H.; Mello, C. M.; Swager, T. M. Synthesis and Application of Poly(Phenylene Ethynylene)s for Bioconjugation: A Conjugated Polymer-Based Fluorogenic Probe for Proteases. *J. Am. Chem. Soc.* **2005**, *127*, 3400–3405.

(19) Gaylord, B. S.; Heeger, A. J.; Bazan, G. C. DNA Detection Using Water-Soluble Conjugated Polymers and Peptide Nucleic Acid Probes. *Proc. Natl. Acad. Sci.* **2002**, *99*, 10954–10957.

(20) Traina, C. A.; Bakus, R. C.; Bazan, G. C. Design and Synthesis of Monofunctionalized, Water-Soluble Conjugated Polymers for Biosensing and Imaging Applications. *J. Am. Chem. Soc.* **2011**, *133*, 12600–12607.

(21) Ho, H. A.; Doré, K.; Boissinot, M.; Bergeron, M. G.; Tanguay, R. M.; Boudreau, D.; Leclerc, M. Direct Molecular Detection of Nucleic Acids by Fluorescence Signal Amplification. *J. Am. Chem. Soc.* **2005**, *127*, 12673–12676.

(22) Kim, T.-H.; Swager, T. M. A Fluorescent Self-Amplifying Wavelength-Responsive Sensory Polymer for Fluoride Ions. *Angew. Chem. Int. Ed.* **2003**, *42*, 4803–4806.

(23) Wang, C. F.; White, J. D.; Lim, T. L.; Hsu, J. H.; Yang, S. C.; Fann, W. S.; Peng, K. Y.; Chen, S. A. Illumination of Exciton Migration in Rodlike Luminescent Conjugated Polymers by Single-Molecule Spectroscopy. *Phys. Rev. B* **2003**, *67*.

(24) Beljonne, D.; Curutchet, C.; Scholes, G. D.; Silbey, R. J. Beyond Förster Resonance Energy Transfer in Biological and Nanoscale Systems. *J. Phys. Chem. B* **2009**, *113*, 6583–6599.

(25) Hennebicq, E.; Pourtois, G.; Scholes, G. D.; Herz, L. M.; Russell, D. M.; Silva, C.; Setayesh, S.; Grimsdale, A. C.; Müllen, K.; Brédas, J.-L.; et al. Exciton Migration in Rigid-Rod Conjugated Polymers: An Improved Förster Model. *J. Am. Chem. Soc.* **2005**, *127*, 4744–4762.

(26) Van Averbeke, B.; Beljonne, D.; Hennebicq, E. Energy Transport along Conjugated Polymer Chains: Through-Space or Through-Bond? *Adv. Funct. Mater.* **2008**, *18*, 492–498.

(27) Van Averbeke, B.; Beljonne, D. Conformational Effects on Excitation Transport along Conjugated Polymer Chains. *J. Phys. Chem. A* **2009**, *113*, 2677–2682.

(28) Harriman, A.; Mallon, L. J.; Elliot, K. J.; Haefele, A.; Ulrich, G.; Ziessel, R. Length Dependence for Intramolecular Energy Transfer in Three- and Four-Color Donor−Spacer−Acceptor Arrays. *J. Am. Chem. Soc.* **2009**, *131*, 13375–13386.

(29) Nesterov, E. E.; Zhu, Z.; Swager, T. M. Conjugation Enhancement of Intramolecular Exciton Migration in Poly(*p* -Phenylene Ethynylene)S. *J. Am. Chem. Soc.* **2005**, *127*, 10083–10088.

(30) Pangeni, D.; Nesterov, E. E. "Higher Energy Gap" Control in Fluorescent Conjugated Polymers: Turn-On Amplified Detection of Organophosphorous Agents. *Macromolecules* **2013**, *46*, 7266–7273.

(31) Lupton, J. M. Single-Molecule Spectroscopy for Plastic Electronics: Materials Analysis from the Bottom-Up. *Adv. Mater.* **2010**, *22*, 1689–1721.

(32) Bolinger, J. C.; Traub, M. C.; Brazard, J.; Adachi, T.; Barbara, P. F.; Vanden Bout, D. A. Conformation and Energy Transfer in Single Conjugated Polymers. *Acc. Chem. Res.* **2012**, *45*, 1992–2001.

(33) Pandey, S. K.; Kim, K.-H.; Tang, K.-T. A Review of Sensor-Based Methods for Monitoring Hydrogen Sulfide. *TrAC Trends Anal. Chem.* **2012**, *32*, 87–99.

(34) Eto, K.; Asada, T.; Arima, K.; Makifuchi, T.; Kimura, H. Brain Hydrogen Sulfide Is Severely Decreased in Alzheimer's Disease. *Biochem. Biophys. Res. Commun.* **2002**, *293*, 1485–1488.

(35) Szabó, C. Hydrogen Sulphide and Its Therapeutic Potential. *Nat. Rev. Drug Discov.* **2007**, *6*, 917–935.

(36) Papapetropoulos, A.; Pyriochou, A.; Altaany, Z.; Yang, G.; Marazioti, A.; Zhou, Z.; Jeschke, M. G.; Branski, L. K.; Herndon, D. N.; Wang, R.; et al. Hydrogen Sulfide Is an Endogenous Stimulator of Angiogenesis. *Proc. Natl. Acad. Sci.* **2009**, *106*, 21972–21977.

(37) Peng, H.; Cheng, Y.; Dai, C.; King, A. L.; Predmore, B. L.; Lefer, D. J.; Wang, B. A Fluorescent Probe for Fast and Quantitative Detection of Hydrogen Sulfide in Blood. *Angew. Chem. Int. Ed.* **2011**, *50*, 9672–9675.

(38) Lippert, A. R.; New, E. J.; Chang, C. J. Reaction-Based Fluorescent Probes for Selective Imaging of Hydrogen Sulfide in Living Cells. *J. Am. Chem. Soc.* **2011**, *133*, 10078–10080.

(39) Qian, Y.; Karpus, J.; Kabil, O.; Zhang, S.-Y.; Zhu, H.-L.; Banerjee, R.; Zhao, J.; He, C. Selective Fluorescent Probes for Live-Cell Monitoring of Sulphide. *Nat. Commun.* **2011**, *2*, 495.

(40) Chen, S.; Chen, Z.; Ren, W.; Ai, H. Reaction-Based Genetically Encoded Fluorescent Hydrogen Sulfide Sensors. *J. Am. Chem. Soc.* **2012**, *134*, 9589–9592.

(41) Montoya, L. A.; Pluth, M. D. Selective Turn-on Fluorescent Probes for Imaging Hydrogen Sulfide in Living Cells. *Chem. Commun.* **2012**, *48,* 4767.

(42) Chen, Y.; Zhu, C.; Yang, Z.; Chen, J.; He, Y.; Jiao, Y.; He, W.; Qiu, L.; Cen, J.; Guo, Z. A Ratiometric Fluorescent Probe for Rapid Detection of Hydrogen Sulfide in Mitochondria. *Angew. Chem. Int. Ed.* **2013**, *52*, 1688–1691.

(43) Chen, W.; Pacheco, A.; Takano, Y.; Day, J. J.; Hanaoka, K.; Xian, M. A Single Fluorescent Probe to Visualize Hydrogen Sulfide and Hydrogen Polysulfides with Different Fluorescence Signals. *Angew. Chem. Int. Ed.* **2016**, *55*, 9993–9996.

(44) Jung, H. S.; Chen, X.; Kim, J. S.; Yoon, J. Recent Progress in Luminescent and Colorimetric Chemosensors for Detection of Thiols. *Chem. Soc. Rev.* **2013**, *42*, 6019.

(45) Hartle, M. D.; Pluth, M. D. A Practical Guide to Working with H_2S at the Interface of Chemistry and Biology. *Chem Soc Rev* **2016**, *45*, 6108–6117.

(46) Tomasulo, M.; Yildiz, I.; Raymo, F. M. PH-Sensitive Quantum Dots. *J. Phys. Chem. B* **2006**, *110*, 3853–3855.

(47) Deniz, E.; Sortino, S.; Raymo, F. M. Fast Fluorescence Photoswitching in a BODIPY−Oxazine Dyad with Excellent Fatigue Resistance. *J. Phys. Chem. Lett.* **2010**, *1*, 1690–1693.

(48) Deniz, E.; Ray, S.; Tomasulo, M.; Impellizzeri, S.; Sortino, S.; Raymo, F. M. Photoswitchable Fluorescent Dyads Incorporating BODIPY and [1,3]Oxazine Components. *J. Phys. Chem. A* **2010**, *114*, 11567–11575.

CHAPTER 3. FLUORESCENCE TURN-ON AMPLIFYING CONJUGATED POLYMER SENSORS FOR CYSTEINE DETECTION

3.1 Introduction

L-cysteine (Cys) is one of the most important and abundant sulfur-containing amino acids for building proteins in organisms as well as regulating antioxidant glutathione (GSH) levels inside cells.[1,2] Deviated concentration of Cys in human body is connected to a variety of syndromes, e.g. hair depigmentation, edema, lethargy, liver damage, leucocyte loss, and Alzheimer's disease.[3–5] Traditional methods for measuring Cys levels such as high performance liquid chromatography,[6] mass spectrometry,[7] and capillary electrophoresis[8] require high instrumental expenses, long data collecting time, and destruction of samples. Importantly, these methods are not optimal for home testing or point-of-care emergency room. To understand the real role of Cys in physiological processes of eukaryotic cells, inorganic nanoparticles and organic fluorescent chemosensors have been developed for *in vitro* and *in vivo* examinations.[9–12] The investigation is significant yet difficult since other biothiols, e.g. GSH, H_2S, and homocysteine (Hcy), can sabotage the analysis. Specifically, concentration level of GSH in living cells is 1-10 mM whereas Cys level is orders of magnitude lower (at the μM level); furthermore, similarity between Hcy and Cys in terms of structure and reactivity renders them to react with the same receptor sites of the sensory molecules.[13,14] Conventionally, development of the fluorescent chemosensors for assaying Cys is mainly based on its affinity toward heavy metal ions and strong nucleophilicity.[15] Therefore, numerous organic reactions have been exploited, including Michael addition,[16] cleavage of sulfonamide and sulfonate ester,[17,18] cleavage of selenium-nitrogen bonds,[19] cleavage of disulfide,[20,21] and cyclization of aldehyde.[22] It has been proven that N-terminal cysteine rapidly forms thiazolidine in the presence of aldehyde in biomimic solution.[23] Strongin *et al.* reported that xanthene derivative **1** containing free aldehyde as a receptor can efficiently monitor Cys and Hcy

concentration down to μM level.[22] Upon the addition of Cys, UV-vis spectrum of the xanthene derivative showed ratiometric behavior and the fluorescence of it was quenched. Barbas III and coworkers demonstrated that a small molecule sensor **2** increased its fluorescence intensity after reacting with Cys, showing the moderate detection range from 100 ppm to 5000 ppm.[24] Lin *et al.* also published a ratiometric fluorescent sensor **3** for Cys and Hcy detection.[25] Composed of an electron rich phenanthroimidazole and electron deficient aldehyde moiety, the pristine small molecule sensor exhibited a fluorescence band at 519 nm, which was assigned as originating from intramolecular charge transfer. Upon cyclization with Cys or Hcy, the intensity of the intramolecular charger transfer band diminished which was accompanied by an intensity increase of a new emission band at 394 nm, originating from the phenanthroimidazole moiety. Hong *et al.* prepared an ortho-hydroxy aldehyde-functionalized coumarin derivative **4**, which acted as a fluorescence turn-on sensor for the detection of Cys and Hcy.[26]

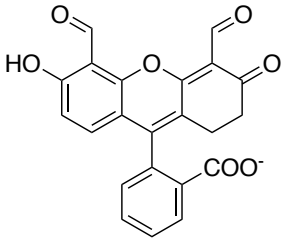

1

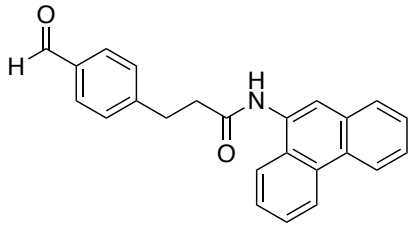

2

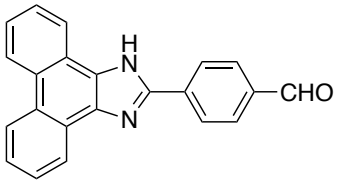

1

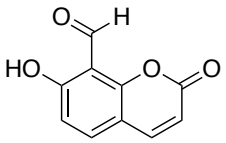

4

In the aqueous solution (HEPES buffer, pH 7.4), the coumarin derivative showed very low fluorescence due to the photoinduced electron transfer from the coumarin to the aldehyde.

Formation of thiazolidine upon reaction of aldehyde with Cys greatly increased the fluorescence up to 100 times in intensity. The author proposed that the enhancement was resulted from the hydrogen bonding between the electron lone pair at the nitrogen of thiazolidine and the hydroxyl group on the coumarin. Generally, design of the biological Cys sensor molecules requires rather complex synthesis and precise adjustment of the electronic characteristics of the sensor (e.g. sensor design based on FRET energy migration mechanism requires achieving spectral overlap between emission of donor and absorbance of acceptor). In a previous study in our group, an anthraldehyde end-capped oligo(*p*-phenylene ethynylene) (OPE) structure was used to modulate excitation energy transfer through the formation of a thiazolidine moiety at the terminus of the π-conjugated oligomer (Figure 3.1).[27]

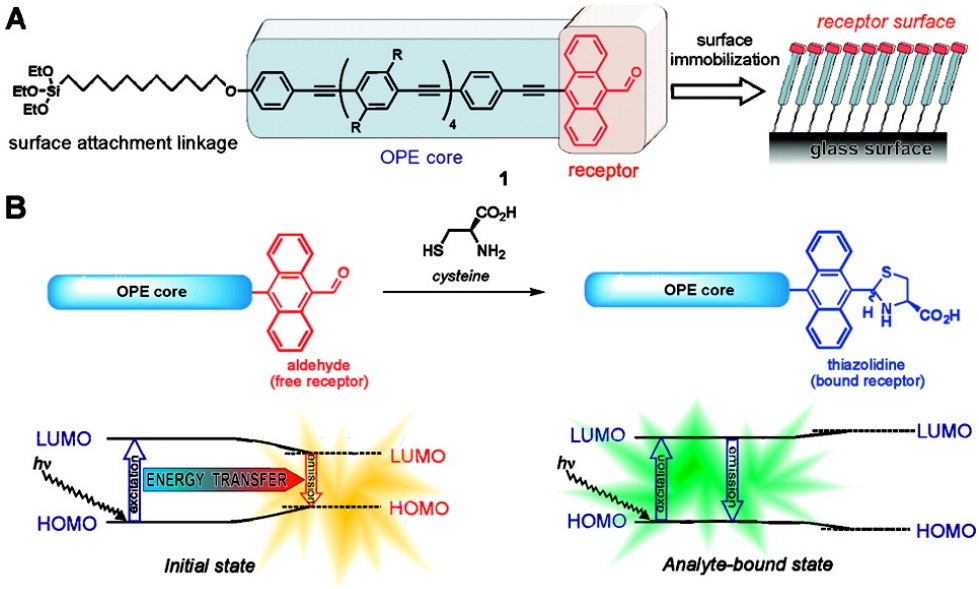

Figure 3.1. (A) General structure of end-functionalized OPE and its immobilization on glass surface; (B) reaction of cysteine and a schematic diagram to show origin of the ratiometric fluorescent response.

These OPEs were self-assembled on a glass surface to form a monolayer-thick film. The OPE monolayer film was exposed to an aqueous solution of Cys at 90 ºC for 20 minutes to allow the analytes react with the aldehyde end-caps through cyclization. Therefore, the reaction with Cys

resulted in a gradual increase in the ratio of fluorescence intensity F_{450}/F_{520}, where F_{450} refers to the anthracenyl end-group emission and F_{520} is emission from the oligo(*p*-phenylene ethynylene) core. The observed ratiometric fluorescence effect stemmed from raising the energy gap of the terminal acceptor fluorophore above the energy gap of the donor conjugated oligomer chromophore. This demonstrated the principle possibility to control excitation energy migration in conjugated oligomers (and polymers) by changing the HOMO-LUMO gap of one of the conjugated units. Recently, we proposed the novel concept of the "higher energy gap" controlled fluorescence amplification and demonstrated how it could be used in design of turn-on fluorescent sensors for the detection of organophosphorous warfare agent mimic diethyl chlorophosphate,[28] and biochemical messenger hydrogen sulfide,[29] respectively. The "higher energy gap" mechanism can be triggered when a target analyte interacts with a receptor along the conjugated polymer backbone and results in increasing the local HOMO-LUMO gap at that site. Unlike conventional fluorescence "turn-on" amplification approaches that often require elaborate synthesis and sophisticated specialized design, e.g. installation of a removable fluorescence quenching moiety or utilizing a scheme where a precursor strongly electronically coupled with polymer backbone would form a high emissive fluorophore upon an analytical reaction. In this part of the project, we decided to apply the "higher energy gap" concept towards the detection of Cys in aqueous environment, utilizing aldehyde reaction with cysteine. Although a number of fluorescent Cys sensors have been described in literature, none of them were amplifying, and therefore could not benefit from the ability to detect a broad range of Cys concentrations.

3.2 Molecular Design of the Cysteine Sensor

To design a "higher energy gap" controlled fluorescence turn-on amplifying conjugated polymer for achieving the Cys detection, poly(naphthylene vinylene) scaffold was employed as

the suitable low energy gap conjugated polymer platform. Similar scaffold has been previously successfully applied in design of amplifying sensors for organophosphate warfare agent mimics diethyl chlorophosphate and biomedical analyte hydrogen sulfide (described in the previous chapter). Among a variety of reported analytical reactions targeting Cys, we identified the reaction of an aldehyde functional group that can efficiently react with Cys to form a thiazolidine five-membered ring. In addition to the relatively simple and straightforward synthetic route, the cyclization to form thiazolidine can efficiently tune the local energy gap of the chromophore without affecting the overall π-electron conjugation in the polymer backbone. Preliminary DFT computational study (at the B3LYP/6-31G* level of theory) indicated that the formation of the thiazolidine unit would increase the HOMO-LUMO gap of the receptor chromophore from 4.01 to 4.15 eV (Figure 3.2). While such a small energy gap change (0.14 eV) was predicted, one can anticipate that, according to the "higher energy gap" mechanism, this could be sufficient to effectively restrict intramolecular exciton migration and result in the amplified turn-on fluorescent response.

3.3 Synthetic Routes for Cys Conjugated Polymer Sensor

The initial synthetic route developed to approach conjugated polymer sensors for Cys detection began from the alkylation of **2-S9** with 1,3-propansultone under basic condition in a solution of butanone-ethanol 1/1 mixture to generate water-soluble potassium sulfonate salt **3-1**, which could be readily purified by precipitation from cold water to give the product in a moderate yield (56%). The water-soluble potassium sulfonate side chain was chosen since triethylene glycol monomethyl ether (TEG) group (used in the H_2S sensor design) provided only limited solubility not sufficient to perform analytical measurements in aqueous media such as in phosphate-buffered saline (PBS) solution. The subsequent Suzuki polymerization of **3-1** and **2-S6** utilizing $Pd(OAc)_2$

and XPhos and K_3PO_4 as base was carried out in aqueous phase (H_2O-THF 1/1) to give Cys polymer sensors **3-P1**, **3-P2**, **3-P3**, and **3-P4**, which were prepared by varying reaction time to achieve different degree of polymerization on the assumption of step-growth mechanism (8 hours for **3-P1**, 24 hours for **3-P2**, 48 hours for **3-P3**, and 72 hours for **3-P4**).

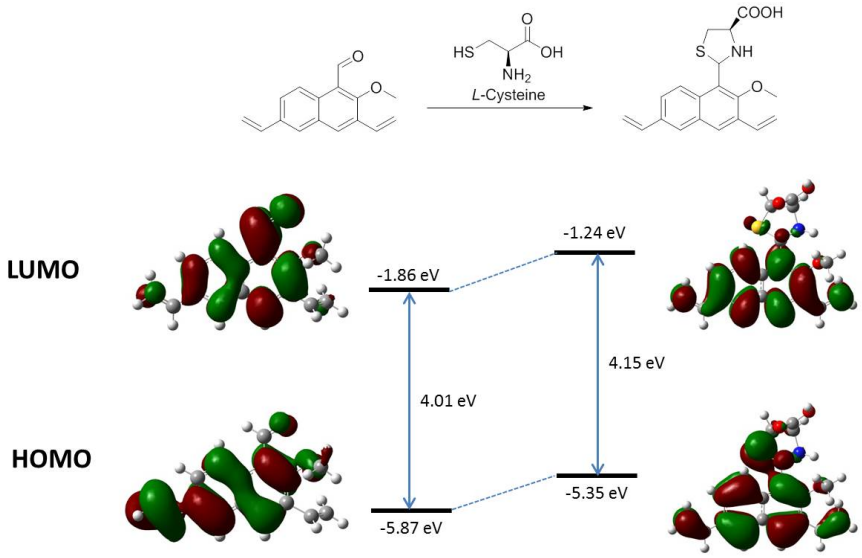

Figure 3.2. DFT studies (at B3LYP/6-31G* level) of the HOMO-LUMO gap change in the aldehyde-functionalized receptor upon reaction with Cys. The molecule was truncated for better simulation efficiency. The computed HOMO and LUMO surfaces of the initial receptor indicate complete electronic delocalization over the entire molecule. Reaction with Cys effectively converted initial aldehyde into thiazoldine leading to the increasing energy gap of the π-conjugated system from 4.01 to 4.15 eV.

All four crude polymers were purified via dialysis in deionized water for 2 days (using a membrane with 3.5 kDa cutoff for **3-P1**, and 8 kDa for other three polymers). We assume that using this approach we obtained polymer sensors with different conjugated backbone lengths. The accurate values of molecular weights of these polymers are yet to be determined as the polymers appear to show heavy intermolecular aggregation during GPC experiments (DMF as eluent). These experiments are currently in progress. Such aggregation indeed could stem from the insufficient solubilizing ability of TEG side chains. To compare the effect of fluorescent amplification in the longer π-conjugated systems with a much shorter system, small molecule reference **3-M1** was

prepared by Suzuki coupling of **3-1** and **2-S12**, and the crude product was then purified by vigorously rinsing with THF and CH_2Cl_2 following by recrystallization from H_2O-EtOH 1/9 to give the product as a light greenish solid in 83% yield. The chemical structure was then elucidated by NMR and further supported by HR-ESI-MS (m/z calc.: 497.1423; found: 497.1427).

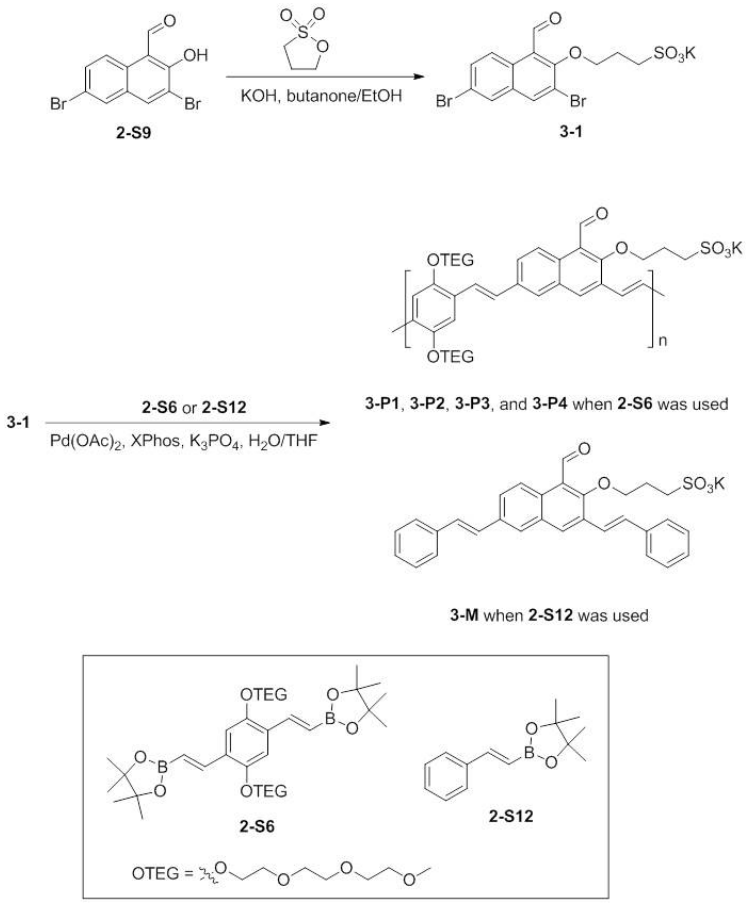

Scheme 3.1. Synthetic route to conjugated polymers for Cys detection (**3-P1**, **3-P2**, **3-P3**, and **3-P4)** and the small molecule analog **3-M1.**

3.4 Photophysical Characteristics and Fluorescent Amplification

We characterized all fluorescent Cys sensor polymers using UV-vis and fluorescence spectroscopies. All the studies were performed using solutions in 1X PBS in ultrapure water, and the analytical reaction with Cys was allowed to run at 50 ºC for 1 hour to reach the equilibrium. The UV-vis absorption spectrum of the small molecule **3-M1** showed a major absorption band at

316 nm with a second, weaker band centered at 400 nm. The latter can be assigned as appearing due to weak intramolecular charge transfer from naphthalene to aldehyde moiety (Figure 3.3). For pristine solutions of polymer sensor **3-P1**, an absorbance band with two maxima at 337 and 394 nm with an onset at 521 nm was observed. For polymer sensor **3-P2**, **3-P3**, and **3-P4**, with presumably higher degree of polymerization, all the UV-vis absorption spectra showed featureless intense broad bands. The significantly higher extinction coefficients indicated a possibility of the heavy aggregation occurring in solutions in the case of polymers with higher molecular weights. The fluorescence spectrum of **3-M1** showed a single band with maximum at 495 nm, whereas the conjugated polymer sensors **3-P1**, **3-P2**, **3-P3**, and **3-P4** were almost non-emissive.

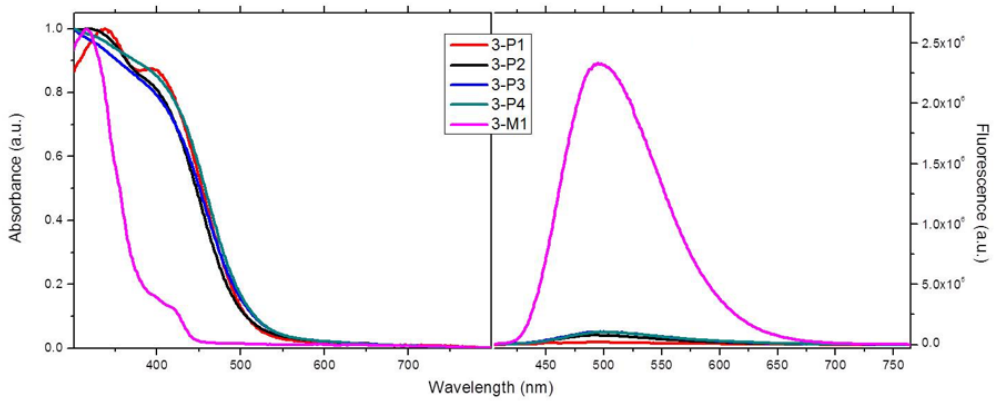

Figure 3.3. UV-vis absorption (normalized, left) and fluorescence (right, inset: normalized FL) spectra of polymer sensors **3-P1**, **3-P2**, **3-P3**, and **3-P4** and small molecule reference **3-M1** in 1X PBS. Concentration: 6.25 μM (**3-P1**, **3-P2**, **3-P3**, and **3-P4**), and 37.5 μM (**3-M1**). (Extinction Coefficients (M^{-1} cm^{-1}): 3136 (**3-P1**), 67696 (**3-P2**), 128971 (**3-P3**), 136229 (**3-P4**), and 15750 (**3-M1**).

Based on general considerations of fluorescent properties of conjugated polymers, we expected that the extended π-conjugation along the polymer backbone should result in bathochromic shifts relative to the model sensor **3-M1** in both UV-vis and fluorescence spectra. However, the normalized fluorescent spectra of the polymer sensors, regardless of their molecular weights, exhibited the same position of the emission maxima as in the small m0olecule sensor **3-**

M1. Upon addition of Cys, the small molecule reference **3-M1** showed a moderate gradual decrease in fluorescence intensity, and insignificant changes in UV-vis absorption spectra, even upon addition of large excess of Cys. The fluorescence intensity decrease (turn-off response) could probably be explained by the heavy atom effect from sulfur upon formation of thiazolidine moiety. Additionally, this could be attributed to the lower solubility of the thiazolidine derivative in the aqueous conditions, causing some material precipitating from the solution. Indeed, we observed accumulation of an insoluble solid from the measured samples after some time.

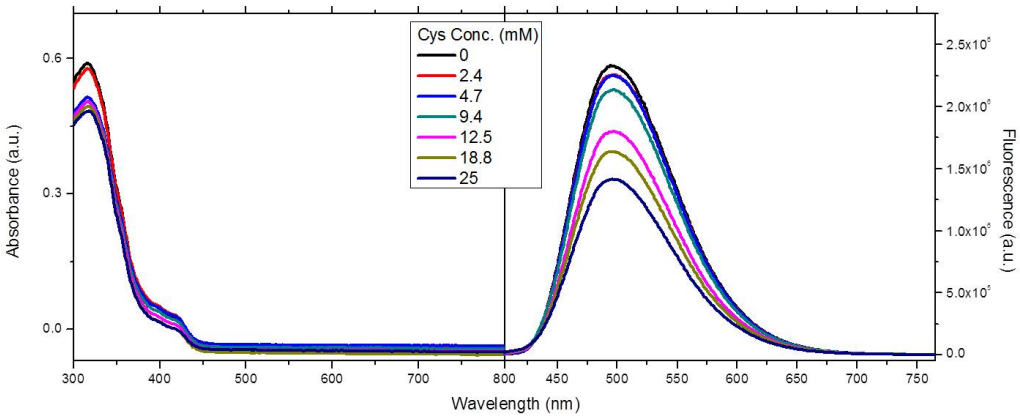

Figure 3.4. Changes in absorption (left) and fluorescence (right) spectra of a 37.5 μM solution of **3-M1** in 1XPBS upon addition of increasing concentrations of Cys.

On the other hand, copolymer **3-P1**, **3-P2**, **3-P3**, and **3-P4** showed rather insignificant changes in UV-vis and fluorescence spectra upon addition of micromolar concentrations of Cys, yet the significant enhancement in fluorescence was observed upon addition of millimolar levels of Cys (Figure 3.5). The narrow Cys detection range could be attributed to the aggregation of the polymer chains in solution. Regarding the amplification ratio, as presented in Figure 3.6, **3-P1** showed an up to 30-fold amplification, and **3-P2**, **3-P3**, and **3-P4** showed smaller, 10 to 15 times, enhancements. The unexpected observation that the polymers with longer chains showed lower fluorescence amplification was contrary to the higher energy gap mechanism, as polymer sensors

with longer conjugated chain length were expected to show higher fluorescent amplification (see Chapter 2). This unexpected behavior could likely result from the poor solubility of the polymer in aqueous media, which induced intermolecular aggregation. Such aggregation would naturally be more prevalent in the case of longer macromolecular chains.

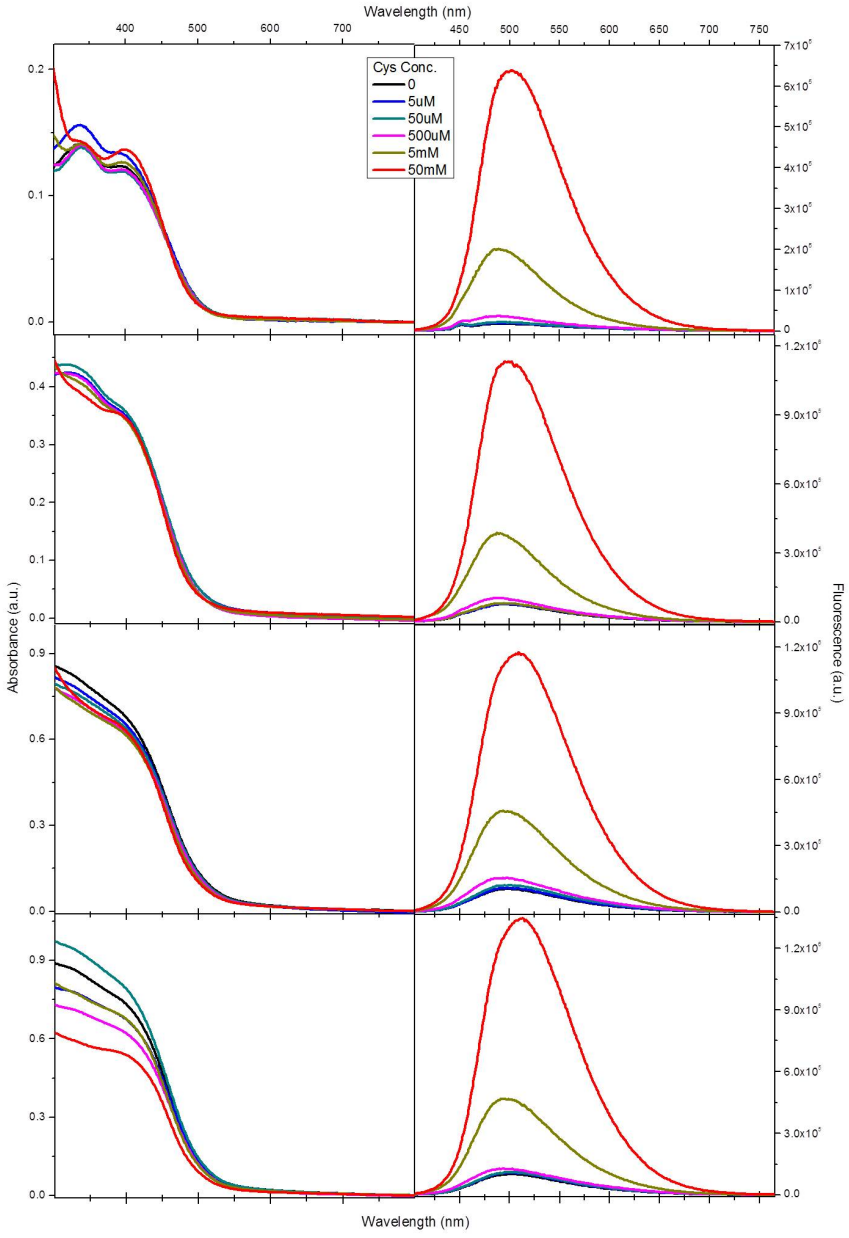

Figure 3.5. Changes in absorption (left) and fluorescence (right) spectra of a 6.25 μM solution of **3-P1**, **3-P2**, **3-P3**, and **3-P4** in 1XPBS upon addition of increasing concentrations of Cys.

The intermolecular aggregation would create numerous close contacts between individual polymer chains which facilitate intermolecular energy transfer via the through-space (Förster-type) mechanism. The possibility of intermolecular energy migration would allow exciton "detour" of the local higher energy site in the conjugated backbone, thereby deactivating the higher energy gap mechanism. Indeed, intermolecular excitation energy transfer is considered to occur more efficiently as compared to the intramolecular pathway.

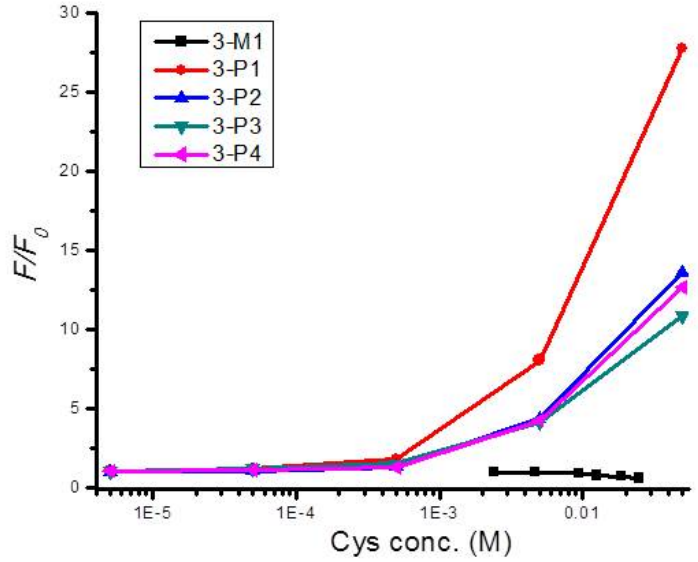

Figure 3.6. Change in integrated fluorescence intensity of polymers **3-P1**, **3-P2**, **3-P3**, and **3-P4** solution in 1XPBS (6.25 μM), and small molecule **3-M1** (37.5 μM) upon addition of increasing concentrations of Cys. The intensity is expressed as a ratio of integrated area of a fluorescent band at each Cys concentration to the fluorescent band in the absence of analyte (F/F_0).

3.5 Conclusions

A series of conjugated polymers functionalized with electronically coupled aldehyde receptor for the detection of cysteine has been prepared. The featureless UV-vis spectra and high extinction coefficients indicated the polymers were highly aggregated in aqueous media. Upon addition of cysteine, the conjugated polymers exhibited substantial amplified fluorescent turn-on

response: sensor **3-P1** showed a 30-times enhancement in fluorescence intensity, and **3-P2**, **3-P3**, and **3-P4** showed 10 to 15-folds amplification, in the minimolar concentration range. This study demonstrated that the "higher energy gap" control mechanism for fluorescence turn-on amplification can be inhibited by intermolecular aggregation and, more importantly, is highly sensitive even to the small increase in local HOMO-LUMO gap at the reactive site. Further continuation of this work requires design and preparation of more water-soluble analogs of the conjugated polymer sensors, in order to minimize the effect of intermolecular aggregation. This work is ongoing.

3.6 References

(1) Lu, S. C. Regulation of Glutathione Synthesis. *Mol. Aspects. Med.* **2009**, *30*, 42–59.

(2) Pham-Huy, L. A.; He, H.; Pham-Huy, C. Free Radicals, Antioxidants in Disease and Health. *Int. J. Biomed. Sci.* **2008**, *4*, 89–96.

(3) Shahrokhian, S. Lead Phthalocyanine as a Selective Carrier for Preparation of a Cysteine-Selective Electrode. *Anal. Chem.* **2001**, *73*, 5972–5978.

(4) Kong, F.; Liu, R.; Chu, R.; Wang, X.; Xu, K.; Tang, B. A Highly Sensitive Near-Infrared Fluorescent Probe for Cysteine and Homocysteine in Living Cells. *Chem. Commun.* **2013**, *49*, 9176-9178.

(5) Yue, Y.; Yin, C.; Huo, F.; Chao, J.; Zhang, Y. Thiol-Chromene Click Chemistry: A Turn-on Fluorescent Probe for Specific Detection of Cysteine and Its Application in Bioimaging. *Sens. Actuators B Chem.* **2016**, *223*, 496–500.

(6) Vacek, J.; Klejdus, B.; Petrlová, J.; Lojková, L.; Kubáň, V. A Hydrophilic Interaction Chromatography Coupled to a Mass Spectrometry for the Determination of Glutathione in Plant Somatic Embryos. *The Analyst* **2006**, *131*, 1167–1174.

(7) Zhang, D.; Liu, Q. Biosensors and Bioelectronics on Smartphone for Portable Biochemical Detection. *Biosens. Bioelectron.* **2016**, *75*, 273–284.

(8) Inoue, T.; Kirchhoff, J. R. Determination of Thiols by Capillary Electrophoresis with Amperometric Detection at a Coenzyme Pyrroloquinoline Quinone Modified Electrode. *Anal. Chem.* **2002**, *74*, 1349–1354.

(9) Chen, H.; Tang, Y.; Lin, W. Recent Progress in the Fluorescent Probes for the Specific Imaging of Small Molecular Weight Thiols in Living Cells. *TrAC Trends Anal. Chem.* **2016**, *76*, 166–181.

(10) Zhou, Y.; Yoon, J. Recent Progress in Fluorescent and Colorimetric Chemosensors for Detection Ofamino Acids. *Chem. Soc. Rev.* **2012**, *41*, 52–67.

(11) Yin, C.; Huo, F.; Zhang, J.; Martínez-Máñez, R.; Yang, Y.; Lv, H.; Li, S. Thiol-Addition Reactions and Their Applications in Thiol Recognition. *Chem. Soc. Rev.* **2013**, *42*, 6032-6059.

(12) Niu, L.-Y.; Chen, Y.-Z.; Zheng, H.-R.; Wu, L.-Z.; Tung, C.-H.; Yang, Q.-Z. Design Strategies of Fluorescent Probes for Selective Detection among Biothiols. *Chem. Soc. Rev.* **2015**, *44*, 6143–6160.

(13) Hassan, S. S. M.; Rechnitz, G. A. Determination of Glutathione and Glutathione Reductase with a Silver Sulfide Membrane Electrode. *Anal. Chem.* **1982**, *54*, 1972–1976.

(14) Jung, H. S.; Chen, X.; Kim, J. S.; Yoon, J. Recent Progress in Luminescent and Colorimetric Chemosensors for Detection of Thiols. *Chem. Soc. Rev.* **2013**, *42*, 6019-6031.

(15) Chow, C.-F.; Chiu, B. K. W.; Lam, M. H. W.; Wong, W.-Y. A Trinuclear Heterobimetallic Ru(II)/Pt(II) Complex as a Chemodosimeter Selective for Sulfhydryl-Containing Amino Acids and Peptides. *J. Am. Chem. Soc.* **2003**, *125*, 7802–7803.

(16) Langmuir, M. E.; Yang, J.-R.; Moussa, A. M.; Laura, R.; LeCompte, K. A. New Naphthopyranone Based Fluorescent Thiol Probes. *Tetrahedron Lett.* **1995**, *36*, 3989–3992.

(17) Maeda, H.; Matsuno, H.; Ushida, M.; Katayama, K.; Saeki, K.; Itoh, N. 2,4-Dinitrobenzenesulfonyl Fluoresceins as Fluorescent Alternatives to Ellman's Reagent in Thiol-Quantification Enzyme Assays. *Angew. Chem. Int. Ed.* **2005**, *44*, 2922–2925.

(18) Han, M. S.; Lytton-Jean, A. K. R.; Oh, B.-K.; Heo, J.; Mirkin, C. A. Colorimetric Screening of DNA-Binding Molecules with Gold Nanoparticle Probes. *Angew. Chem. Int. Ed.* **2006**, *45*, 1807–1810.

u.3

(19) Tang, B.; Yin, L.; Wang, X.; Chen, Z.; Tong, L.; Xu, K. A Fast-Response, Highly Sensitive and Specific Organoselenium Fluorescent Probe for Thiols and Its Application in Bioimaging. *Chem. Commun.* **2009**, *35*, 5293-5295.

(20) Zhu, J.; Dhimitruka, I.; Pei, D. 5-(2-Aminoethyl)Dithio-2-Nitrobenzoate as a More Base-Stable Alternative to Ellman's Reagent. *Org. Lett.* **2004**, *6*, 3809–3812.

(21) Pullela, P. K.; Chiku, T.; Carvan, M. J.; Sem, D. S. Fluorescence-Based Detection of Thiols in Vitro and in Vivo Using Dithiol Probes. *Anal. Biochem.* **2006**, *352*, 265–273.

(22) Rusin, O.; St. Luce, N. N.; Agbaria, R. A.; Escobedo, J. O.; Jiang, S.; Warner, I. M.; Dawan, F. B.; Lian, K.; Strongin, R. M. Visual Detection of Cysteine and Homocysteine. *J. Am. Chem. Soc.* **2004**, *126*, 438–439.

(23) Tolbert, T. J.; Wong, C.-H. New Methods for Proteomic Research: Preparation of Proteins with N-Terminal Cysteines for Labeling and Conjugation This Research Was Supported by the NIH (R37 GM44154). *Angew. Chem. Int. Ed.* **2002**, *41*, 2171-2174.

(24) Tanaka, F.; Mase, N.; Barbas III, C. F. Determination of Cysteine Concentration by Fluorescence Increase: Reaction of Cysteine with a Fluorogenic Aldehyde. *Chem. Commun.* **2004**, *15*, 1762-1763.

(25) Lin, W.; Long, L.; Yuan, L.; Cao, Z.; Chen, B.; Tan, W. A Ratiometric Fluorescent Probe for Cysteine and Homocysteine Displaying a Large Emission Shift. *Org. Lett.* **2008**, *10*, 5577–5580.

(26) Lee, K.-S.; Kim, T.-K.; Lee, J. H.; Kim, H.-J.; Hong, J.-I. Fluorescence Turn-on Probe for Homocysteine and Cysteine in Water. *Chem. Commun.* **2008**, *46*, 6173-6175.

(27) Acharya, J. R.; Zhang, H.; Li, X.; Nesterov, E. E. Chemically Controlled Amplified Ratiometric Fluorescence in Surface-Immobilized End-Capped Oligo(*p*-Phenylene Ethynylene)S. *J. Am. Chem. Soc.* **2009**, *131*, 880–881.

(28) Pangeni, D.; Nesterov, E. E. "Higher Energy Gap" Control in Fluorescent Conjugated Polymers: Turn-On Amplified Detection of Organophosphorous Agents. *Macromolecules* **2013**, *46*, 7266–7273.

(29) Chiang, C.-H.; Pangeni, D.; Nesterov, E. E. Higher Energy Gap Control of Fluorescence in Conjugated Polymers: *Turn-On* Amplifying Chemosensor for Hydrogen Sulfide. *Macromolecules* **2017**, *46*, 6961-6966.

CHAPTER 4. CONJUGATED POLYMER THIN FILMS WITH ORDERED MOLECULAR ORGANIZATION AND MORPHOLOGY BY STEPWISE SURFACE-INITIATED POLYMERIZATION

4.1 Introduction

Performance of conjugated polymers based electronic and optoelectronic devices greatly depends on intrinsic electronic properties of polymers and their organizations as bulk materials.[1–3] While uniform alignments of conjugated polymer chains provide potential benefits for charge injection and charge transportation process, fine adjustment on it and further manipulation of mesoscale morphology in thin films remain a significant challenge.[4] Currently, one most utilized solution-based approach is spin-casting that utilizes centrifugal force to randomly disperse polymer molecules onto substrates where the physical adsorbed thin films can be easily removed mechanically or chemically. Chemisorption of appropriate end groups, such as alkoxysilane or phosphonate, of conjugated polymers (grafting-to) yields more robust thin films yet the polymer chains tend to form "mushroom" aggregates in solution prior to binding with surface.[5–7] The "mushroom" architectures result in limited grafting density. On the other hand, surface-initiated polymerization (grafting-from) has been extensively harnessed in preparation of conjugated polymer thin films, such as polythiophene[8–10], polyfluorene[11], poly(*p*-phenylene)[12,13], and poly(*p*-phenylene ethynylene)[14]. It is evident that this purification-free approach can produce very thick films with highly dense interchain packing. Furthermore, monomers used for surface-initiated polymerization do not require solubilizing side chains, which are major sites where oxidation , therefore, photo- and thermal degradation start. The solubilizing chains usually hinder the polymer packing resulting in effective "dilution" of the "semiconducting" fraction in bulk materials. However, this method is limited to chain-growth polymerization, and requires problematic immobilization of air-sensitive imitators, and sophisticated experimental settings.[15] One

intermediary technique is to implement solution polymerization in the presence of a substrate decorated with functional groups which can take part in polymerization (grafting-through).[16,17] Step-growth polymerization can occur spontaneously in the solution and on the surface thereby causing rough polymer thin films.

Alternating donor-acceptor conjugated copolymers allow one to chemically manage electronic properties of bulky materials since extent of orbital coherence between electron donating and accepting moieties can bring the band gap below 2.0 eV (a threshold for practical applications as semiconducting materials), as a result of lowering the required energy for the π-π^* transition.[18–21] Such low band gap conjugated polymers exhibit several promising redox and photoelectronic properties, e.g. broad and long wavelength absorption, solid-state charge transfer, and multiple charge states in a small potential window. Among various low band gap conjugated polymers, poly(*p*-arylene ethynylene)s (PAEs) are especially attracting due to its unique linear rigid π–conjugated backbone and exceptional ability to transfer photoexcitation energy.[22–27] Furthermore, relatively simple and straightforward synthesis of monomers, mild and highly reproducible polymerization conditions which can tolerate numerous functional groups, including sulfonate, amine, carboxylate, hydroxy, and biologically active ligands indeed facilitate the generalizing of PAEs.

In a previous study, our group demonstrated preparation of semiconducting thin films of poly(bithiophenetriazole fluorene) and poly(triazole fluorene) using surface-initiated stepwise click polymerization.[28] The robustness, regioselectivity and chemoselectivity of Cu(I)-catalyzed acetylene-azide click reaction allowed to prepare highly organized anisotropic semiconducting polymer thin films with precise control of thickness and polymer molecular structure. However, the triazole units were not completely "conjugated" in a sense that they possess properties of

"cross-conjugated" units, and thus do not allow complete π-electron delocalization. In this chapter we describe our development, for the first time, of a simple and efficient procedure for the highly ordered truly conjugated immobilized poly(*p*-phenylene ethynylene) (PPE) thin films (Figure 4.1) consisting of precisely defined alternating donor-acceptor units using surface-initiated stepwise Sonogashira polymerization under mild reaction condition.

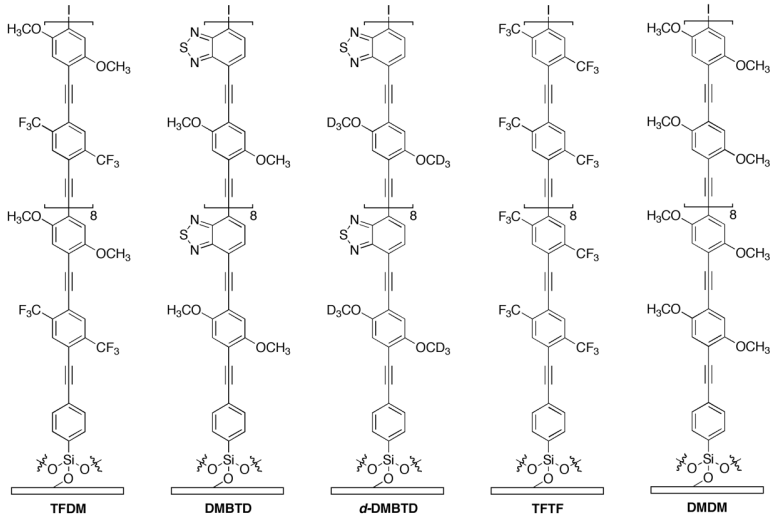

Figure 4.1. Chemical structures of surface-confined PPE polymer thin films prepared in this study.

4.2 Synthetic Strategy towards Surface-Confined PPE Thin Films

The surface-confined initiator **4-1**, triethoxy(4-iodophenyl)silane, was prepared from commercially available 1,4-diiodobenzene through halogen-lithium exchange reaction following by the quenching of organolithium compound with tetraethoxysilane, as shown in scheme 4-1. The initiator **4-1** was covalently immobilized onto the homogeneous inorganic oxide substrate to generate surface-immobilized self-assembled monolayer **4-SAM1**. To prepare **DMDM** semiconducting polymer thin film, **4-SAM1** was immersed into a solution of 1,4-dimethoxy-2,5-diethynylbenzene (**2**), $Pd(PPh_3)_4$, and CuI in toluene/diisopropylamine at 40 ºC for 30 minutes to obtain an ethynyl-terminated thin film (step A). After thoroughly rinsing with toluene under inert gas atmosphere to remove unbounded reactants, catalysts, and reaction byproducts, the ethynyl-terminated thin film was then immersed into a solution of 1,4-diiodo-2,5-dimethoxybenzene (**5**),

$Pd(PPh_3)_4$, and CuI in toluene/diisopropylamine at 40 ºC for 30 minutes followed by vigorous washing with toluene and sonication for 3 minutes to obtain an iodo-terminated thin film (step B). The conjugated polymer thin film **DMDM** was prepared by alternation of steps A and B for 9 times, and exhibited robust chemical and mechanical tolerance. We further demonstrated the preparation of an n-type polymeric semiconductor **TFTF**, and low band gap conjugated polymer thin films **TFDM** and **DMBTD**, following the same approach and utilizing different diethynyl- and/or diiodo-monomers. While dimerization of diethynyl-functional monomers could occur in the presence of trace amount of Cu(I) and oxygen, neither self-coupling nor polymeric aggregates were observed during the entire reaction period.

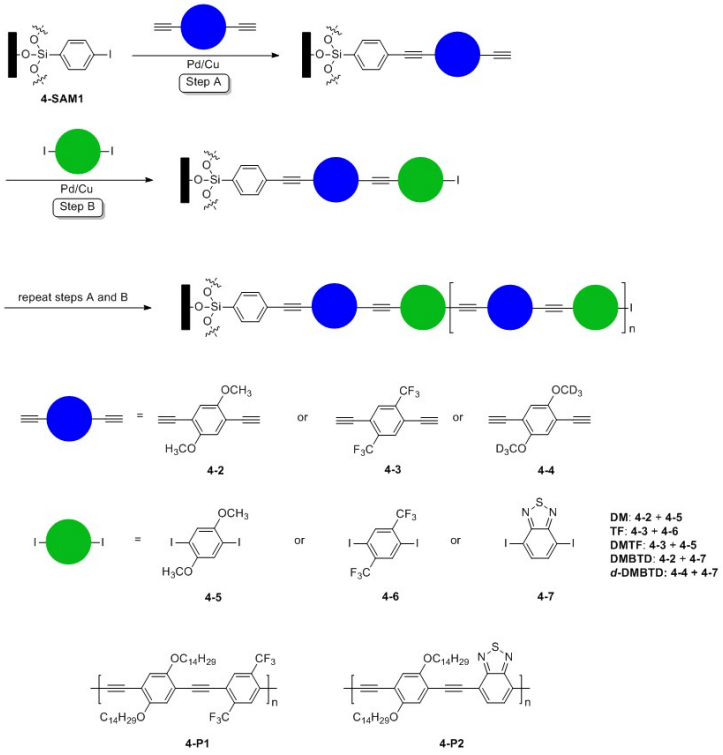

Scheme 4.1. Preparation of semiconducting PPE thin films via stepwise surface-imitated Sonogashira polymerization.

Furthermore, for the best quality of the polymer films, the reaction solutions were prepared freshly at every single step, thereby maintaining the well-defined reactants concentrations, and minimizing formation of possible byproducts generated in reaction media over more extended reaction times.

4.3 Photophysical Characteristics of the Surface-Confined PPE Thin Films.

The evolution of the polymer thin films could be tracked by UV-vis absorption (Figure 4.2). The initiator surface-immobilized monolayer **4-SAM1** displayed a distinct UV-vis absorbance maximum at 239 nm corresponding to π-π* transition of the phenyl group. We then measured the UV-vis progression of the thin films after each coupling cycle (one step A followed by one step B) at the iodo-termination step, in order to avoid potential oxidation of the ethynyl terminal group during the UV–vis measurements. In **DMDM** thin films, absorbance maximum (λ_{abs} 409 nm) showed a significant bathochromic shift (170 nm) accompanied by a linear increase in the absorption intensity: this appeared as a clear evidence for the extension of π-electron delocalization. Furthermore, the featureless long wavelength onset tailing beyond the detection range of the spectrometer indicated possible significant intermolecular electronic delocalization as a result of the close packed macromolecular chain arrangement on the surface. Likewise, **TFTF** thin film showed absorbance maximum at 351 nm with a red shift of 112 nm with respect to the initiator monolayer, and the linear increase of optical absorbance referred to the gradual growth of the polymer film. In the alternating donor-acceptor **TFDM** thin film, a broad absorption band featured a dual maximum at 330 and 405 nm, the latter can be assigned as a charge transfer band between the donor and acceptor moieties. Incorporating a stronger electron acceptor monomeric block 2,1,3-benzothiadiazole, semiconducting film **DMBTD** exhibited a broad absorbance with two maxima at 329 and 466 nm. It is worth noticing that the severe red-tailing of the long wavelength onset of the absorption band made an accurate determination of the energy band gap impossible. The energy band gaps of the four semiconducting polymer thin films determined using UV-vis spectroscopy and electrochemical studies are presented in Table 4.1.

The semiconducting polymers prepared by surface-initiated stepwise Sonogashira polymerization are expected to display uniform chain alignment in the direction perpendicular to the substrate surface and form a highly ordered densely packed bulk film. This is due to the highly rigid rod-like nature of the PPE macromolecules. To compare the polymer chain organization in surface-

confined thin films with the structure of thin films prepared by spin-casting method, the corresponding soluble analogs of **TFDM** and **DMBTD**, conjugated polymers **4-P1** (M_n 5.9 kDa; PDI 1.8) and **4-P2** (M_n 22.3 kDa; PDI 3.1) were synthesized by conventional Sonogashira polymerization. As the analog of **TFDM**, the solution of **4-P1** in $CHCl_3$ showed a UV-vis absorbance maximum at 443 nm, which was assigned to charge transfer between electron donating and accepting units. The spin-casted **4-P1** thin film showed a similar absorbance signature with an additional shoulder at 500 nm and an onset-tail implying the increased intermolecular electronic delocalization. In sharp contrast, the UV-vis of **TFDM** showed a 40 nm hypsochromic shift relative to **4-P1** in $CHCl_3$. In the case of **DMBTD**, a blue shift in absorption (40 nm) was observed compared to the soluble analog **4-P2** in toluene (λ_{abs} 524 nm), while its spin-casted thin film showed a 40 nm bathochromic shift.

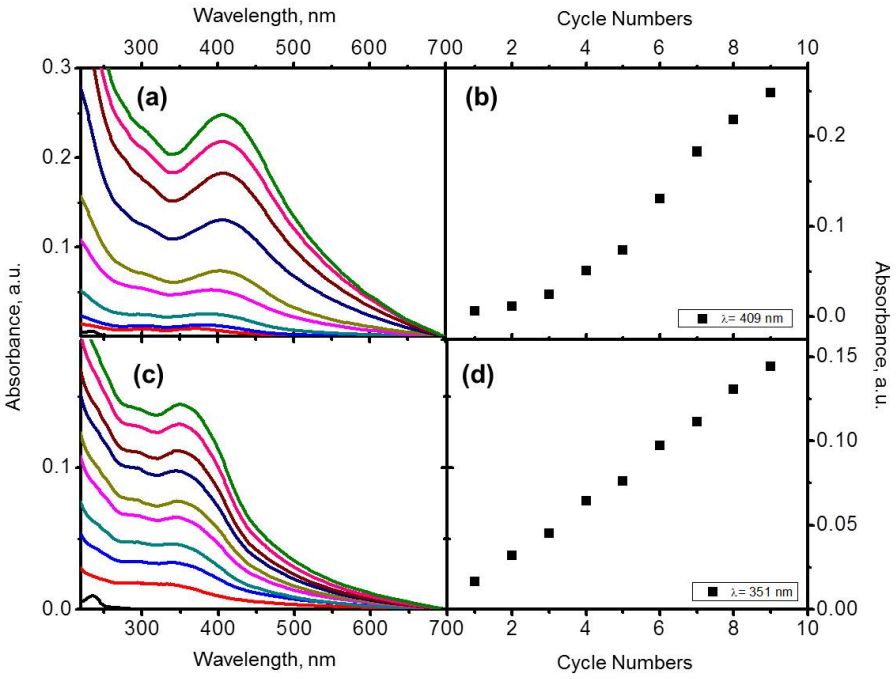

Figure 4.2. UV-vis tracking of the growth of thin films of (a) **DMDM** and (c) **TFTF**; linear relationship of E_{abs} and cycle numbers of (b) **DMDM** and (d) **TFTF.**

These unusual results indicated that the alignment of polymer chains in the thin films prepared by surface-initiated polymerization was intrinsically different from the nanoscale organization of the thin films prepared by spin-casting of the soluble analogs. Bathochromic shifts

in absorption spectra are usually reported for spin-cast films because spin-casting procedure mechanically disperses isolated polymers on substrates leading to random molecular alignments. However, the substantial hypsochromic shifts in absorption spectra of **TFDM** and **DMBTD** thin films would be the consequence of a predominant normal to surface uniform alignment of the polymer backbones, in which the neighboring interacting π-conjugated units could form face-to-face stacked aggregates (similar to H-aggregates). Nevertheless, the broad bands with long wavelength tailing in absorption spectra of the thin films could stem from the mixture of face-to-face and head-to-tail aggregates (similar to J-aggregates).

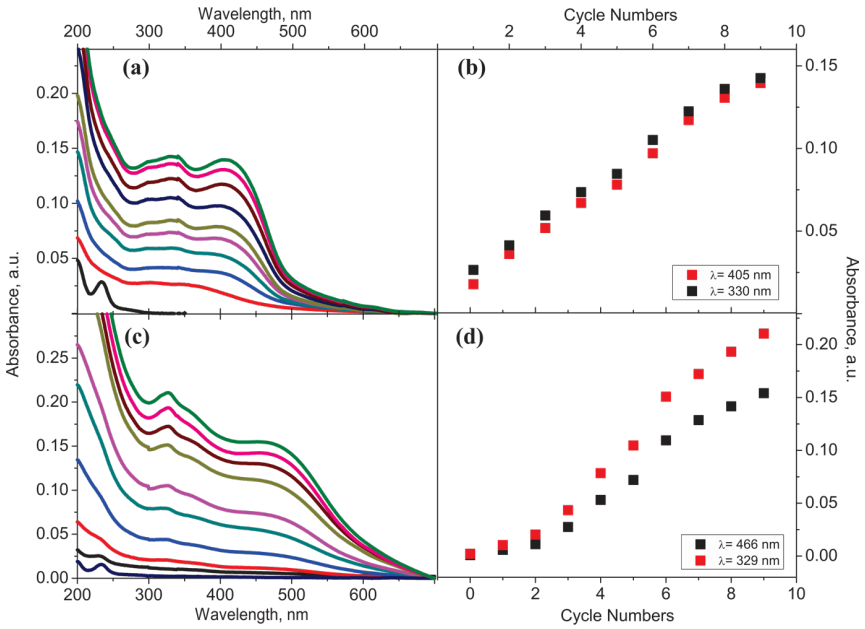

Figure 4.3. UV-vis tracking of the growth of thin films of (a) **TFDM** and (c) **DMBTD**; linear relationship of E_{abs} and cycle numbers of (b) **TFDM** and (d) **DMBTD.**

4.4 Morphology and Uniformity of PPE Thin Films.

The surface morphology of **TFDM** and **DMBTD** thin films was analyzed by atomic force microscopy (AFM). Both thin films revealed a dense surface coverage with exceedingly smooth morphology. The thin film of **DMBTD** was composed of numerous uniform circular domains of average diameter 35 nm (Figure 4.6) with an approximate RMS roughness of 2.4 nm. The similarly shaped circular domains (60 nm in average diameter) were also observed in **TFDM** thin film

(Figure 4.5). The formation of circular domains could stem from the polymer backbone structure and supramolecular alignment of the surface-confined polymer in the bulk thin films. The dense surface morphology with circular domains for the thin films was highly reproducible throughout this study.

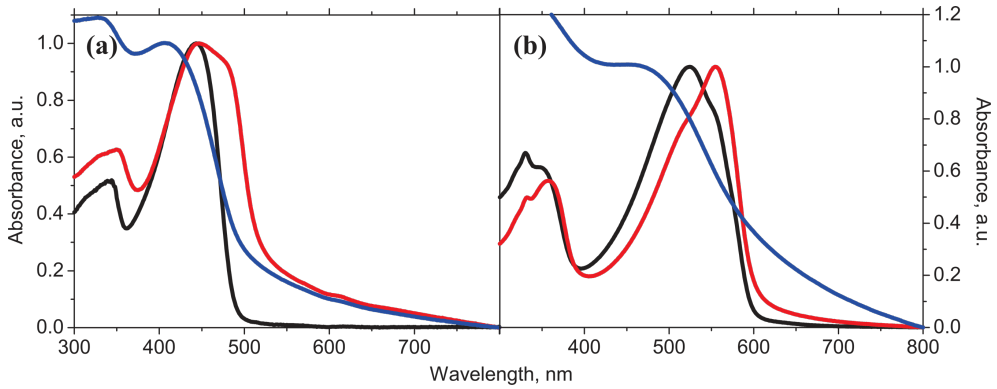

Figure 4.4. (a) Superimposed UV-vis spectra of **TFDM** from solution (black), spin-casting (red) and grafting-from (blue); (b) Supreimposed UV-vis spectra of **DMBTD** from solution (black), spin-casting (red) and grafting-from (blue).

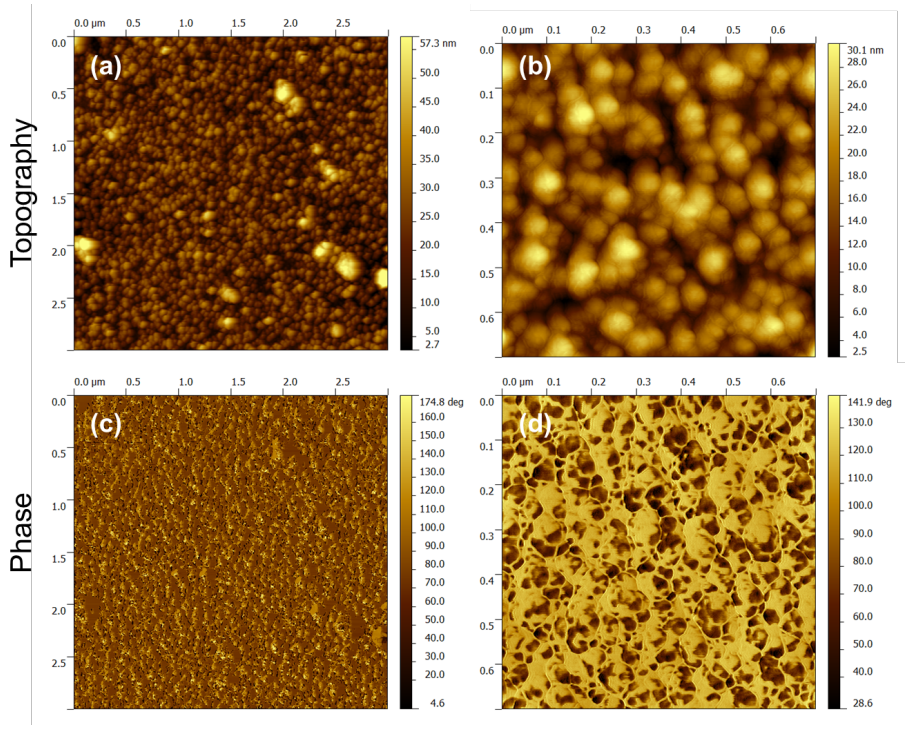

Figure 4.5. Representative tapping mode AFM image of **TFDM** on quartz substrate. The topography (a) and phase (c) in 3 μm x 3 μm scan area; and the zoom-in topography (b) and phase (d) in 0.7 μm x 0.7 μm scan area.

To further evaluate nanoscale details and across-the-film structure of the semiconducting thin films, we prepared deuterated **DMBTD** (***d*-DMBTD**) thin films for neutron reflectometry studies. Neutron scattering is considered as a "soft" method, compared to X-ray scattering, and shows high sensitivity to deuterium element than hydrogen since they possess different scattering cross-section for neutrons. In the scattering length density (SLD) profile based on the best fitting model (Figure 4.X), we clearly observed the thickness of ***d*-DMBTD** around 14.5 nm, which was in a good match with the theoretical value (13.2 nm) assuming the polymer chains were aligned normally to the substrate. The constant scattering length density (SLD) of approximately 2.8×10^{-6} $Å^{-2}$ across 80% of the thin film thickness and the corresponding mass density of this high-density region calculated from this SLD value was 0.87 g cm^{-3}, indicating that the thin film consisted of densely packed ***d*-DMBTD** polymer chains.

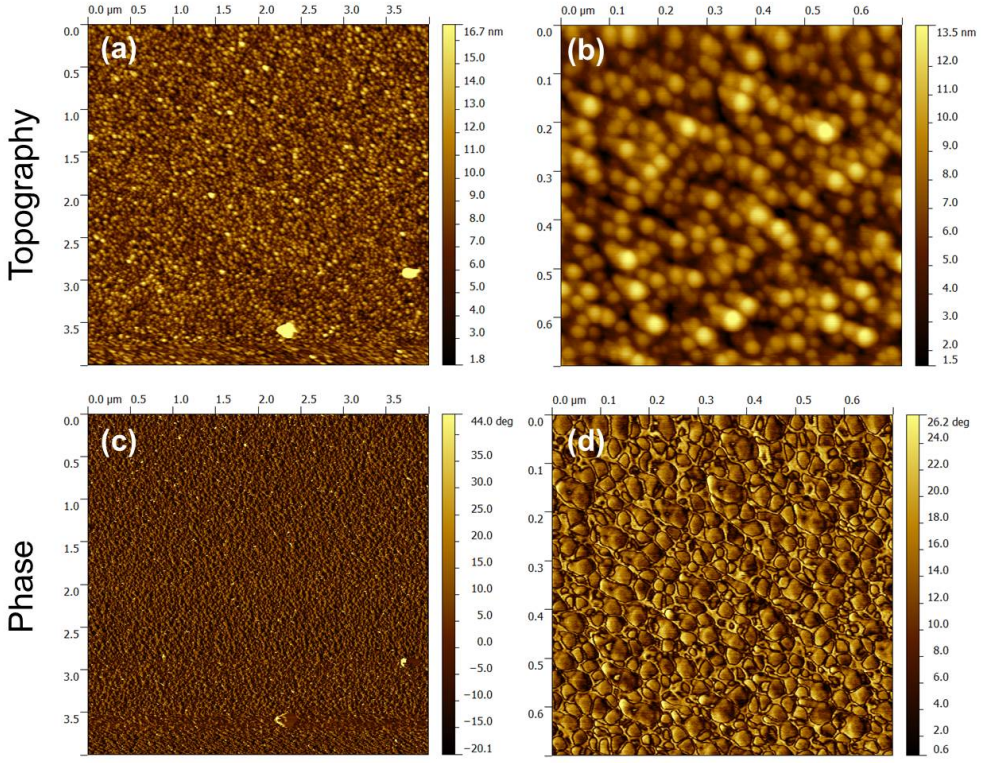

Figure 4.6. Representative tapping mode AFM image of **DMBTD** on quartz substrate. The topography (a) and phase (c) in 4 µm x 4 µm scan area; and the zoom-in topography (b) and phase (d) in 0.7 µm x 0.7 µm scan area.

4.5 Electrochemical Properties of PPE Thin Films.

All the PPE thin films were found remarkably stable and unaffected by prolonged sonication in organic solvents ($CHCl_3$, toluene, THF, acetone, MeOH, and EtOH) and water. Electrochemical studies of the thin films were conducted by cyclic voltammetry (CV) using thin films on ITO substrates as working electrodes and 0.1 M solution of *n*-Bu_4NPF_6 in acetonitrile as the supporting electrolyte. **DMDM**, **TFTF**, and **TFDM** showed irreversible oxidation or reduction features over the scans, but we were able to acquire information about their electronic energy levels before the degradation. As shown in table 4.1, the highest occupied molecular orbital energy level of **DMDM** (E_{HOMO}) was estimated at –5.99 eV against vacuum level. The lowest

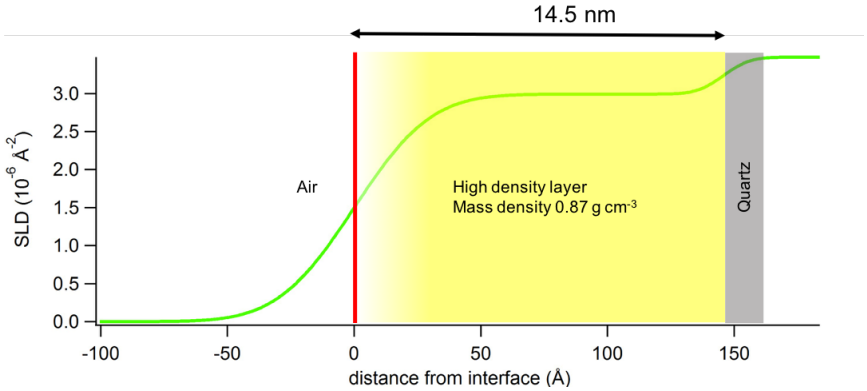

Figure 4.7. Neutron reflectometry study of ***d*-DMBTD** thin film prepared by surface-initiated stepwise Sonogashira polymerization on a quartz substrate.

Table 4.1. Electrochemical Onset Potentials and Electronic Energy Levels of the Polymer Thin Films.

	φ_{ox}(V vs Fc/Fc^+)/ E_{HOMO} (eV)[a]	φ_{red}(V vs Fc/Fc^+)/ E_{LUMO} (eV)[b]	E_g^{ec} (eV)	E_g^{opt} (eV)[c]
DM	0.89/-5.99	n.a.[d]/-3.51[e]	n.a.[d]	2.48
TF	n.a.[d]/-6.52[e]	-1.17/-3.93	n.a.[d]	2.59
TFDM	1.05/-6.15	-1.37/-3.73	2.42	2.45
DMBTD	0.54/-5.64	-0.86/-4.24	1.40	1.87
4-P1	0.89/-5.99	-1.43/-3.67	2.32	2.38
4-P2	0.56/-5.66	-1.33/-3.77	1.89	2.04

[a]Calculated according to the equation: $E_{HOMO} = -(\varphi_{ox} + 5.1)$ (eV). [b]Calculated according to the equation: $E_{LUMO} = -(\varphi_{red} + 5.1)$ (eV). [C]Estimated from the onset wavelength of the absorption spectra: $E_g^{opt} = 1240/\lambda_{onset}$. [d]Measurement on the cyclic voltammograms is unavailable. [e]Calculated according to the equation: $E_g^{opt} = E_{LUMO} - E_{HOMO}$.

unoccupied molecular orbital energy level of **TFTF** (E_{LUMO}) was determined at –3.93 eV. The E_{HOMO} and E_{LUMO} of **TFDM** were at –615 and –3.73 eV, respectively. These energy levels were in line with the values found from common semiconducting polymers. **DMBTD** gave E_{HOMO} at –5.64 eV and E_{LUMO} at -4.24 eV, and as expected, its energy band gap was slightly lower than 2.0 eV due to the strong donor-acceptor electronic coupling.

4.6 Conclusions

We have developed preparation of surface-confined semiconducting poly(*p*-phenylene ethynylene) thin films *via* stepwise Sonogashira polymerization. This efficient and yet unprecedented approach allowed us to prepare PPE thin film with precise structure and controlled nanoscale morphology. All the thin films showed excellent chemical and mechanical tolerance. Both **TFDM** and **DMBTD** showed unusual hyposchromic shifts in E_{abs} and long vibronic tails relative to their spin-casting counterparts, which was due to the highly dense uniform packing and face-to-face stacking of the π-conjugated units. AFM studies showed smooth morphology for **DMBTF** and good RMS roughness. Furthermore, the thickness of ***d*-DMBTF** thin film obtained using neutron reflectometry exhibited excellent match to the theoretical value assuming uniform normal-to-surface orientation of the conjugated macromolecules.

4.7 References

(1) Lee, J. K.; Ma, W. L.; Brabec, C. J.; Yuen, J.; Moon, J. S.; Kim, J. Y.; Lee, K.; Bazan, G. C.; Heeger, A. J. Processing Additives for Improved Efficiency from Bulk Heterojunction Solar Cells. *J. Am. Chem. Soc.* **2008**, *130*, 3619–3623.

(2) Li, G.; Shrotriya, V.; Huang, J.; Yao, Y.; Moriarty, T.; Emery, K.; Yang, Y. High-Efficiency Solution Processable Polymer Photovoltaic Cells by Self-Organization of Polymer Blends. *Nat. Mater.* **2005**, *4*, 864–868.

(3) Park, L. Y.; Munro, A. M.; Ginger, D. S. Controlling Film Morphology in Conjugated Polymer:Fullerene Blends with Surface Patterning. *J. Am. Chem. Soc.* **2008**, *130*, 15916–15926.

(4) Geng, R.; Roy, A.; Zhao, W.; Subedi, R. C.; Li, X.; Locklin, J.; Nguyen, T. D. Engineering of Spin Injection and Spin Transport in Organic Spin Valves Using π-Conjugated Polymer Brushes. *Adv. Funct. Mater.* **2016**, *26*, 3999–4006.

(5) Paoprasert, P.; Spalenka, J. W.; Peterson, D. L.; Ruther, R. E.; Hamers, R. J.; Evans, P. G.; Gopalan, P. Grafting of Poly(3-Hexylthiophene) Brushes on Oxides Using Click Chemistry. *J Mater Chem* **2010**, *20*, 2651–2658.

(6) Moon, J. H.; Swager, T. M. Poly(*p*-Phenylene Ethynylene) Brushes. *Macromolecules* **2002**, *35*, 6086–6089.

(7) Notestein, J. M.; Canlas, C.; Siegfried, J.; Moore, J. S. Covalent Grafting of *m*-Phenylene-Ethynylene Oligomers to Oxide Surfaces. *Chem. Mater.* **2010**, *22*, 5319–5327.

(8) Youm, S. G.; Hwang, E.; Chavez, C. A.; Li, X.; Chatterjee, S.; Lusker, K. L.; Lu, L.; Strzalka, J.; Ankner, J. F.; Losovyj, Y.; et al. Polythiophene Thin Films by Surface-Initiated Polymerization: Mechanistic and Structural Studies. *Chem. Mater.* **2016**, *28*, 4787–4804.

(9) Senkovskyy, V.; Khanduyeva, N.; Komber, H.; Oertel, U.; Stamm, M.; Kuckling, D.; Kiriy, A. Conductive Polymer Brushes of Regioregular Head-to-Tail Poly(3-Alkylthiophenes) via Catalyst-Transfer Surface-Initiated Polycondensation. *J. Am. Chem. Soc.* **2007**, *129*, 6626–6632.

(10) Khanduyeva, N.; Senkovskyy, V.; Beryozkina, T.; Horecha, M.; Stamm, M.; Uhrich, C.; Riede, M.; Leo, K.; Kiriy, A. Surface Engineering Using Kumada Catalyst-Transfer Polycondensation (KCTP): Preparation and Structuring of Poly(3-Hexylthiophene)-Based Graft Copolymer Brushes. *J. Am. Chem. Soc.* **2009**, *131*, 153–161.

(11) Beryozkina, T.; Boyko, K.; Khanduyeva, N.; Senkovskyy, V.; Horecha, M.; Oertel, U.; Simon, F.; Stamm, M.; Kiriy, A. Grafting of Polyfluorene by Surface-Initiated Suzuki Polycondensation. *Angew. Chem. Int. Ed.* **2009**, *48*, 2695–2698.

(12) Sontag, S. K.; Marshall, N.; Locklin, J. Formation of Conjugated Polymer Brushes by Surface-Initiated Catalyst-Transfer Polycondensation. *Chem. Commun.* **2009**, *23*, 3354-3356.

(13) Marshall, N.; Sontag, S. K.; Locklin, J. Substituted Poly(*p*-Phenylene) Thin Films via Surface-Initiated Kumada-Type Catalyst Transfer Polycondensation. *Macromolecules* **2010**, *43*, 2137–2144.

(14) Kang, S.; Ono, R. J.; Bielawski, C. W. Controlled Catalyst Transfer Polycondensation and Surface-Initiated Polymerization of a *p*-Phenyleneethynylene-Based Monomer. *J. Am. Chem. Soc.* **2013**, *135*, 4984–4987.

(15) Marshall, N.; Sontag, S. K.; Locklin, J. Surface-Initiated Polymerization of Conjugated Polymers. *Chem. Commun.* **2011**, *47*, 5681-5689.

(16) Jhaveri, S. B.; Peterson, J. J.; Carter, K. R. Poly(9,9-Dihexylfluorene) Layers Grown via Surface-Directed Ni(0) Condensation Polymerization. *Langmuir* **2009**, *25*, 9552–9556.

(17) Beinhoff, M.; Appapillai, A. T.; Underwood, L. D.; Frommer, J. E.; Carter, K. R. Patterned Polyfluorene Surfaces by Functionalization of Nanoimprinted Polymeric Features. *Langmuir* **2006**, *22*, 2411–2414.

(18) Müllen, K.; Pisula, W. Donor–Acceptor Polymers. *J. Am. Chem. Soc.* **2015**, *137*, 9503–9505.

(21) Wu, J.-S.; Cheng, S.-W.; Cheng, Y.-J.; Hsu, C.-S. Donor–acceptor Conjugated Polymers Based on Multifused Ladder-Type Arenes for Organic Solar Cells. *Chem Soc Rev* **2015**, *44*, 1113–1154.

(22) Bunz, U. H. F. Poly(Aryleneethynylene)s: Syntheses, Properties, Structures, and Applications. *Chem. Rev.* **2000**, *100*, 1605–1644.

(23) Seehafer, K.; Bender, M.; Bunz, U. H. F. Aggregation, Acidochromicity, and Metallochromicity of a Pyridine-Based Poly(Aryleneethynylene). *Macromolecules* **2014**, *47*, 922–927.

(24) Woody, K. B.; Bullock, J. E.; Parkin, S. R.; Watson, M. D. Alternating Arene−Perfluoroarene Poly(Phenylene Ethynylenes). *Macromolecules* **2007**, *40*, 4470–4473.

(25) Pawle, R. H.; Agarwal, A.; Malveira, S.; Smith, Z. C.; Thomas, S. W. Bandgap Engineering of Conjugated Materials with Nonconjugated Side Chains. *Macromolecules* **2014**, *47*, 2250–2256.

(26) Dutta, T.; Woody, K. B.; Parkin, S. R.; Watson, M. D.; Gierschner, J. Conjugated Polymers with Large Effective Stokes Shift: Benzobisdioxole-Based Poly(Phenylene Ethynylene)s. *J. Am. Chem. Soc.* **2009**, *131*, 17321–17327.

(27) Bunz, U. H. F. Poly(Aryleneethynylene)s. *Macromol. Rapid Commun.* **2009**, *30*, 772–805.

(28) Hwang, E.; Lusker, K. L.; Garno, J. C.; Losovyj, Y.; Nesterov, E. E. Semiconducting Polymer Thin Films by Surface-Confined Stepwise Click Polymerization. *Chem. Commun.* **2011**, *47*, 11990-11992.

CHAPTER 5. EXPERIMENTAL SECTION

5.1 General Considerations

All reactions were performed under an atmosphere of dry nitrogen, except those that required Schlenk techniques, which were conducted under an atmosphere of ultrapure argon. Melting points were determined in open capillaries and were uncorrected. Chromatographic separations were carried out on silica gel (Sorbent Technologies, 60 Å, 40-63 μm, pH = 6.0-7.0) slurry packed into glass columns. Toluene, THF, DCM, ether, and hexane were dried by passing through columns of activated alumina and *N,N*-dimethylformamide (DMF) was dried through a column of molecular sieves both contained in a PS-400 Solvent Purification System from Innovative Technologies, Inc. The water content in the solvents was periodically controlled by coulometric titration on a Mettler Toledo DL 32 diaphragm-less coulometric titrator. Tetrabutylammonium hexafluorophosphate for electrochemical measurements was obtained from Aldrich and used after recrystallization from ethanol. Isopropylmagnesium chloride (2.0 M solution in THF) was purchased from Acros Organic, organometallic reagents were titrated with salicylaldehyde phenylhydrazone prior to use.[1] High purity $Pd(PPh_3)_4$ was obtained from Stem, while all other reagents were obtained from Sigma-Aldrich and Alfa Aesar and used as received. Indium tin oxide (ITO) coated glass slides (25x75x1.1 mm^3 polished float glass, 8-12 Ohm/sq. surface resistivity) were purchased from Delta Technologies, Ltd. 75x25 mm^2 sized polished rectangular quartz slides were purchased from Chemglass. ^1H NMR spectra were recorded at 400 MHz or 500 MHz unless otherwise indicated and were reported in parts per million downfield from tetramethylsilane. GPC analysis of polymers was performed with an Agilent 1100 chromatograph equipped with two PLgel 5 μm MIXED-C and one PLgel 5 μM 1000 Å columns connected in series, using THF as a mobile phase, and calibrated against polystyrene standard.

Dialysis purification was carried out using Spectrum Laboratories, Inc. Spectra/Por® dialysis tubing with MWCO 3.5kDa or 8kDa. DFT computations were performed under Windows version of Gaussian 09 computational package.[2] UV-vis absorption spectra were recorded on an Agilent Cary 5000 UV-Vis-NIR spectrometer. Fluorescence studies were carried out using a PTI QuantaMaster4/2006SE spectrofluorimeter. Electrochemical measurements were carried out using a three-electrode system with Pt button working electrode (diameter 2mm), $Ag/AgNO_3$ non-aqueous reference electrode, and Pt wire counter electrode. Polymer thin film attached ITO substrate was used to replace Pt button working electrode when solid state measurement was necessary. The reference electrode was checked against ferrocene standard every time before and after the experiments were performed, and the measured potentials were corrected based on the Fc/Fc^+ redox potential value. All experiments were carried out in 0.1 M Bu_4NPF_6 solution in THF or DCM as supporting electrolyte. High resolution mass spectra were obtained at the LSU Department of Chemistry Mass Spectrometry Facility.

5.2 Substrate Cleaning and Activation

Rectangular quartz slides (75 x 25mm) were cut using a ceramic cutting. The glass pieces were then washed with hexane, DMC, acetone, methanol, and then water for 30 minutes each under sonication. The slides were then thoroughly dried under a flow of nitrogen. The cleaned slides were placed in 20 mL scintillation vials and filled with freshly prepared piranha solution (7:3 H_2SO_4:30% H_2O_2) until the cover slip was submerged. (**CAUTION:** Piranha solutions are extremely corrosive and oxidizing. It must be prepared carefully due to exothermic mixing. Ensure that all contact surfaces are clean and free of any solvents from previous washings or other organic contaminants or else explosive conditions can be generated.) The vials were placed at rt for 1 h, then the slide removed and rinsed with copious amounts of Millipore-filtered water. The

rinsed slides were then dried under a flow of nitrogen and protected from dust and other particulates for 3 hours and were then ready for immobilization. ITO was activated using "basic piranha" (NH_4OH:H_2O_2:Water, 1:1:5) and prewashed using the same procedure as the glass slides. And placed at 75°C for 1, then the slide removed and rinsed with copious amounts of Millipore-filtered water. The rinsed slides were then dried under a flow of nitrogen and protected from dust and other particulates for 3 hours and were then ready for immobilization.

5.3 Atomic Force Microscopy

Samples were characterized with a model 5500 atomic force microscope (AFM) equipped with Picoscan v5.3.3 software (Agilent Technologies, Chandler, Az). Images were acquired using tapping mode in ambient condition. Nanoshaving was conducted using contact mode. Oxide-sharpened silicon nitride cantilevers with force constants ranging from 0.1 to 0.6 N/m were used for imaging (Veeco Probes, Santa Barbara, CA). Digital images were processed with Gwyddion open source software (version 2.9), which is supported by the Czech Metrology Institute.[3]

5.4 Neutron Reflectometry

Neutron reflectivity measurements were performed at the Spallation Neutron Source Liquids Reflectometer (SNS-LR, Beamline 4B) at the ORNL. The reflectivity data were collected using a sequence of 3.25-Å-wide continuous wavelength bands (selected from 2.63 Å < λ < 16.63 Å) and incident angles (ranging over 0.60° < θ < 2.71°), where λ is the neutron wavelength and θ is the scattering angle. Using these settings, the momentum transfer, $q = (4\pi \sin \theta/\lambda)$ was varied over a range of 0.008 $Å^{-1} < q < 0.22$ $Å^{-1}$. Reflectivity curves were assembled by combining seven different wavelength and angle data sets together, maintaining a constant sample footprint and relative instrumental resolution of $\delta q/q = 0.023$ by varying the incident-beam apertures.

The reduced data consisted of absolute neutron reflectivity (R) *vs.* neutron momentum transfer q. *Layers*[4] and *Motofit*[5] software were used to fit the measured reflectivity curves, providing the reflectivity of a model scattering length density profile, which can be analyzed to determine the structure of the thin films. One or two layers were used to model the depth profiles of the films. The scattering length density, thickness, and roughness of each layer was freely varied in the fitting procedure. The quality of fit was gauged by minimizing χ^2 between data and model reflectivity curves.

5.5 Supporting Information Associated to Chapter II

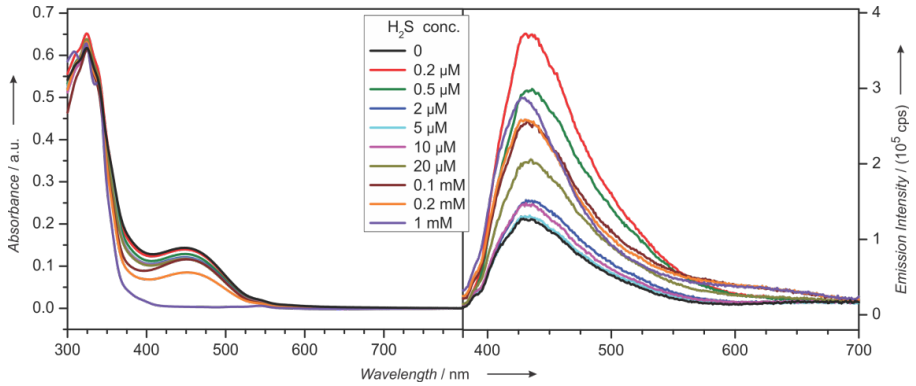

Figure 5.1. Change in absorption (left) and fluorescence (right) spectra of a 13.3 μM solution of the small-molecule sensor **2-M1** in acetonitrile upon addition of increasing concentrations of H_2S (the spectra were acquired in 6 min after H_2S addition).

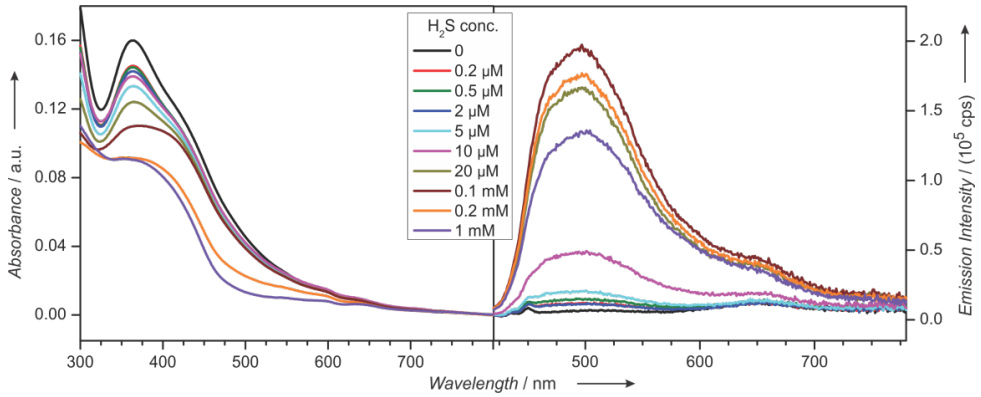

Figure 5.2. Change in absorption (left) and fluorescence (right) spectra of a 10.8 μM solution of the lower molecular weight polymer sensor **2-P1b** in acetonitrile upon addition of increasing concentrations of H_2S (the spectra were acquired in 6 min after H_2S addition).

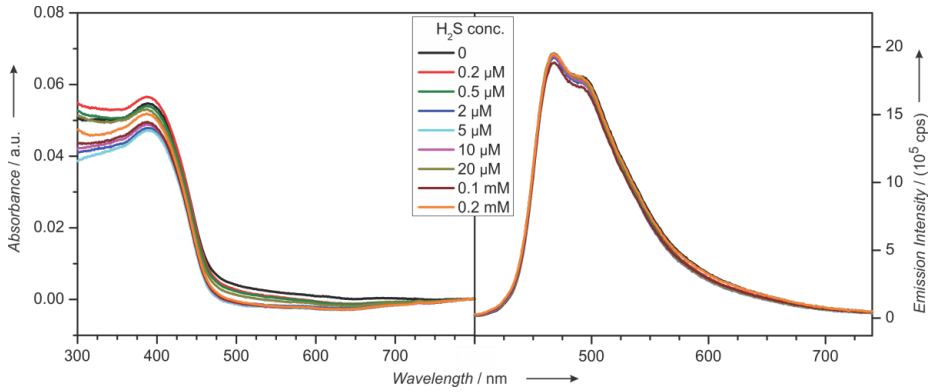

Figure 5.3. Absorption (left) and fluorescence (right) spectra of a 10.0 μM solution of the control polymer **2-P2** in acetonitrile upon addition of increasing concentrations of H_2S (the spectra were acquired in 6 min after H_2S addition).

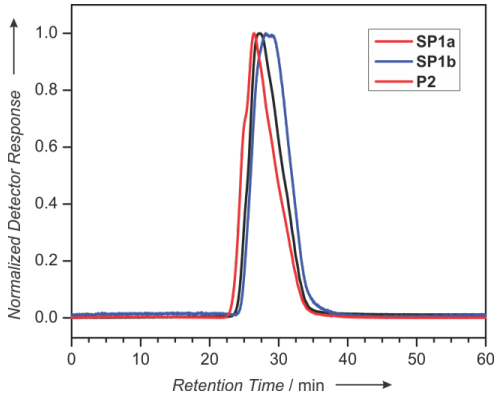

Figure 5.4. GPC elution traces for conjugated polymers **2-SP1a** and **2-SP1b** (precursors to sensor polymers **2-P1a** and **2-P1b**), and **2-P2**. Experimental conditions: solvent THF, flow rate 0.7 mL min^{-1}, UV/vis absorbance detection at 450 nm.

5.6 Supporting Information Associated to Chapter IV

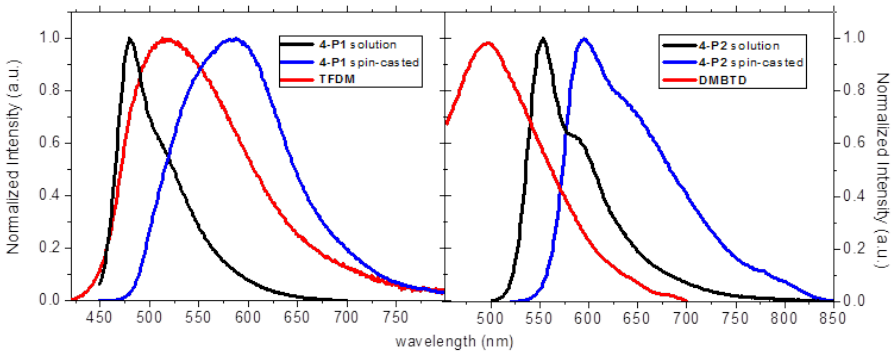

Figure 5.5. Photoluminescence spectra of **TFDM**, **4-P1** in DCM, and spin-casted **4-P1** (left), and **DMBTD**, **4-P2** in toluene, and spin-casted **4-P2**.

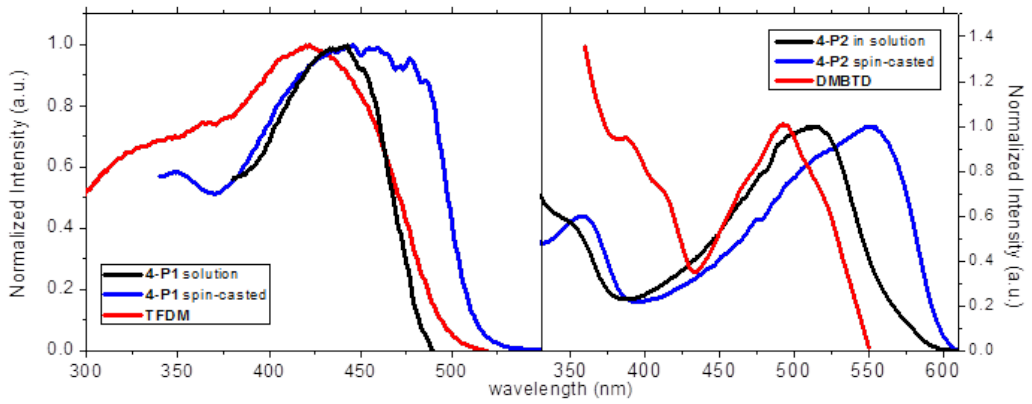

Figure 5.6. Excitation spectra of **TFDM**, **4-P1** in DCM, and spin-casted **4-P1** (left), and **DMBTD**, **4-P2** in toluene, and spin-casted **4-P2**.

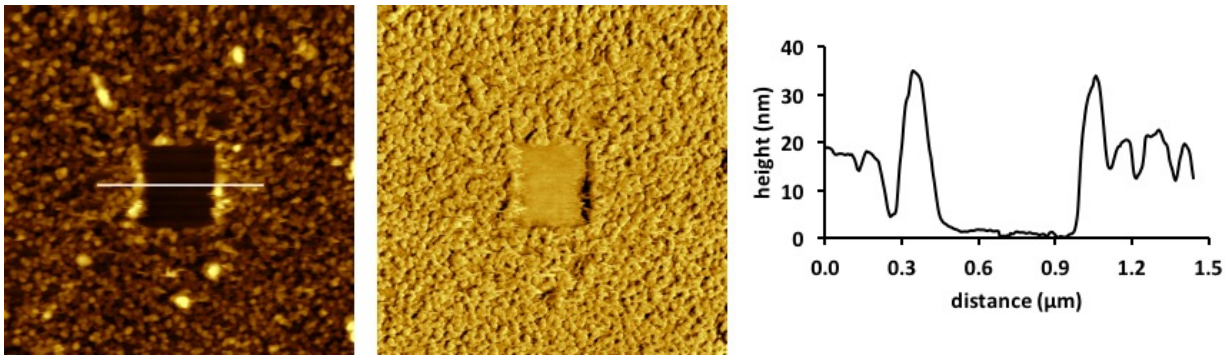

Figure 5.7. Determination of **TFDM** film thickness by "nanoshaving" to reference the quartz substrate as a baseline in a scanning area of 3 µm x 3 µm; topography (left), phase (middle) and cursor profile (right).

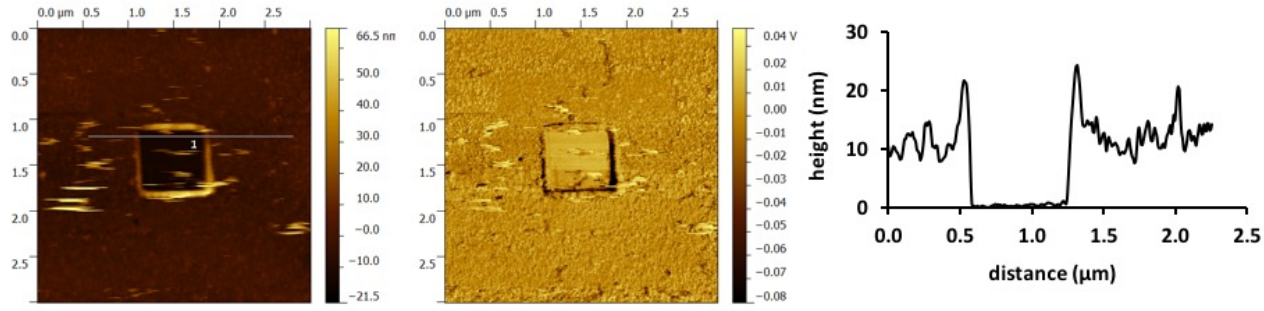

Figure 5.8. Determination of **DMBTD** film thickness by "nanoshaving" to reference the quartz substrate as a baseline in a scanning area of 3 µm x 3 µm; topography (left), phase (middle) and cursor profile (right).

5.7 Synthetic Details

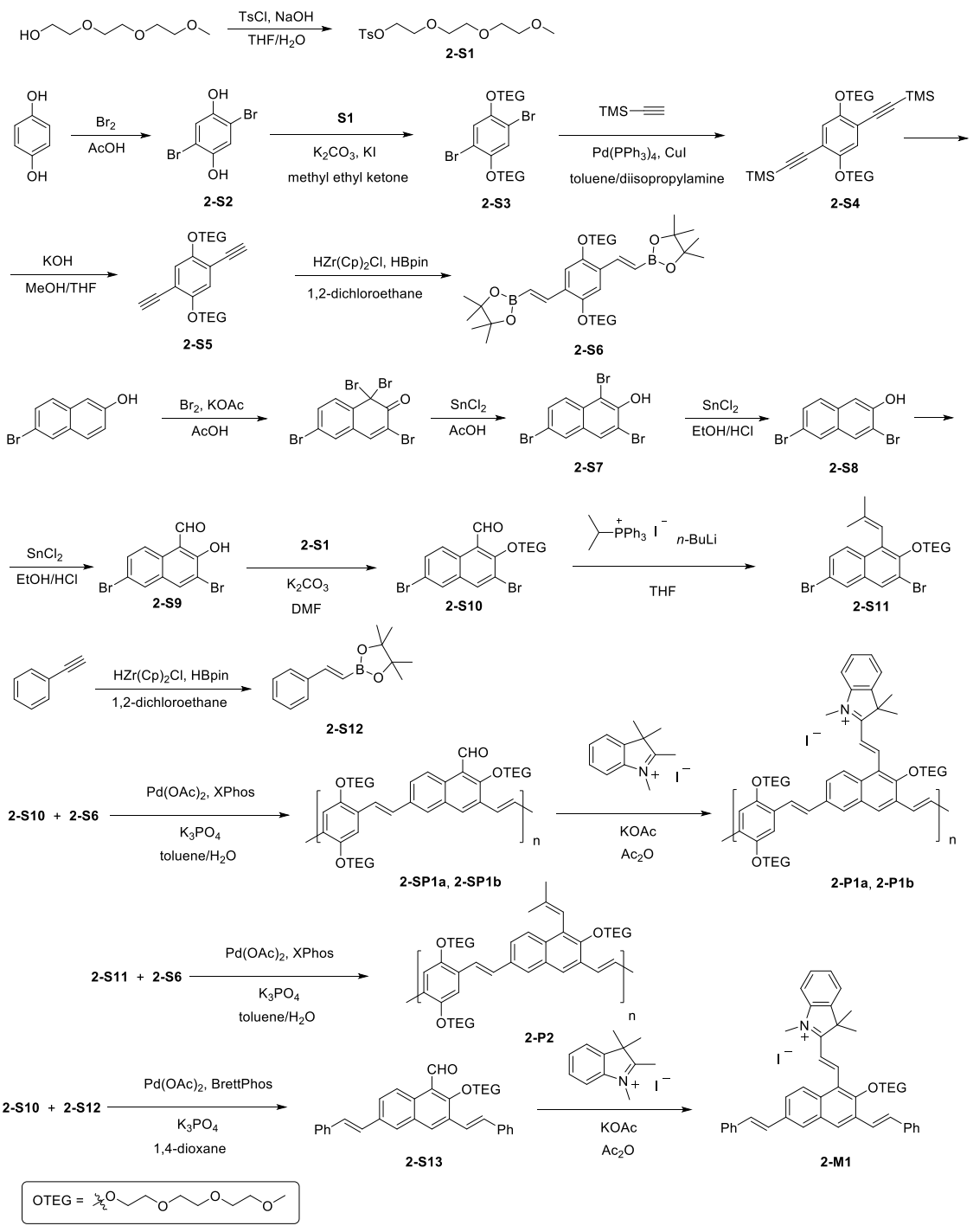

Scheme 5.1. Synthesis of polymer sensors **2-P1a-b**, control polymer **2-P2**, and small-molecule sensor **2-M1**.

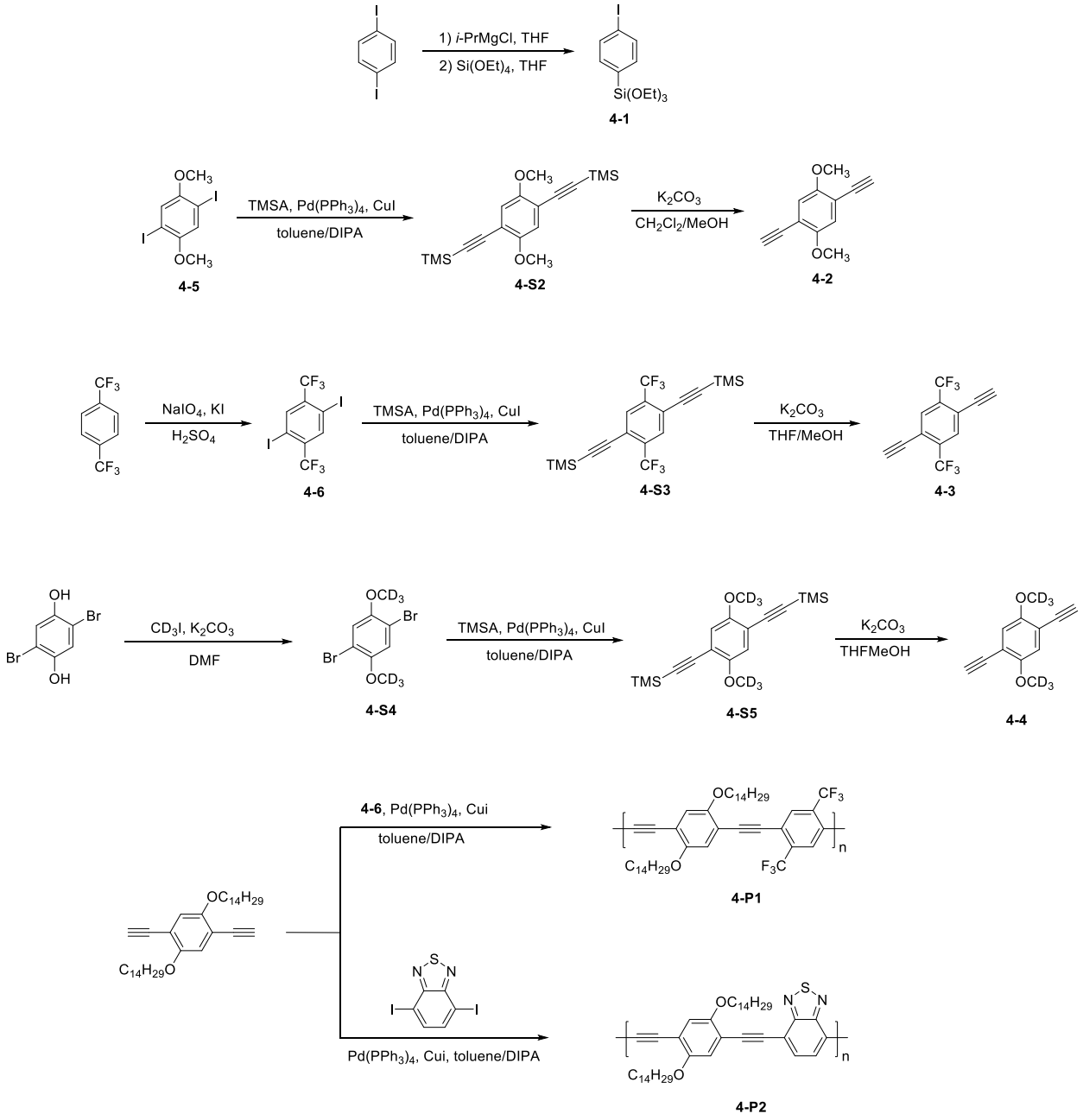

Scheme 5.2. Synthesis of small molecule building blocks, and soluble polymer **4-P1** and **4-P2**.

Triethylene glycol monomethyl ether tosylate (2-S1)[6] **and 1,4-dibromo-2,5-bis(2-(2-(2-methoxyethoxy)ethoxy)ethoxy)benzene (2-S3)**[7] were prepared generally following established literature procedures.

1,4-bis(2-(2-(2-Methoxyethoxy)ethoxy)ethoxy)-2,5-((trimethylsilyl)ethynyl)ben-zene (2-S4). A solution of 1.75 g (17.8 mmol) of trimethylsilylacetylene, 2.53 g (4.46 mmol) of **2-S3**, 103 mg (88.7 μmol) of $Pd(PPh_3)_4$, and 25.1 mg (0.131 mmol) of CuI in 150 mL of toluene/*i*-Pr_2NH (7:3) mixture was stirred in a sealed Airfree flask at 70 °C for 48 h. After allowing to cool down to room temperature, the reaction mixture was filtered through a glass filter, and the filtrate was concentrated in vacuo. The crude product was purified by column chromatography on silica gel (eluent ethyl acetate – CH_2Cl_2 (1:5)) to afford 2.15 g (78%) of **2-S4** as a colorless liquid that slowly solidified into a white waxy solid, R_f 0.38. ^{1}H NMR (400 MHz, $CDCl_3$) δ 6.93 (s, 2H), 4.14 (t, *J* = 4.8 Hz, 4H), 3.89 (t, *J* = 4.8 Hz, 4H), 3.81 (t, *J* = 4.8 Hz, 4H), 3.70-3.66 (m, 8H), 3.57 (t, *J* = 4.8 Hz, 4H), 3.40 (s, 6H), 0.27 (s, 18H).

1,4-bis(2-(2-(2-Methoxyethoxy)ethoxy)ethoxy)-2,5-diethynylbenzene (2-S5). A solution of 317 mg (5.65 mmol) of KOH in 132 mL of MeOH/THF (1:3) was added into a solution of 1.41 g (2.35 mmol) of **2-S4** in 48 mL of THF, and the resulting solution was stirred at room temperature for 1 h. The reaction mixture was poured into water, extracted with dichloromethane (3 X 100 mL) and the organic fraction was washed with water (3 X 100 mL), dried over Na_2SO_4, and concentrated in vacuo. The crude product was purified by column chromatography on silica gel (eluent ethyl acetate – CH_2Cl_2 (1:5)) to afford 990 mg (85%) of **2-S5** as a colorless liquid that slowly solidified into a white waxy solid at low temperature, R_f 0.43. ^{1}H NMR (400 MHz, $CDCl_3$) δ 6.99 (s, 2H), 4.15 (t, *J* = 4.8 Hz, 4H), 3.86 (t, *J* = 4.8 Hz, 4H), 3.77 (t, *J* = 4.8 Hz, 4H), 3.68-3.64 (m, 8H), 3.55 (t, *J* = 4.8 Hz, 4H), 3.37 (s, 6H), 3.33 (s, 2H).

1,4-bis(2-(2-(2-Methoxyethoxy)ethoxy)ethoxy)-2,5-bis((4,4,5,5-tetramethyl-1,3,2-dioxaborolan-1-yl)benzene (2-S6). A mixture of 800 mg (1.78 mmol) of **2-S5**, 707 mg (4.09 mmol) of pinacolborane, and 46.0 mg (0.178 mmol) of $ZrCp_2HCl$ in 20 mL of 1,2-dichloroethane

was stirred in a sealed Airfree flask at 65 °C for 72 h. After allowing to cool down to room temperature, the reaction mixture was poured into water, extracted with dichloromethane (3 X 100 mL), and the organic fraction was washed with water (3 X 100 mL), and dried over Na_2SO_4. Concentration in vacuo afforded crude product that was further purified by column chromatography on silica gel (eluent ethyl acetate – CH_2Cl_2 (1:1)) to afford 1.00 g (64%) of **2-S6** as a yellow sticky liquid that slowly solidified into a yellow solid at low temperature, R_f 0.30. ^{1}H NMR (400 MHz, $CDCl_3$) δ 7.70 (d, J = 18.6 Hz, 2H), 7.10 (s, 2H), 6.14 (d, J =18.6 Hz, 2H), 4.15-4.09 (m, 4H), 3.90-3.84 (m, 4H), 3.77-3.74 (m, 4H), 3.71-3.66 (m, 12H), 3.56-3.54 (m, 4H), 3.37 (s, 6H), 1.30 (s, 24H).

3,6-Dibromo-2-hydroxy-1-naphthaldehyde (2-S9) was prepared starting from 6-bromo-2-naphthol following the previously described procedure.[8]

3,6-Dibromo-2-(2-(2-methoxyethoxy)ethoxy)ethoxy)-1-naphthaldehyde (2-S10). A mixture of 1.03 g (3.03 mmol) of **2-S9**, 2.89 g (9.09 mmol) of **2-S1**, and 1.26 g (9.09 mmol) of K_2CO_3 in 15 mL of DMF was stirred at 80 °C for 48 h. After allowing to cool to room temperature, the reaction mixture was poured into ethyl acetate, washed successively with H_2O (3 X 50 mL) and brine, extracted with ethyl acetate (3 X 50 mL), and dried over Na_2SO_4. After concentrating in vacuo, the crude product was purified by column chromatography (eluent ethyl acetate – hexane (1:5)) to afford 1.19 g (82%) of **2-S10** as a yellow liquid which was slowly solidified as a white waxy solid at low temperature, R_f 0.43. ^{1}H NMR (400 MHz, $CDCl_3$) δ 10.82 (s, 1H), 9.09 (d, J = 9.2 Hz, 1H), 8.22 (s, 1H), 7.90 (d, J = 2.1 Hz, 1H), 7.70 (dd, J_1 = 9.2 Hz, J_2 = 2.1 Hz, 1H), 4.36 (t, J = 4.8 Hz, 2H), 3.92 (t, J = 4.8 Hz, 2H), 3.73-3.71 (m, 2H), 3.68-3.64 (m, 4H), 3.54 (t, J = 4.8 Hz, 2H), 3.37 (s, 3H).

3,6-Dibromo-2-(2-(2-(2-methoxyethoxy)ethoxy)ethoxy)-1-(2-methylprop-1-enyl)-naphthalene (2-S11). A solution of *n*-BuLi in hexanes (0.48 mL (0.768 mmol) of 1.6 M solution) was added dropwise into a solution of 327 mg (0.756 mmol) of isopropyltriphenylphosphonium iodide in 10 mL of THF at 0 °C. The resulting mixture was stirred at this temperature for 1 h, followed by addition of a solution of 200 mg (0.420 mmol) of **2-S10** in 10 mL of THF. The reaction mixture was stirred at room temperature for 16 h, then 10 mL of H_2O was added and the resulting mixture was stirred for 30 min. The solvents were removed under reduced pressure, and the residue was diluted with ethyl acetate and filtered through a pad of Celite. The filtrate was washed with water (3 X 100 mL), extracted with ethyl acetate (3 X 100 mL), dried over Na_2SO_4, and concentrated in vacuo. The crude product was purified by column chromatography on silica gel (eluent ethyl acetate – hexane (1:5)) to yield 193 mg (92%) of **2-S11** as a clear liquid, R_f 0.52. ^{1}H NMR (400 MHz, $CDCl_3$) δ 7.91 (s, 1H), 7.85 (s, 1H), 7.69 (d, J = 9.0 Hz, 1H), 7.50 (d, J = 9.0 Hz, 1H), 6.35 (s, 1H), 4.05 (t, J = 5.1 Hz, 2H), 3.84 (t, J = 5.1 Hz, 2H), 3.75 (t, J = 5.1 Hz, 2H), 3.70-3.65 (m, 4H), 3.55 (t, J = 5.1 Hz, 2H), 3.38 (s, 3H), 2.03 (s, 3H), 1.49 (s, 3H).

(*E*)-4,4,5,5-tetramethyl-2-styryl-1,3,2-dioxaborolane (2-S12). A mixture of 500 mg (4.89 mmol) of phenylacetylene, 1.82 g (14.3 mmol) of pinacolborane, and 126 mg (0.489 mmol) of $ZrCp_2HCl$ in 20 mL of 1,2-dichloroethane was stirred in a sealed Airfree flask at 65 °C for 72 h. After allowing to cool down to room temperature, the reaction mixture was poured into H_2O, extracted with dichloromethane (3 X 100 mL), washed with H_2O (3 X 100 mL), and dried over Na_2SO_4. Concentration in vacuo afforded crude product that was further purified by column chromatography on silica gel (eluent hexane – CH_2Cl_2 (3:1)) to afford 630 mg (59%) of **2-5** as a yellow sticky liquid, R_f 0.51 ^{1}H NMR (400 MHz, $CDCl_3$) δ 7.59 (d, J = 8.0 Hz, 2H), 7.42-7.29 (m, 4H), 6.19 (d, J = 18.4 Hz, 1H), 1.34 (s, 12H).

Precursor polymer 2-SP1a. A solution of 961 mg (4.53 mmol) of K_3PO_4 in 2 mL of H_2O was added into a solution of 297 mg (0.623 mmol) of **2-S10**, 400 mg (0.566 mmol) of **S6**, 6.00 mg (26.7 μmol) of $Pd(OAc)_2$ and 27.1 mg (56.8 μmol) of XPhos in 10 mL of toluene, and the resulting solution was stirred in a sealed Airfree flask at 60 °C for 60 h. After allowing to cool down to room temperature, the reaction mixture was precipitated in MeOH resulting in 261 mg (60%) of **2-SP1a** as a yellow sticky solid, M_n 20.3 kDa, PDI 2.44 (GPC, vs. polystyrene). ^{1}H NMR (400 MHz, CD_2Cl_2) δ 10.86 (s, 1H), 9.13 (s, 1H), 8.34 (s, 1H), 7.94 (s, 2H), 7.77-7.62 (m, 3H), 7.40-7.32 (m, 3H), 4.37-4.20 (m, 6H), 3.97-3.42 (m, 30H), 3.31-3.24 (m, 9H).

Precursor polymer 2-SP1b. A solution of 0.18 g (0.85 mmol) of K_3PO_4 in 1 mL of H_2O was added into a solution of 55 mg (0.12 mmol) of **2-S10**, 74 mg (0.11 mmol) of **2-S6**, 1.0 mg (5.3 μmol) of $Pd(OAc)_2$ and 42 mg (11 μmol) of XPhos in 5 mL of toluene, and the resulting solution was stirred in a sealed Airfree flask at 60 °C for 20 h. After allowing to cool down to room temperature, the reaction mixture was precipitated in MeOH resulting in 18 mg (20%) of **2-SP1b** as a yellow sticky solid, M_n 11.3 kDa, PDI 2.14 (GPC, vs. polystyrene). ^{1}H NMR spectrum was similar to that of polymer **2-SP1a**.

Polymer 2-P1a. A solution of 38 mg (49 μmol) of **2-SP1a**, 0.45 g (1.5 mmol) of 1,2,3,3-tetramethyl-3H-indolium iodide, and 0.15 g (1.5 mmol) of KOAc in 2 mL of Ac_2O was stirred at 80 °C for 2 h. The reaction mixture was allowed to cool down to room temperature, and Ac_2O was removed in vacuo. The residue was dissolved in dichloromethane, and precipitated in hexane, and the resulting brown solid was washed successively with ethyl acetate and acetone. The crude product was further purified by dialysis from acetonitrile for 24 h to afford 38 mg (81%) of **2-P1a** as a red sticky solid. The number average molecular weight M_n 27.7 kDa was calculated based on M_n of the precursor polymer **2-SP1a**. ^{1}H NMR (400 MHz, CD_2Cl_2) δ 8.95-8.91 (m, 1H), 8.40-8.33

(m, 2H), 8.12-8.02 (m, 3H), 7.81-7.58 (m, 7H), 7.48-7.27 (m, 3H), 4.33-4.28 (m, 9H), 3.99-3.43 (m, 30H), 3.31-3.24 (m, 9H), 2.03 (s, 6H).

Polymer 2-P1b was prepared following the procedure for polymer **2-P1a**, using 10 mg (13 μmol) of **2-SP1b**, 0.12 g (0.39 mmol) of 1,2,3,3-tetramethyl-3H-indolium iodide, and 38 mg (0.39 mmol) of KOAc in 1 mL of Ac_2O. This yielded 2 mg (17%) of **2-P1b** as a red sticky solid. The number average molecular weight M_n 15.5 kDa was calculated based on M_n of the precursor polymer **SP1b**. ^{1}H NMR spectrum was similar to that of polymer **2-P1a**.

Control polymer 2-P2. A solution of 0.26 g (1.2 mmol) of K_3PO_4 in 1 mL of H_2O was added into a solution of 80 mg (0.16 mmol) of **2-S11**, 0.11 g (0.15 mmol) of **2-S6**, 1.7 mg (7.6 μmol) of $Pd(OAc)_2$ and 7.1 mg (15 μmol) of XPhos in 5 mL of toluene, and the resulting solution was stirred in a sealed Airfree flask at 60 °C for 72 h. After allowing to cool down to room temperature, the reaction mixture was precipitated in MeOH to afford 50 mg (42%) of **2-P3** as a yellow sticky solid, M_n 15.9 kDa, PDI 2.24 (GPC, vs. polystyrene). ^{1}H NMR (400 MHz, CD_2Cl_2) δ 8.09-6.95 (m, 10H), 6.45-6.34 (m, 1H), 4.30- 3.28 (m, 45H), 2.06 (s, 3H), 1.58 (s, 3H).

3,6-bis(2-Phenylethenyl)-2-(2-(2-methoxyethoxy)ethoxy)ethoxy)-1-naphthaldehyde (2-S13). A solution of 401 mg (1.89 mmol) of K_3PO_4 in 2 mL of H_2O was added into a solution of 150 mg (0.315 mmol) of **2-S10**, 0.181 mg (0.79 mmol) of **2-S12**, 4.2 mg (16 μmol) of $Pd(OAc)_2$ and 17 mg (32 μmol) of BrettPhos in 5 mL of 1,4-dioxane, and the resulting solution was stirred in a sealed Airfree flask at 80 °C for 72 h. After allowing to cool down to room temperature, the reaction mixture was poured into H_2O, extracted with dichloromethane (3 X 50 mL), washed with H_2O (3 X 50 mL), and dried over Na_2SO_4. Concentration in vacuo afforded crude product that was further purified by column chromatography on silica gel (eluent ethyl acetate – CH_2Cl_2 (1:10)) to

afford 120 mg (73%) of **2-S13** as a yellow sticky solid, R_f 0.44. ^{1}H NMR (400 MHz, $CDCl_3$) δ 10.90 (s, 1H), 9.18 (d, J = 9.5 Hz, 1H), 8.30 (s, 1H), 7.86 (s, 1H), 7.85 (d, J = 8.0 Hz, 1H), 7.62 (d, J = 11.4 Hz, 2H), 7.59-7.53 (m, 3H), 7.44-7.38 (m, 4H), 7.34-7.28 (m, 3H), 7.26-7.25 (m, 2H), 4.24 (t, J = 4.3 Hz, 2H), 3.89 (t, J = 4.3 Hz, 2H), 3.75-3.73 (m, 2H), 3.71-3.69 (m, 2H), 3.65-3.63 (m, 2H), 3.54-3.52 (m, 2H), 3.36 (s, 3H).

Small-molecule sensor 2-M1. A solution of 60 mg (0.11 mmol) of **2-S13**, 38 mg (0.13 mmol) of 1,2,3,3-tetramethyl-3H-indolium iodide, and 3 mg (32 μmol) of KOAc in 1 mL of Ac_2O was stirred at 80 °C for 2 h. The reaction mixture was allowed to cool down to room temperature, and the solvent was removed under reduced pressure. The residue was dissolved in dichloromethane, precipitated in hexane, and the resulting brown solid was washed thoroughly with ethyl acetate to afford 18 mg (24%) of **2-M1** as a red sticky solid. ^{1}H NMR (400 MHz, CD_2Cl_2) δ 8.89 (d, J = 16.4 Hz, 1H), 8.34 (s, 1H), 8.31(d, J = 8.7 Hz, 1H), 8.05 (d, J = 16.4 Hz, 1H), 8.01-7.99 (m, 2H), 7.78-7.76 (m, 1H), 7.70-7.61 (m, 7H), 7.56 (d, J = 16.4 Hz, 1H), 7.46-7.29 (m, 9H), 4.29 (s, 3H), 4.22-4.20 (m, 2H), 3.91-3.89 (m, 2H), 3.71-3.69 (m, 2H), 3.61-3.59 (m, 2H), 3.53-3.51 (m, 2H), 3.46-3.44 (m, 2H), 3.27 (s, 3H), 2.00 (s, 6H).

Potassium 3-(3,6-dibromo-1-formylnaphthalen-2-yloxy)propane-1-sulfonate (3-1). A mixture of 26 mg (0.46 mmol) KOH in 1 mL of ethanol was added into a solution of 100 mg (0.3 mmol) of 9 in 3 mL of methyl ethyl ketone at 70 °C. A solution of 56 mg (0.46 mmol) 43 of 1,3-propanesultone in 1 mL of methyl ethyl ketone was added into the reaction mixture and stirred for overnight. After cooling down to rt, the reaction mixture was poured into acetone and white solid was precipitated. The white solid was collected after centrifuge and recrystallized from hot water to afford 77 mg (56%) of 10 as a white solid. ^{1}H NMR (d_6-DMSO, 400 MHz): δ 10.61 (s, 1H), 8.96 (d, 1H), 8.70 (s, 1H), 8.29 (s, 1H), 7.85 (d, 1H), 4.23 (t, 2H), 2.65 (t, 2H), 2.17 (m, 2H).

Copolymer 3-P1, 3-P2, 3-P3, and 3-P4. Polymerization of copolymer **3-P1, 3-P2, 3-P3,** and **3-P4** was performed using stock solutions of 120 mg (0.57 mmol) of K_3PO_4 in 12 mL of H_2O, 50 mg (0.07 mmol) of **2-S6** in 4 mL of THF, 32 mg (0.07 mmol) of **3-1** in 4 mL of THF, 0.3 mg (1.4 μmol) of $Pd(OAc)_2$ in 2 mL of THF and 1.7 mg (3.5 μmol) of XPhos in 2 mL of THF. Every stock solution was divided into four portions with equal volume, and resulting portions of reaction reagents and starting materials were then combined to give four reacting solutions with exactly the same concentrations. The reactions were conducted in 20 mL polycarbonate-capped glass vials at 55 °C in glove box. The reactions were then workup individually after 8 h for **3-P1**, 24 h for **3-P2**, 48 h for **3-P3**, and 72 h for **3-P4**. After allowing to cool down to room temperature, the reaction mixture was precipitated in acetone following by dialysis from deionized water for 2 days (3.5 kDa cutoff for **3-P1**, and 8 kDa for others) to yield 10 mg of **3-P1** (72%), 5 mg of **3-P2** (36%), 6 mg of **3-P3** (44%), and 6 mg of **3-P4** (44%) as yellow sticky solid. ^{1}H NMR of **3-P1** (d_6-DMSO, 400 MHz) δ 10.73 (s, 1H), 9.03 (s, 1H), 8.56 (s, 1H), 8.11-7.02 (br, 8H), 4.28-3.88 (br, 9H), 3.66-3.26 (br, 17H), 3.19-3.08 (m, 6H) 2.70 (s, 2H), 2.19 (s, 2H).

Small-molecule sensor 3-M1. A solution of 70 mg (0.33 mmol) of K_3PO_4 in 2 mL of H_2O was added into a solution of 25 mg (0.06 mmol) of **3-1**, 38 mg (0.17 mmol) of **2-S12**, 0.6 mg (2.8 μmol) of $Pd(OAc)_2$ and 3 mg (5.5 μmol) of XPhos in 2 mL of toluene, and the resulting solution was stirred in a sealed Airfree flask at 70 °C for 72 h. After allowing to cool down to room temperature, the reaction mixture was poured into acetone to form solid crude product. The solid was then vigorously washing with CH_2Cl_2 and THF to afford 22 mg (83%) of **2-S13** as a light greenish solid. ^{1}H NMR (d_6-DMSO, 400 MHz) δ 10.72 (s, 1H), 9.04 (d, J = 8.0 Hz, 1H), 8.67 (s, 1H), 8.12 (s, 1H), 8.15 (d, J = 12.0 Hz, 1H), 7.73-7.67 (m, 4H), 7.65 (d, J = 12.0 Hz, 1H), 7.46-

7.40 (m, 6H), 7.36-7.31 (m, 3H), 4.18 (t, J = 8.0 Hz, 2H), 2.68 (t, J = 8.0 Hz, 2H), 2.17 (t, J = 8.0 Hz, 2H). HR-ESI-MS (m/z calc.: 497.1423; found: 497.1427).

Triethoxy(4-iodophenyl)silane (4-1) was synthesized through a modified literature procedure.[1] A solution of 0.7 mL (6.67 mmol of 1.85 M solution in THF) *i*-PrMgCl was added dropwise to a solution of 2.0 g (6.06 mmol) 1,4-diiodobenzene in 15 mL of anhydrous THF at −40 °C under N_2 atmosphere. The resulting mixture was stirred for 6 h to give a solution of (4-iodophenyl)magnesium chloride. The as prepared solution of (4-iodophenyl)magnesium chloride was added dropwise via cannula to a solution of 3.12 g (30.3 mmol) $Si(OEt)_4$ in 5 mL of anhydrous THF. The resulting solution was stirred at −40 °C for 1 h and then allowed to warm to rt overnight. The reaction mixture was diluted with 100mL of CH_2Cl_2, washed with H_2O, and extracted with CH_2Cl_2. The organic fraction was washed with brine, dried over Na_2SO_4, and concentrated in vacuo. The crude mixture was purified by Kugelrohr distillation (8 mm Hg, over temperature 130 °C) to give 0.67 g (32%) of **4-1** as a clear liquid. ^{1}H NMR($CDCl_3$, 400 MHz) δ 7.76 (d, J = 8.0 Hz, 2H), 7.41 (d, J = 8.0 Hz, 2H), 3.88 (q, J = 6.8 Hz, 6H), 1.26 (t, J = 6.8 Hz, 12H).

1,4-Diiodo-2,5-dimethoxybenzene (4-5) was prepared as described in the literature.[9]

1,4-Dimethoxy-2,5-bis(trimethylsilylethynyl)benzene (4-S2). 1.51 g (15.39 mmol) of (trimethylsilyl)acetylene was added to a mixture of 2 g (5.13 mmol) of **4-5**, 119 mg (0.1 mmol) of $Pd(PPh_3)_4$ and 29 mg (0.15 mmol) of CuI in 150 mL of toluene - *i*-Pr_2NH (7:3). The resulting mixture was stirred at 70 °C in a sealed air-free flask for 48 h. After cooling down to rt, the mixture was concentrated in vacuo, and the crude product was purified by column chromatography on silica gel eluted with CH_2Cl_2 - hexane (1:3) to afford 1.36 g (90%) of **4-S2** as a white solid. ^{1}H NMR($CDCl_3$, 400 MHz) δ 6.93 (s, 2H), 3.85 (s, 6H), 0.28 (s, 18H).

1,4-Dimethoxy-2,5-diethynylbenzene (4-2). A solution of 1.3 g (3.93 mmol) of **4-S2** in 5 mL of CH_2Cl_2 was added into a mixture of 5.44 g (39.3 mmol) of K_2CO_3 in 80 mL of MeOH - CH_2Cl_2 (1:1). The resulting mixture was stirred at room temperature for 1 h. The mixture was filtered and the filtrate was collected and then diluted in 100 mL of CH_2Cl_2, washed with H_2O for three times, and then extracted with 100 mL of CH_2Cl_2 for three times. The resulting organic fraction was washed with brine, dried over Na_2SO_4, and concentrated in vacuo. The crude product was purified by column chromatography on silica gel eluted with CH_2Cl_2 - hexane (1:3) to afford 695 mg (95%) of **4-2** as a white solid. ^{1}H NMR($CDCl_3$, 400 MHz) δ 6.98 (s, 2H), 3.86 (s, 6H), 3.40 (s, 2H).

1,4-Diiodo-2,5-bis(trifluoromethyl)benzene (4-6) was synthesized through a modified literature procedure.[10] 3 g (14.01 mmol) of 1,4-bis(trifluoromethyl)benzene was added into a mixture of 4.50 g (21.02 mmol) of $NaIO_4$, 6.98 g (42.03 mmole) of KI in 100 mL of H_2SO_4 at rt. The resulting mixture was stirred at 90 °C for 16 h. After cooling to rt, the mixture was poured into ice, washed with H_2O, and filtered. The residual was collected, washed with $NaS_2O_{3\,(aq)}$, extracted with CH_2Cl_2. The resulting organic fraction was washed with brine, dried over Na_2SO_4, concentrated in vacuo, and recrystallized from hexane to afford 3.24 g (50%) of **4-6** as a white solid. ^{1}H NMR($CDCl_3$, 400 MHz) δ 8.22 (s, 2H).

1,4-Bis(trifluoromethyl)-2,5-bis(trimethylsilylethynyl)benzene (4-S3) was prepared utilizing the same procedure as **4-S2**. 1.7 g (97%) of **4-S3** as a white solid was acquired. ^{1}H NMR($CDCl_3$, 400 MHz) δ 7.84 (s, 2H), 0.28 (s, 18H).

1,4-Bis(trifluoromethyl)-2,5-diethynylbenzene (4-3). A solution of 1.7 g (4.18 mmol) of **4-S3** in 5 mL of THF was added into a mixture of 5.78 g (41.82 mmol) of K_2CO_3 in 80 mL of MeOH - THF (1:1). The resulting mixture was stirred at room temperature for 1 h. The mixture

was filtered and the filtrate was collected and then diluted in 100 mL of CH_2Cl_2, washed with H_2O for three times, and then extracted with 100 mL of CH_2Cl_2 for three times. The resulting organic fraction was washed with brine, dried over Na_2SO_4, and concentrated in vacuo. The crude product was purified by column chromatography on silica gel eluted with CH_2Cl_2 - hexane (1:3) to afford 987 mg (90%) of **4-3** as a white solid. ^{1}H NMR($CDCl_3$, 400 MHz) δ 7.94 (s, 2H), 3.86 (s, 2H).

1,4-Dibromo-2,5-d$_6$-dimethoxybenzene (4-S4). A solution of 1 g (3.73 mmol) of 2,5-dibromohydroquinone, 1.35 g (9.33 mmol) of d_3-methyl iodide, and 2.06 g (14.92 mmol) of K_2CO_3 in 25 mL of DMF was stirred at 40 °C for 48 h. After cooling down to rt, the mixture was filtrated and the filtrate was purified by column chromatography on silica gel (DCM – hexane (3:1)) to yield 900 mg (80%) of **4-S4** as a white solid, R_f 0.34. ^{1}H NMR (400 MHz, $CDCl_3$) δ 7.10 (s, 2H).

1,4-d$_6$-Dimethoxy-2,5-bis(trimethylsilylethynyl)benzene (4-S5). 709 g (7.22 mmol) of (trimethylsilyl)acetylene was added to a mixture of 650 g (2.41 mmol) of **4-S4**, 139 mg (0.12 mmol) of $Pd(PPh_3)_4$ and 46 mg (0.24 mmol) of CuI in 100 mL of toluene - *i*-Pr_2NH (7:3). The resulting mixture was stirred at 70 °C in a sealed air-free flask for 48 h. After cooling down to rt, the mixture was concentrated in vacuo, and the crude product was purified by column chromatography on silica gel eluted with CH_2Cl_2 - hexane (1:3) to afford 510 mg (63%) of **4-S5** as a white solid. ^{1}H NMR($CDCl_3$, 400 MHz) δ 6.90 (s, 2H), 0.27 (s, 18H).

1,4-d$_6$-Dimethoxy-2,5-diethynylbenzene (4-4). A solution of 510 mg (1.52 mmol) of **4-S5** in 10 mL of THF was added into a mixture of 204 mg (3.64 mmol) of KOH in 40 mL of MeOH - THF (1:1). The resulting mixture was stirred at room temperature for 1 h. The mixture was filtered and the filtrate was collected and then diluted in 100 mL of CH_2Cl_2, washed with H_2O for three times, and then extracted with 100 mL of CH_2Cl_2 for three times. The resulting organic fraction was washed with brine, dried over Na_2SO_4, and concentrated in vacuo. The crude product was

purified by column chromatography on silica gel eluted with CH_2Cl_2 - hexane (1:3) to afford 276 mg (95%) of **4-4** as a white solid. ^{1}H NMR($CDCl_3$, 400 MHz) δ 6.98 (s, 2H), 3.40 (s, 2H).

Alternating donor-acceptor type conjugated polymer **4-P1**. 35 mg (0.064 mmol) of 1,4-Bis(tetradecyloxy-2,5-diethynyl)benzene, 30 mg (0.064 mmol) of **4-6**, 1.4 mg (2 mmol%) of $Pd(PPh_3)_4$ and 0.24 mg (2 mmol%) of CuI in 10 mL of toluene - *i*-Pr_2NH (7:3). The resulting mixture was stirred at 70 °C in a sealed air-free flask for 72 h. After cooling down to rt, the mixture was poured into 50 mL of acetone to afford 30 mg (63% Mn 5.9 kDa PDI 1.8) of **4-P1** as a yellow solid. ^{1}H NMR($CDCl_3$, 400 MHz) δ 7.98 (m, 2H), 7.02 (s, 2H), 4.05 (m, 4H), 1.87 (m, 4H), 1.43 (m, 44H), 0.89 (m, 6H).

Alternating donor-acceptor type conjugated polymer **4-7**. 20 mg (0.036 mmol) of 1,4-Bis(tetradecyloxy-2,5-diethynylbenzene, 14 mg (0.036 mmol) of 4,7-diiodobenzo[*c*][1,2,5]-thiadiazole, 0.8 mg (2 mmol%) of $Pd(PPh_3)_4$ and 0.2 mg (2 mmol%) of CuI in 5 mL of toluene - *i*-Pr_2NH (7:3). The resulting mixture was stirred at 70 °C in a sealed air-free flask for 72 h. After cooling down to rt, the mixture was poured into 50 mL of acetone to afford 20 mg (80% Mn 22.3 kDa PDI 3.1) of **4-P2** as a red solid. ^{1}H NMR(CD_2Cl_2, 400 MHz) δ 7.82 (s, 2H), 7.19 (s, 2H), 4.13 (t, 4H), 1.92 (t, 4H), 1.4 (m, 44H), 0.86 (m, 6H)

5.8 References

(1) Love, B. E.; Jones, E. G. The Use of Salicylaldehyde Phenylhydrazone as an Indicator for the Titration of Organometallic Reagents. *J. Org. Chem.* **1999**, *64*, 3755–3756.

(2) Frisch, M. J.; Trucks, G. W.; Schlegel, H. B.; Scuseria, G. E.; Robb, M. A.; Cheeseman, J. R.; Scalmani, G.; Barone, V.; Petersson, G. A.; Nakatsuji, H.; et al. *Gaussian 09, Revision A.02*; Gaissoan, Inc.: Wallingford CT, 2016.

(3) *Gwyddion 2.9*; Metrology Institute, 2010.

(4) Layers Is an Excel Spreadsheet for Modeling Neutron Reflectivity Data Developed by John F. Ankner at the Oak Ridge National Laboratory.

(5) Nelson, A. Co-Refinement of Multiple-Contrast Neutron/X-Ray Reflectivity Data Using *MOTOFIT*. *J. Appl. Crystallogr.* **2006**, *39*, 273–276.

(6) Tanaka, M.; Yoshioka, K.; Hirata, Y.; Fujimaki, M.; Kuwahara, M.; Niwa, O. Design and Fabrication of Biosensing Interface for Waveguide-Mode Sensor. *Langmuir* **2013**, *29*, 13111–13120.

(7) Song, I. Y.; Kim, M.; Park, T. Effect of Ion-Chelating Chain Lengths in Thiophene-Based Monomers on in Situ Photoelectrochemical Polymerization and Photovoltaic Performances. *ACS Appl. Mater. Interfaces* **2015**, *7*, 11482–11489.

(8) Pangeni, D.; Nesterov, E. E. "Higher Energy Gap" Control in Fluorescent Conjugated Polymers: Turn-On Amplified Detection of Organophosphorous Agents. *Macromolecules* **2013**, *46*, 7266–7273.

(9) Li, J.; Kendig, C. E.; Nesterov, E. E. Chemosensory Performance of Molecularly Imprinted Fluorescent Conjugated Polymer Materials. *J. Am. Chem. Soc.* **2007**, *129*, 15911–15918.

(10) Kim, Y.; Whitten, J. E.; Swager, T. M. High Ionization Potential Conjugated Polymers. *J. Am. Chem. Soc.* **2005**, *127*, 12122–12130.

CONCLUSIONS

A CP sensor **2-P1a** (M_n ~27.7 kDa) incorporates an H_2S naphthalene cyanine receptor which is part of the poly(arylene vinylene) π-conjugated backbone. Adding increasing concentrations (200 nM to 0.1 mM) of aqueous H_2S to a dilute solution of **2-P1a** in acetonitrile produced a substantial gradual increase of the fluorescent emission, up to 74-fold as an integrated intensity ratio F/F_0. The lack of a significant change in the absorption spectra as well as negligible wavelength shift accompanying the fluorescence enhancement indicated only the minor electronic perturbations in the extended π-electron conjugated system of **2-P1a** upon reaction with H_2S. The corresponding small-molecule sensor **2-M1** (prepared as a reference) produced no detectable change in the absorption spectrum and only an approximately 2.5-fold enhancement in F/F_0. Thus, the small-molecule sensor demonstrated a rather insignificant *turn-on* fluorescent response and a narrow analyte detection range. According to the "higher energy gap" mechanism, we expected that the sensing performance would be greatly affected by the polymer conjugation length, since this mechanism is based on restricting the intramolecular exciton migration in the CP π-conjugated backbone. Indeed, a CP sensor **2-P1b** (M_n ~15.5 kDa) with a lower degree of polymerization displayed a much-diminished *turn-on* sensing performance, with only a 30-fold maximum increase in F/F_0 and approximately 20 times lower H_2S sensitivity than the polymer **2-P1a**. This illustrated that the overall short conjugation length in **2-P1b** was responsible for a more limited intramolecular exciton migration and thus a smaller fluorescent enhancement upon creating higher energy gap exciton "roadblocks" in the CP backbone.

To prove that the "roadblocks" responsible for the *turn-on* amplified fluorescence enhancement were created via the reaction of H_2S with the cyanine moiety, we checked a control polymer **2-P2** which, as was expected, showed absolutely no response on H_2S addition. As an

excellent illustration of the power of the "higher energy gap" concept in fluorescent sensor design, the polymer sensor **2-P1a** demonstrated a superior *turn-on* response, with approximately 10 times higher detection sensitivity and a broad analyte detection range, all in a dramatic contrast with the poor sensing performance of the small molecule analogue **2-M1**.

To better understand the minimal requirements to the energy gap modulation for achieving an amplified fluorescence response in the "higher energy gap" mechanism, we turned to the cysteine sensor based on the reaction of an aromatic aldehyde with cysteine to form thiazolidine. Preliminary DFT (B3LYP/6-31G*) computations indicated that such a conversion would result in the energy gap change of approximately 0.1 eV. Such change normally would be too small to use in the design of conventional sensors, however it could be sufficient within the framework of the "higher energy gap" mechanism. Four CP sensors **3-P1**, **3-P2**, **3-P3**, and **3-P4** were prepared by step-growth Suzuki polymerization using various reaction times to achieve different degree of polymerization. The goal was to obtain polymer sensors with different π-conjugation length. The accurate values of molecular weight of these polymers are yet to be determined as the polymers appear to show strong intermolecular aggregation during GPC experiments. Indeed, the featureless UV/vis spectra and unusually high extinction coefficients also indicated that the polymers were highly aggregated in aqueous media. Such aggregation could stem from the insufficient solubilizing ability of the side chains in aqueous environment.

Regarding the amplification ratio, CP sensor **3-P1** exhibited an up to 30-fold F/F_0 whereas **3-P2**, **3-P3**, and **3-P4** exhibited smaller, 10 to 15-fold enhancements, and all four polymers showed rather insignificant changes in absorption spectra after adding millimolar levels of cysteine. In contrast, small molecule sensor **3-M1** showed a moderate decrease in fluorescence intensity, due to the insufficient energy gap change.

Although, to our satisfaction, the "higher energy gap" based polymer sensors showed a reasonable *turn-on* response in the situation where a small-molecule sensor was not operational, we were not satisfied with a relatively small magnitude of the *turn-on* response. The less than desired sensing performance could be caused by poor solubility of the polymer in aqueous media, which induced intermolecular aggregation. Such aggregation could be responsible for numerous close contacts between individual polymer chains which would facilitate intermolecular exciton migration via the through-space mechanism. The possibility of intermolecular energy migration would allow an exciton "detour" of the local higher energy gap site in the CP backbone, thereby diminishing the effect of the higher energy gap mechanism.

Uniform alignment and improved molecular organization of CP chains in thin films could provide potential benefits for charge injection and charge transport processes in thin-film electronic and optoelectronic devices. However, fine adjustment and further fine-tuning of mesoscale morphology in films remain a significant and not yet solved challenge. In Chapter 4, we developed a precision stepwise Sonogashira polymerization to prepare a series of highly packed surface-immobilized PPE films with complete structural and morphological control. This method involves preparing thin films by adding one monomer repeating unit at a time using Sonogashira coupling protocol, and can be extended towards preparation of polymer chains of up to 20-30 repeating units.

In UV/vis spectra, all surface-confined PPE films showed significant bathochromic shift accompanied by a linear increase in the optical density: a clear evidence for the extension of the π-electron delocalization. It is worth noticing that the absorbance maxima in surface-confined precision polymers were hypsochromically shifted relative to the spectra of spin-cast reference films films. This unusual (and previously unobserved) phenomenon could stem from the

interruption of continuous intramolecular π-conjugation caused by the alternating and uniform CP backbone twisting formed during the stepwise polymerization in the densely packed film. Indeed, atomic force microscopy studies on **TFDM** and **DMBTD** films exhibited highly dense packing and dramatic difference in morphology from the corresponding spin-cast films. To confirm the hypothesis of alternating backbone twisting, grazing-incidence wide-angle X-ray scattering studies showed that PPE films were amorphous and deficient of interchain π-π stacking as a result of torsional twisting. From the neutron reflectometry (NR) studies, we obtained the thickness of a deuterated **DMBTD** film at 14.5 nm, which was in a good match with the theoretical value (13.2 nm) considering the polymer chains were aligned normally to the substrate. The mass density obtained the scattering length density in NR studies was 0.87 g cm^{-3} indicating that the **DMBTD** film consisted of densely and uniformly packed polymer chains. In conclusion, the PPE films prepared by precision surface-confined stepwise Sonogashira polymerization showed unique and previously unobtainable thin-film morphology and polymer structure, which resulted in interesting electronic properties potentially well-suited for the applications in devices requiring enhanced charge transport across the film (e.g. organic light-emitting devices).

APPENDIX A: PERMISSIONS

THE AMERICAN ASSOCIATION FOR THE ADVANCEMENT OF SCIENCE LICENSE TERMS AND CONDITIONS

Nov 04, 2017

This Agreement between Louisiana state university -- Chien-Hung Chiang ("You") and The American Association for the Advancement of Science ("The American Association for the Advancement of Science") consists of your license details and the terms and conditions provided by The American Association for the Advancement of Science and Copyright Clearance Center.

License Number	4222191265734
License date	Nov 04, 2017
Licensed Content Publisher	The American Association for the Advancement of Science
Licensed Content Publication	Science
Licensed Content Title	Coherent Intrachain Energy Migration in a Conjugated Polymer at Room Temperature
Licensed Content Author	Elisabetta Collini,Gregory D. Scholes
Licensed Content Date	Jan 16, 2009
Licensed Content Volume	323
Licensed Content Issue	5912
Volume number	323
Issue number	5912
Type of Use	Thesis / Dissertation
Requestor type	Scientist/individual at a research institution
Format	Print and electronic
Portion	Figure
Number of figures/tables	1
Order reference number	
Title of your thesis / dissertation	Higher energy gap of fluorescence in conjugated polymers
Expected completion date	Nov 2017
Estimated size(pages)	100
Requestor Location	Louisiana state university 232 Choppin Hall BATON ROUGE, LA 70808 United States Attn: Louisiana state university
Billing Type	Invoice
Billing Address	Louisiana state university 232 Choppin Hall

RightsLink®

Home | Account Info | Help

Title:	Conjugation Enhancement of Intramolecular Exciton Migration in Poly(p-phenylene ethynylene)s
Author:	Evgueni E. Nesterov, Zhengguo Zhu, Timothy M. Swager
Publication:	Journal of the American Chemical Society
Publisher:	American Chemical Society
Date:	Jul 1, 2005

Logged in as:
Chien-Hung Chiang
Louisiana state university
Account #:
3001190298

LOGOUT

PERMISSION/LICENSE IS GRANTED FOR YOUR ORDER AT NO CHARGE

This type of permission/license, instead of the standard Terms & Conditions, is sent to you because no fee is being charged for your order. Please note the following:

- Permission is granted for your request in both print and electronic formats, and translations.
- If figures and/or tables were requested, they may be adapted or used in part.
- Please print this page for your records and send a copy of it to your publisher/graduate school.
- Appropriate credit for the requested material should be given as follows: "Reprinted (adapted) with permission from (COMPLETE REFERENCE CITATION). Copyright (YEAR) American Chemical Society." Insert appropriate information in place of the capitalized words.
- One-time permission is granted only for the use specified in your request. No additional uses are granted (such as derivative works or other editions). For any other uses, please submit a new request.

If credit is given to another source for the material you requested, permission must be obtained from that source.

BACK CLOSE WINDOW

Title: Method for enhancing the sensitivity of fluorescent chemosensors: energy migration in conjugated polymers

Author: Qin Zhou, Timothy M. Swager

Publication: Journal of the American Chemical Society

Publisher: American Chemical Society

Date: Jul 1, 1995

PERMISSION/LICENSE IS GRANTED FOR YOUR ORDER AT NO CHARGE

This type of permission/license, instead of the standard Terms & Conditions, is sent to you because no fee is being charged for your order. Please note the following:

- Permission is granted for your request in both print and electronic formats, and translations.
- If figures and/or tables were requested, they may be adapted or used in part.
- Please print this page for your records and send a copy of it to your publisher/graduate school.
- Appropriate credit for the requested material should be given as follows: "Reprinted (adapted) with permission from (COMPLETE REFERENCE CITATION). Copyright (YEAR) American Chemical Society." Insert appropriate information in place of the capitalized words.
- One-time permission is granted only for the use specified in your request. No additional uses are granted (such as derivative works or other editions). For any other uses, please submit a new request.

If credit is given to another source for the material you requested, permission must be obtained from that source.

JOHN WILEY AND SONS LICENSE TERMS AND CONDITIONS

Aug 31, 2017

This Agreement between Louisiana state university -- Chien-Hung Chiang ("You") and John Wiley and Sons ("John Wiley and Sons") consists of your license details and the terms and conditions provided by John Wiley and Sons and Copyright Clearance Center.

License Number	4179681046870
License date	Aug 31, 2017
Licensed Content Publisher	John Wiley and Sons
Licensed Content Publication	Angewandte Chemie International Edition
Licensed Content Title	A Fluorescent Self-Amplifying Wavelength-Responsive Sensory Polymer for Fluoride Ions
Licensed Content Author	Tae-Hyun Kim,Timothy M. Swager
Licensed Content Date	Sep 23, 2003
Licensed Content Pages	4
Type of use	Dissertation/Thesis
Requestor type	University/Academic
Format	Print and electronic
Portion	Figure/table
Number of figures/tables	1
Original Wiley figure/table number(s)	figure 2
Will you be translating?	No
Title of your thesis / dissertation	Higher energy gap of fluorescence in conjugated polymers
Expected completion date	Nov 2017
Expected size (number of pages)	100
Requestor Location	Louisiana state university 232 Choppin Hall BATON ROUGE, LA 70808 United States Attn: Louisiana state university
Publisher Tax ID	EU826007151
Billing Type	Invoice
Billing Address	Louisiana state university 232 Choppin Hall BATON ROUGE, LA 70808

Title: "Higher Energy Gap" Control in Fluorescent Conjugated Polymers: Turn-On Amplified Detection of Organophosphorous Agents

Author: Deepa Pangeni, Evgueni E. Nesterov

Publication: Macromolecules

Publisher: American Chemical Society

Date: Sep 1, 2013

PERMISSION/LICENSE IS GRANTED FOR YOUR ORDER AT NO CHARGE

This type of permission/license, instead of the standard Terms & Conditions, is sent to you because no fee is being charged for your order. Please note the following:

- Permission is granted for your request in both print and electronic formats, and translations.
- If figures and/or tables were requested, they may be adapted or used in part.
- Please print this page for your records and send a copy of it to your publisher/graduate school.
- Appropriate credit for the requested material should be given as follows: "Reprinted (adapted) with permission from (COMPLETE REFERENCE CITATION). Copyright (YEAR) American Chemical Society." Insert appropriate information in place of the capitalized words.
- One-time permission is granted only for the use specified in your request. No additional uses are granted (such as derivative works or other editions). For any other uses, please submit a new request.

If credit is given to another source for the material you requested, permission must be obtained from that source.

BACK | CLOSE WINDOW

APPENDIX B: ^{1}H NMR SPECTRA OF KEY COMPOUNDS

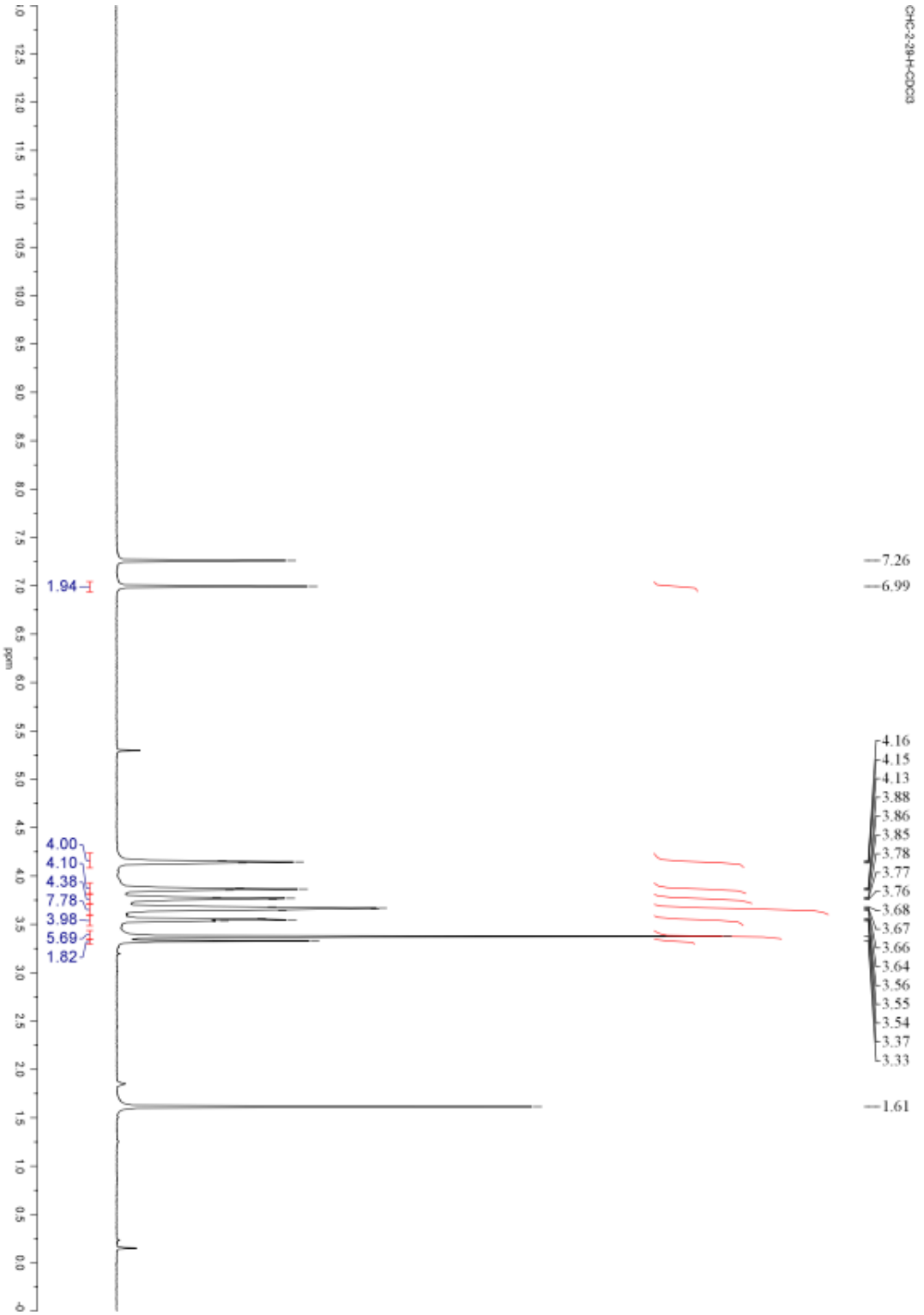

Figure Appendix B.1.^{1}H NMR spectrum of compound **2-S5** ($CDCl_3$, 400 MHz).

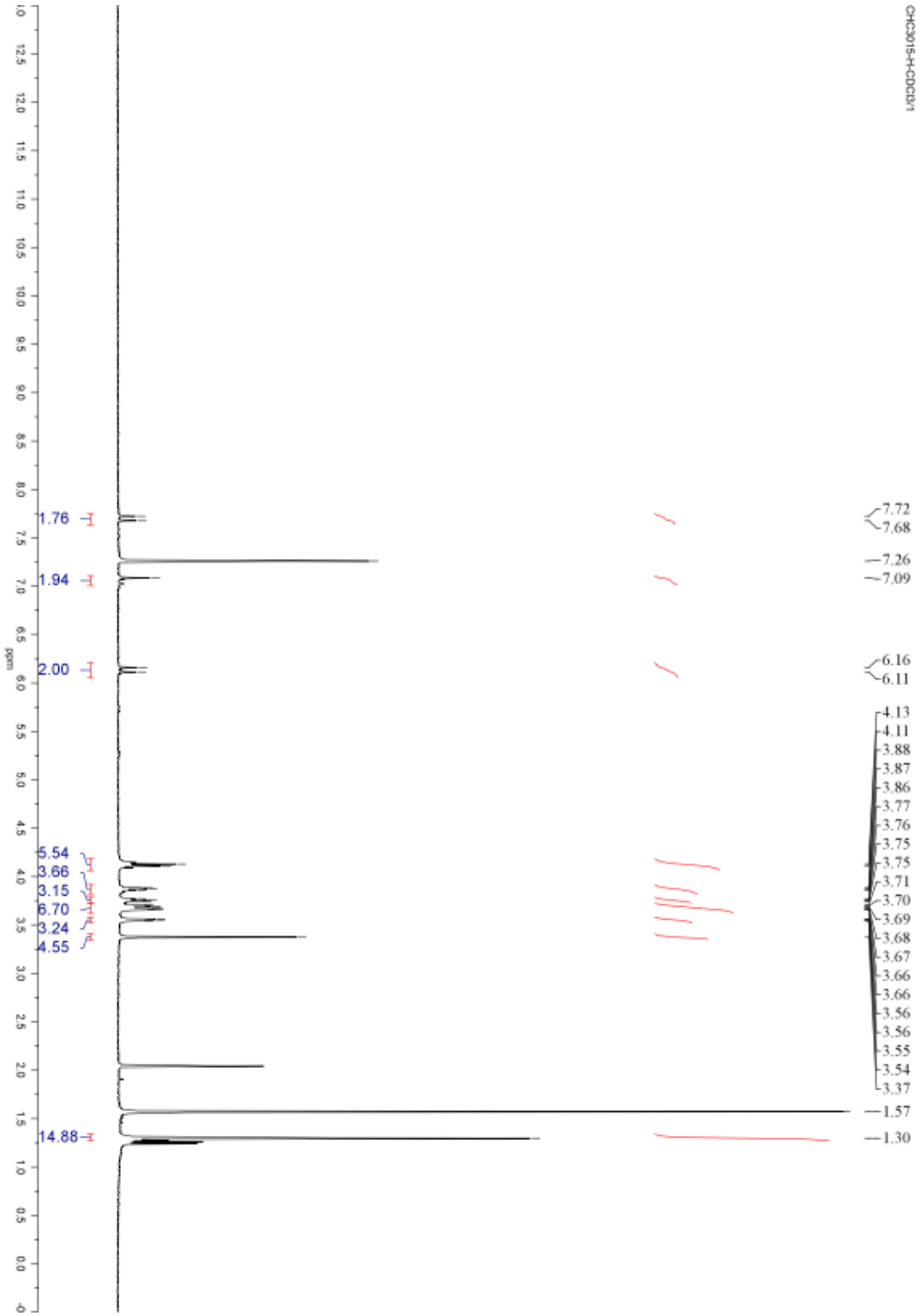

Figure Appendix B.2.^{1}H NMR spectrum of compound **2-S6** ($CDCl_3$, 400 MHz).

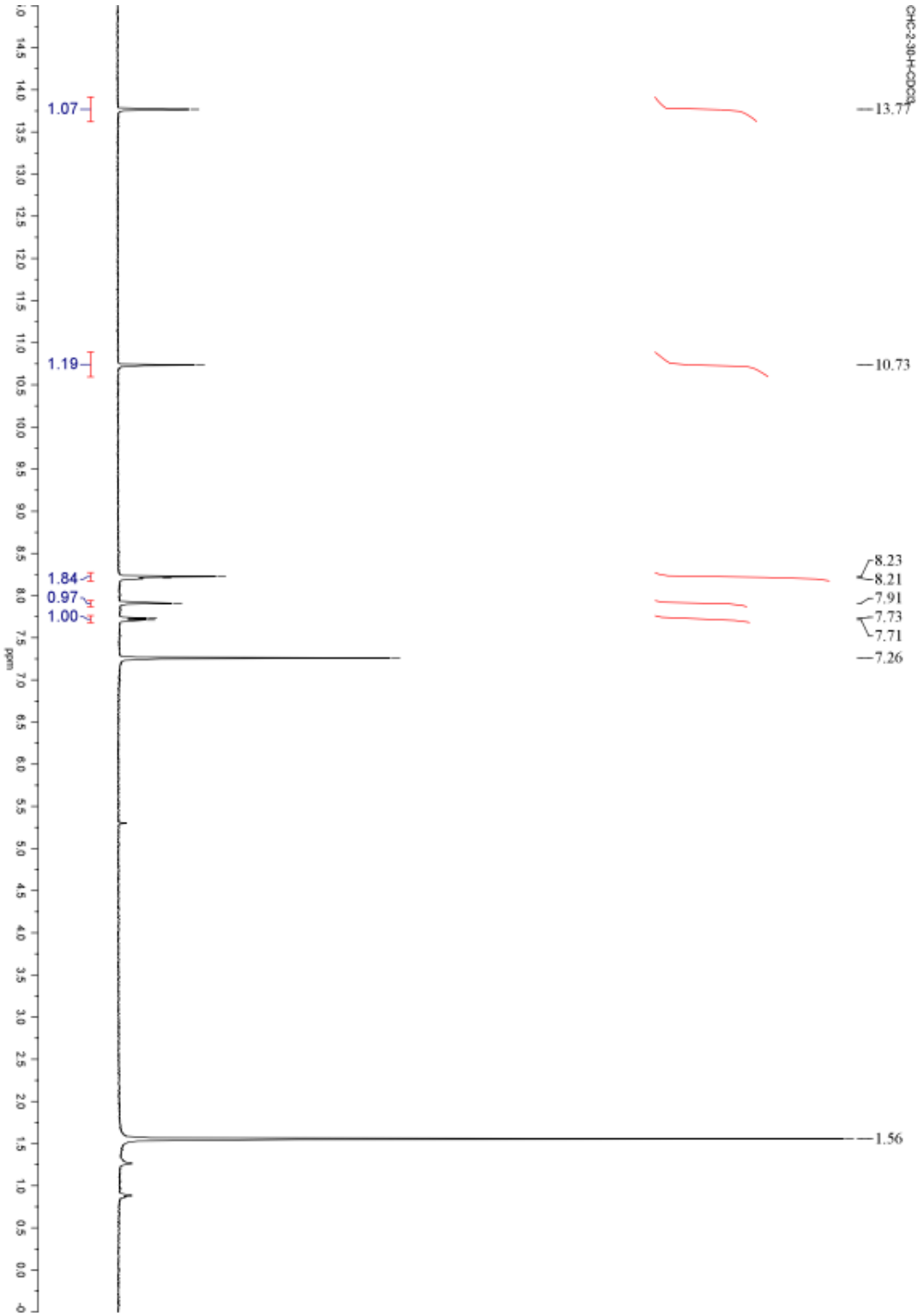

Figure Appendix B.3.[1]H NMR spectrum of compound **2-S9** ($CDCl_3$, 400 MHz).

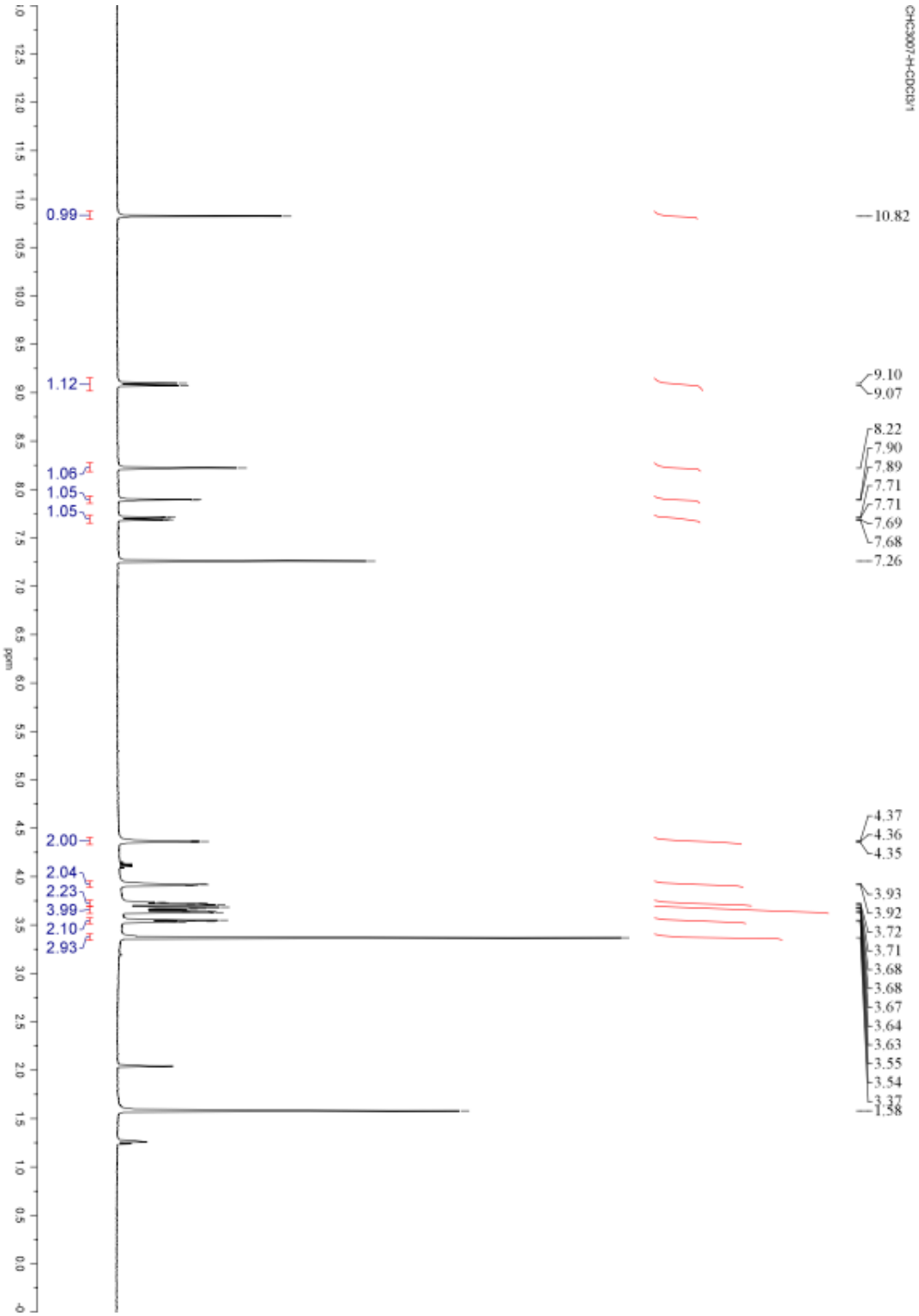

Figure Appendix B.4.^{1}H NMR spectrum of compound **2-S10** ($CDCl_3$, 400 MHz).

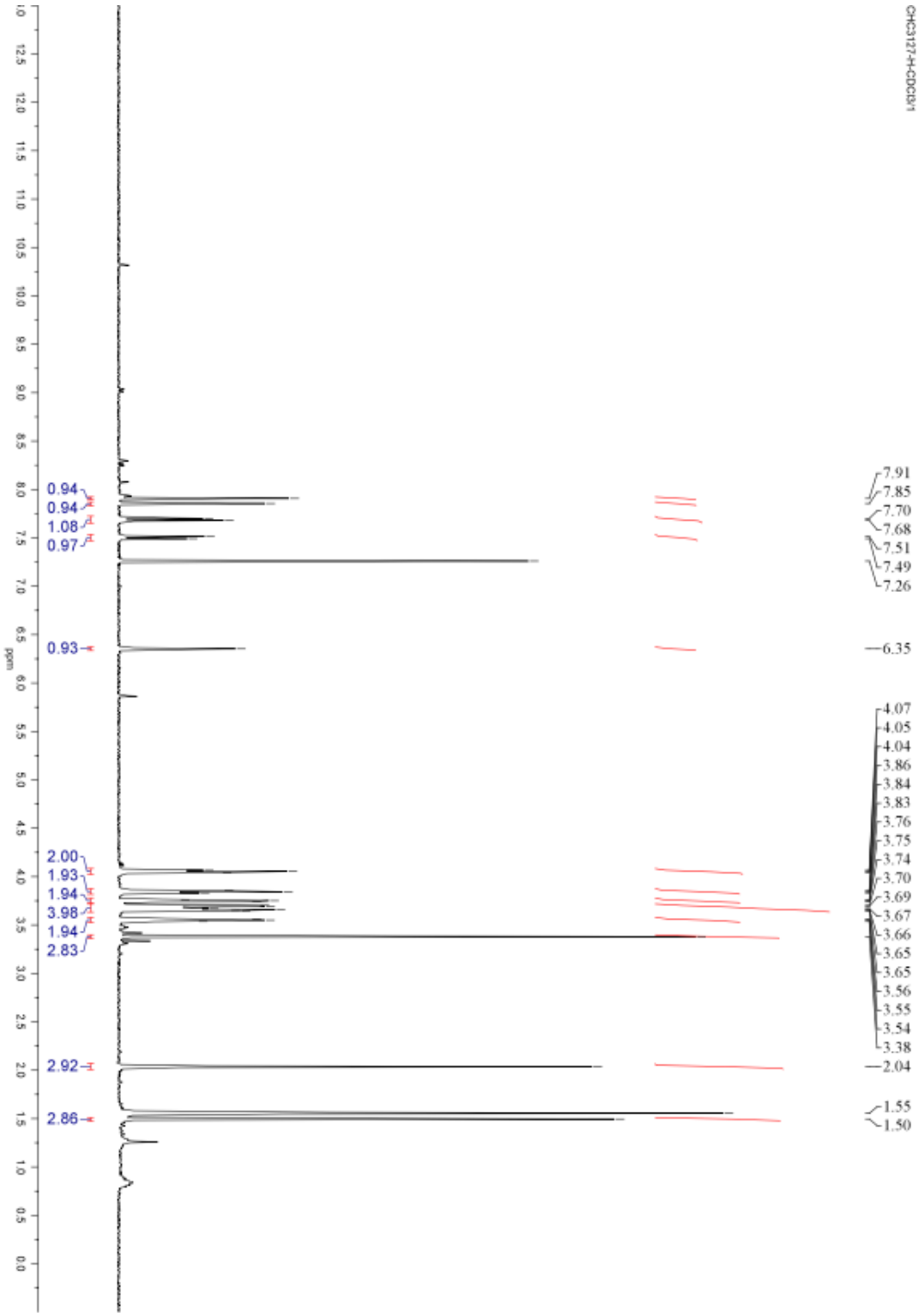

Figure Appendix B.5.^{1}H NMR spectrum of compound **2-S11** ($CDCl_3$, 400 MHz).

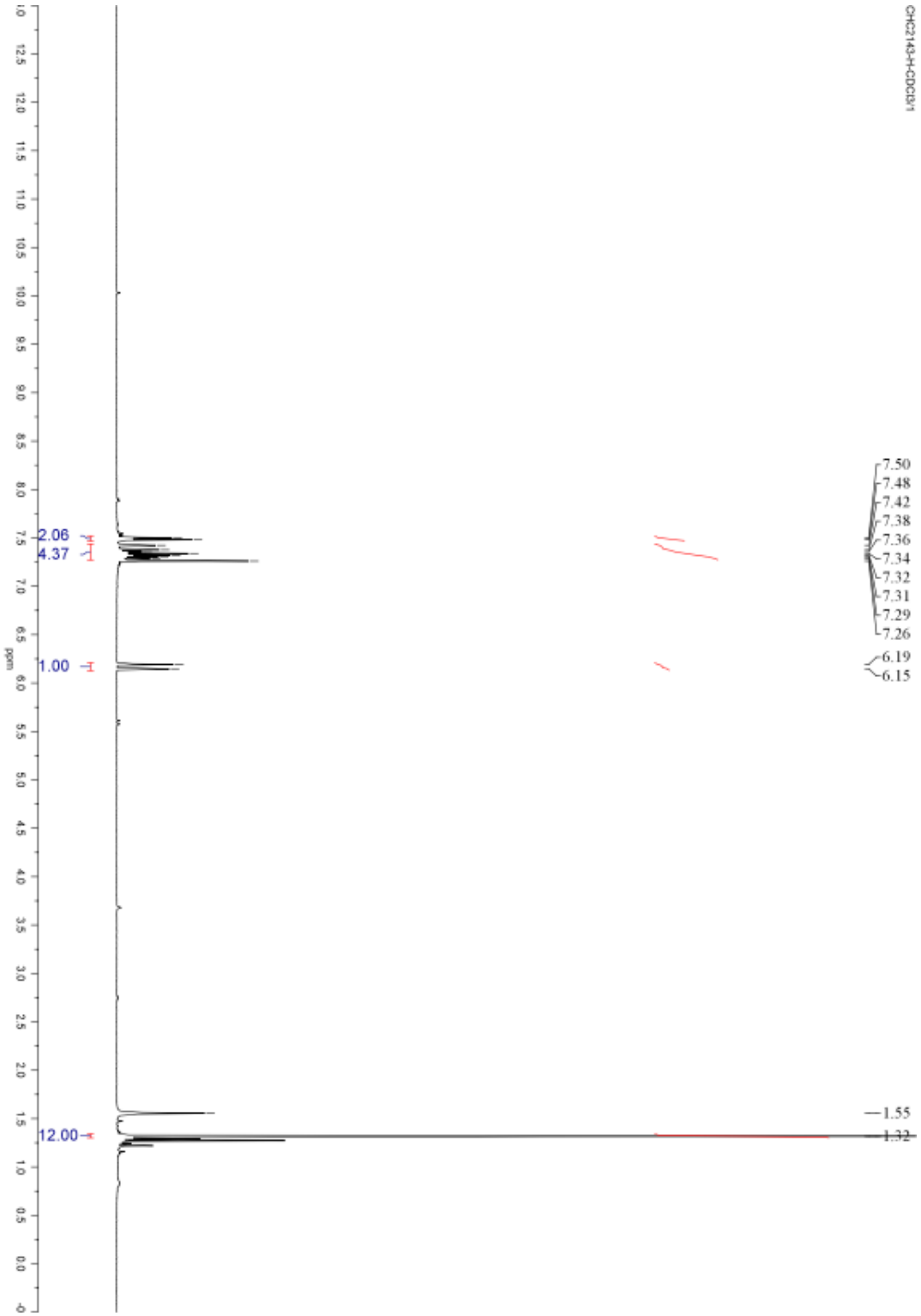

Figure Appendix B.6.^{1}H NMR spectrum of compound **2-S12** ($CDCl_3$, 400 MHz).

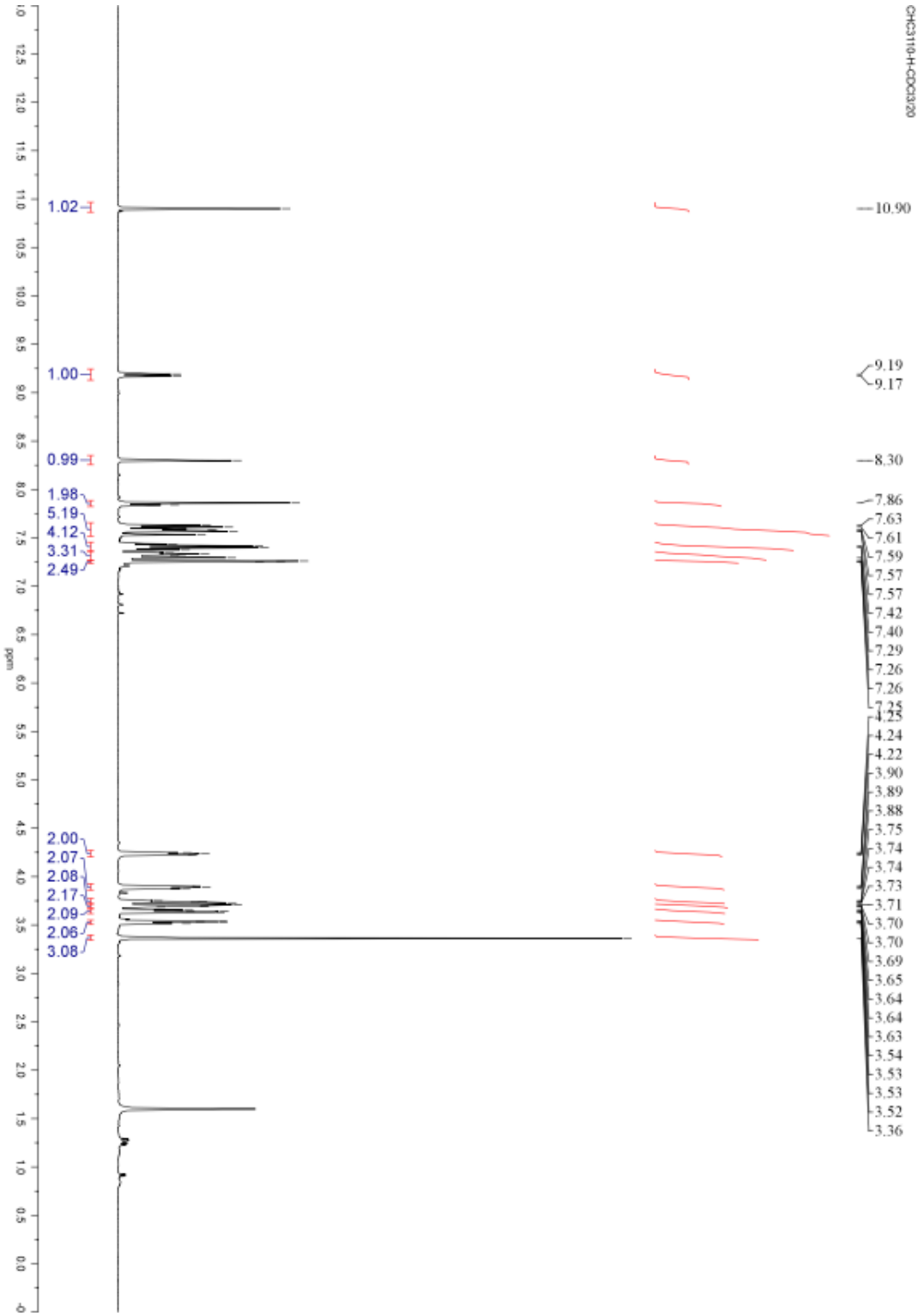

Figure Appendix B.7.^{1}H NMR spectrum of compound **2-S13** ($CDCl_3$, 400 MHz).

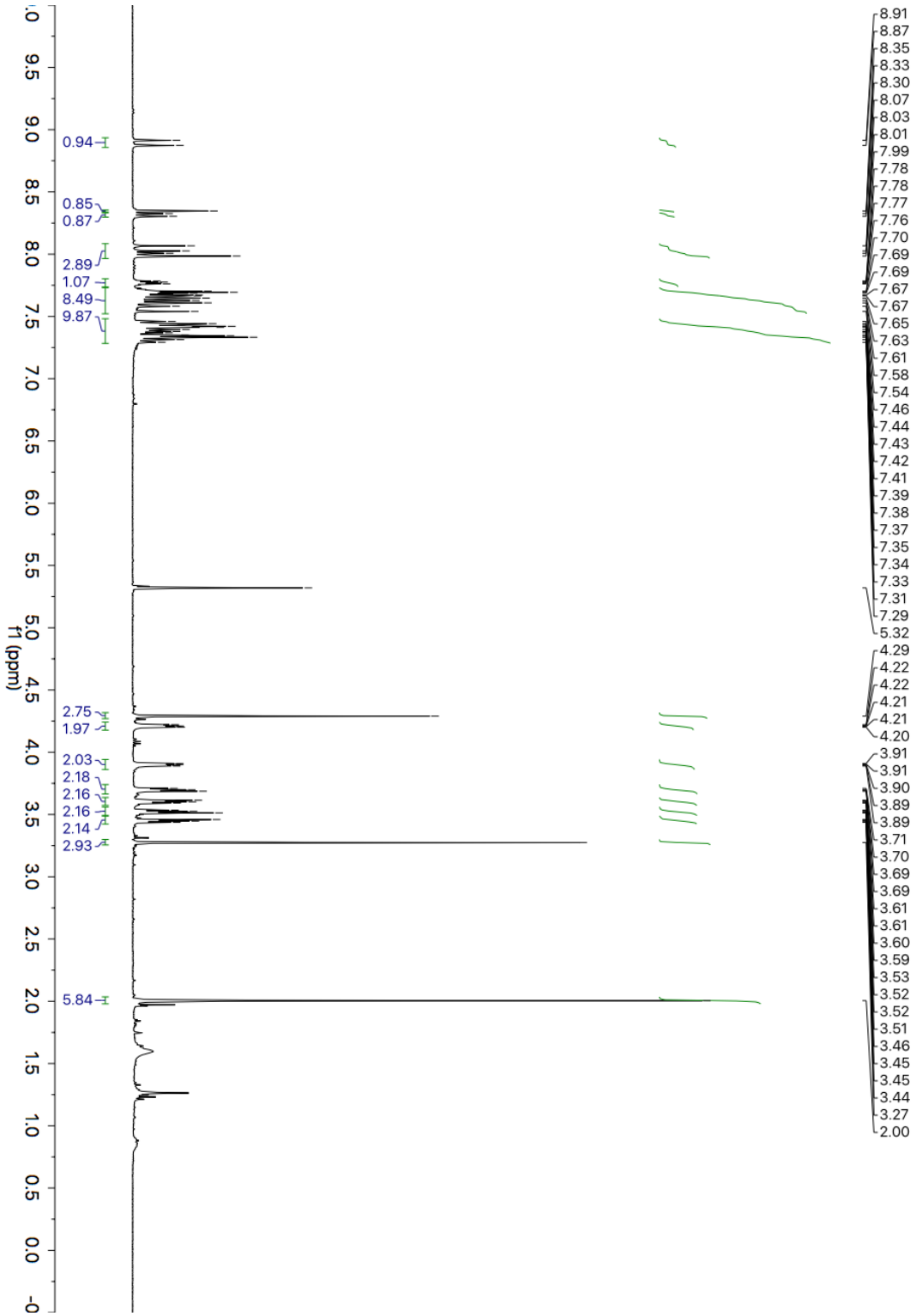

Figure Appendix B.8.^{1}H NMR spectrum of compound **2-M1** (CD_2Cl_2, 400 MHz).

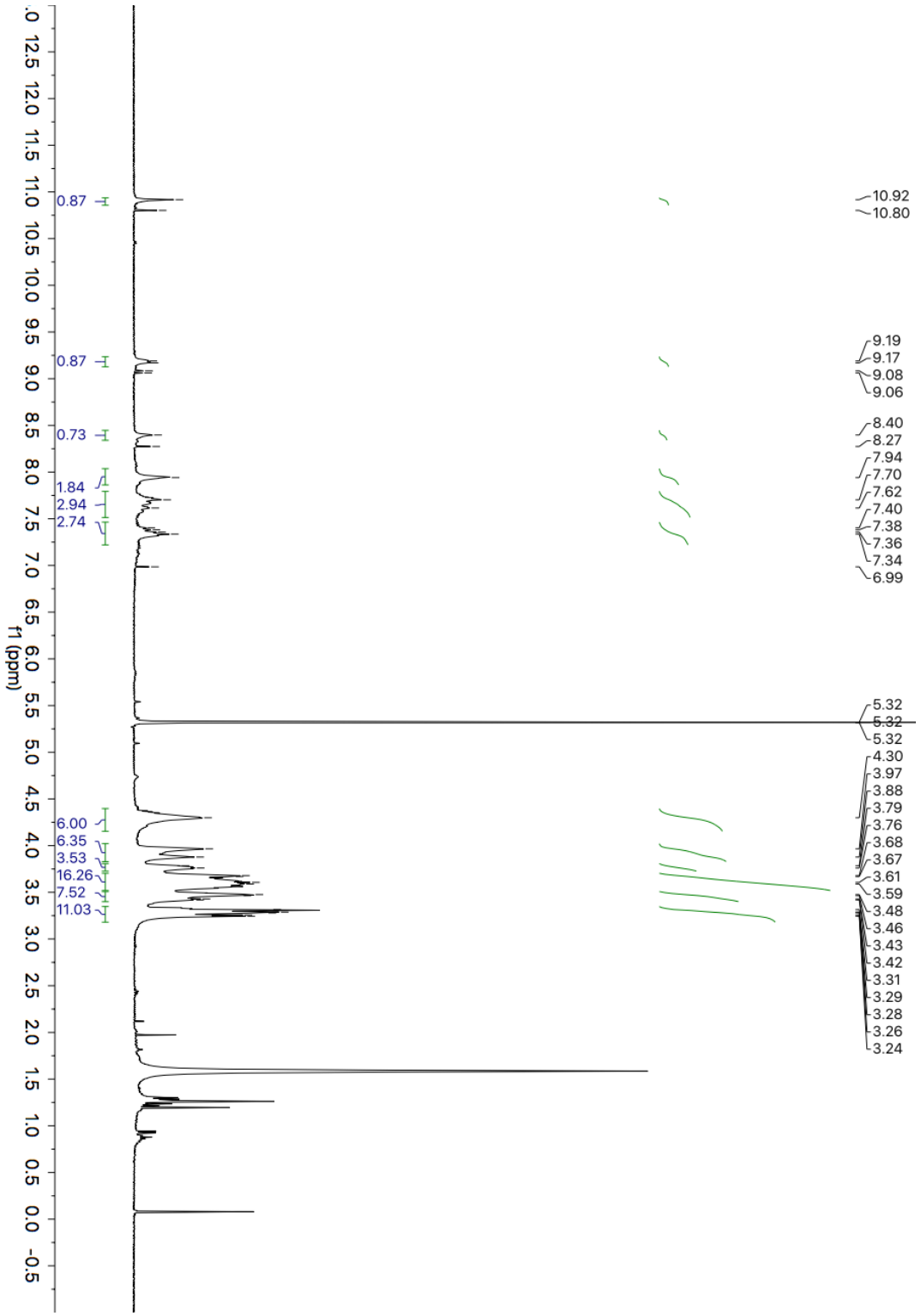

Figure Appendix B.9.^{1}H NMR spectrum of compound **2-SP1a** (CD_2Cl_2, 400 MHz).

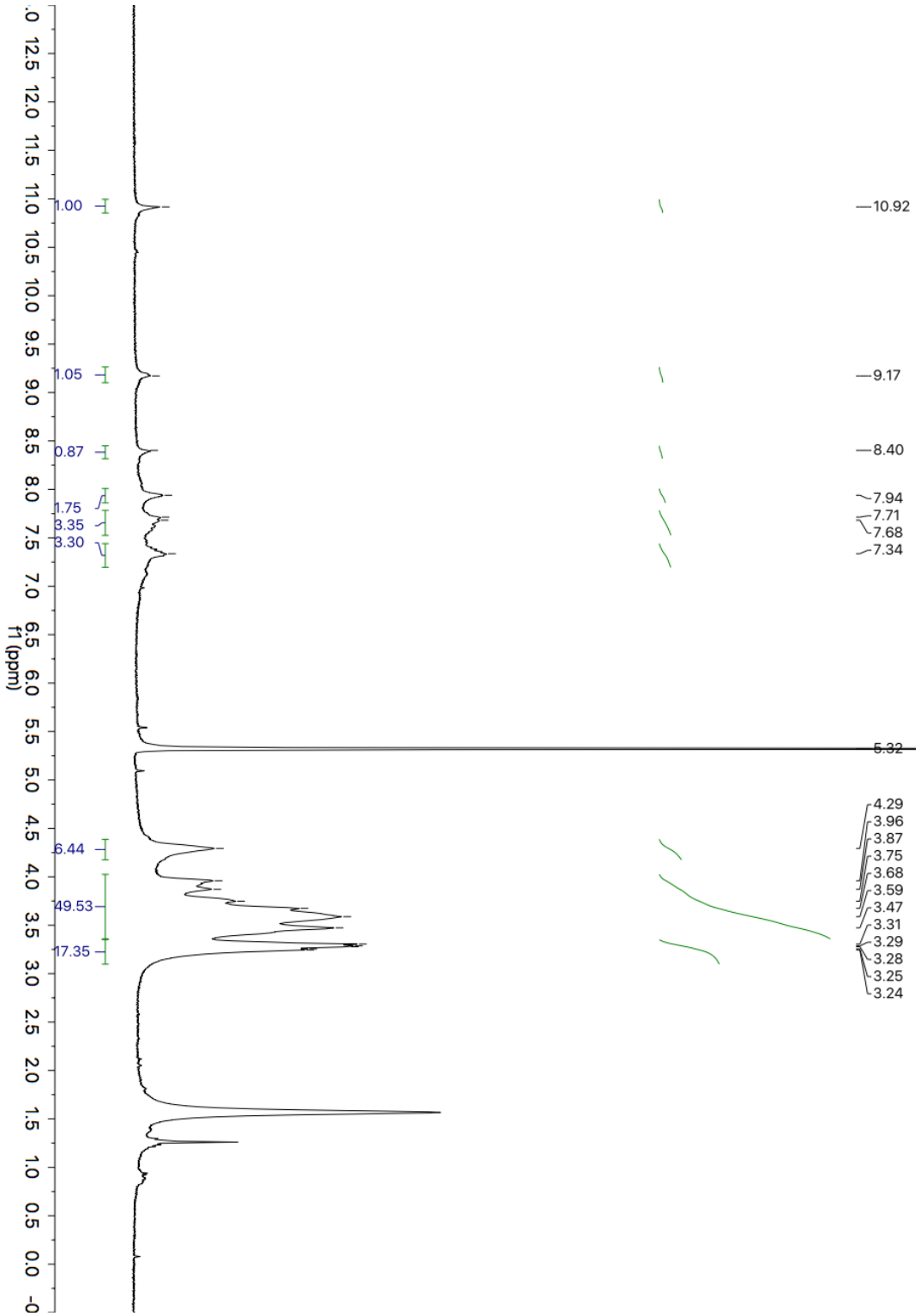

Figure Appendix B.10.^{1}H NMR spectrum of compound **2-SP1b** (CD_2Cl_2, 400 MHz).

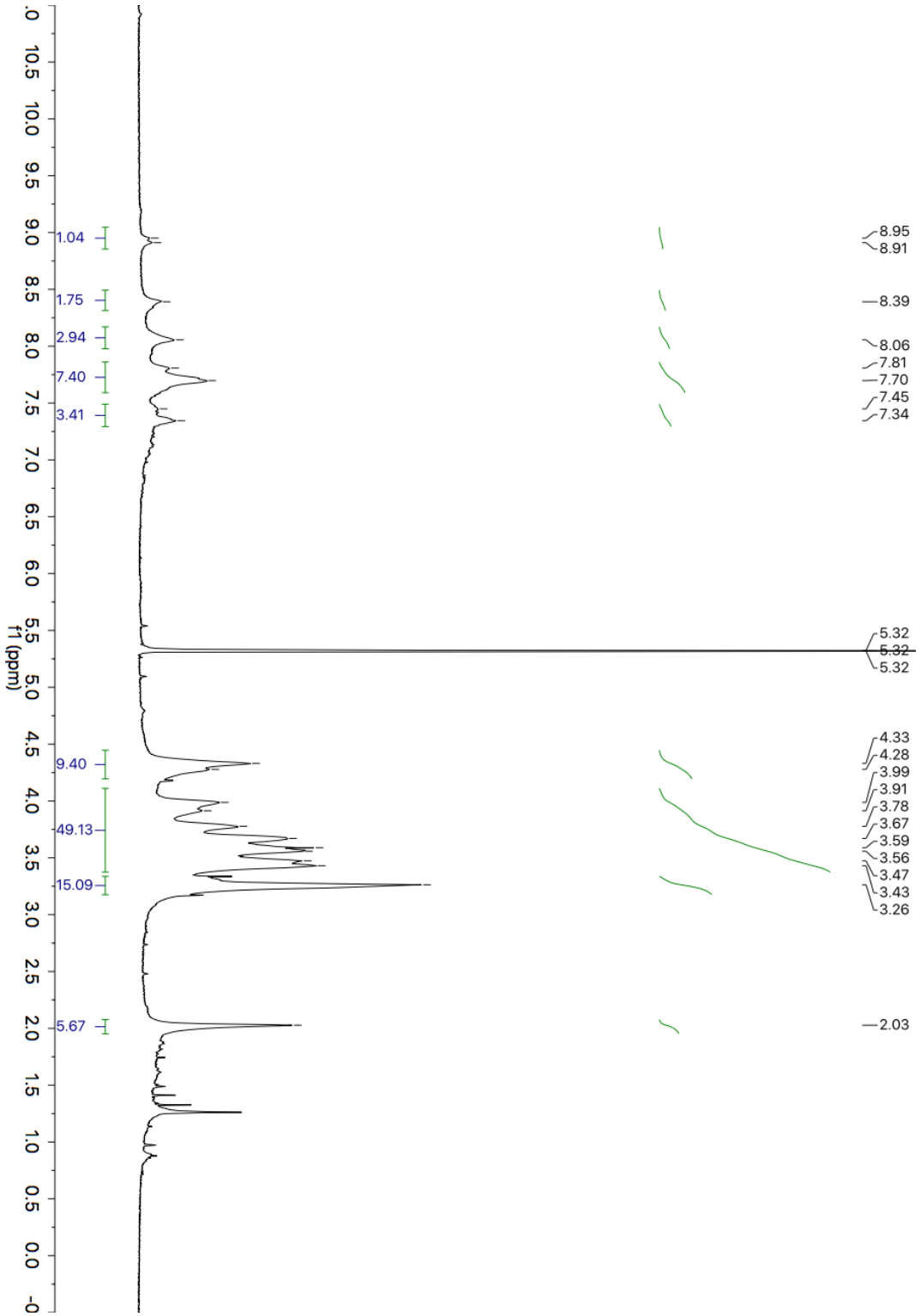

Figure Appendix B.11.[1]H NMR spectrum of compound **2-P1a** (CD_2Cl_2, 400 MHz).

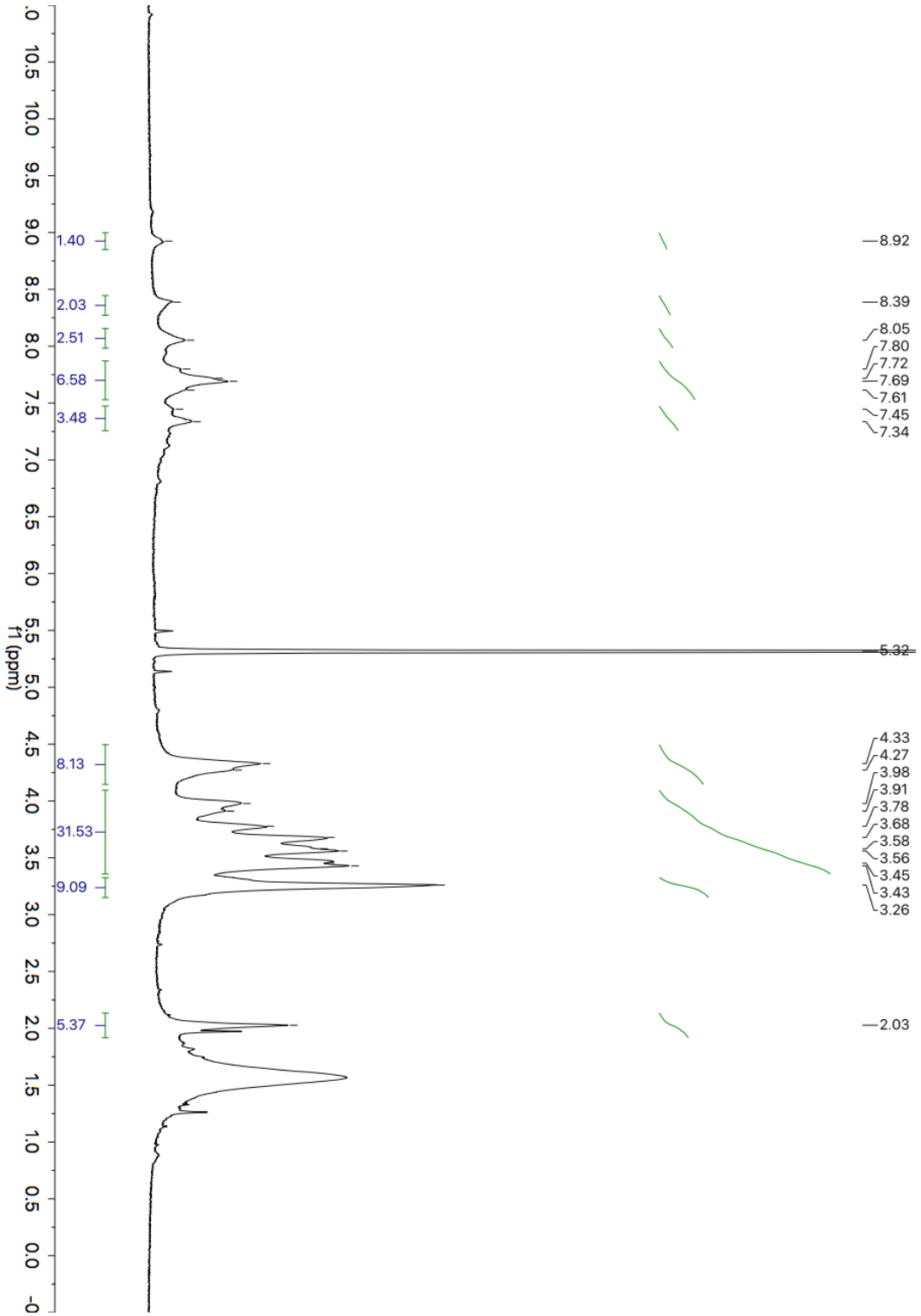

Figure Appendix B.12.[1]H NMR spectrum of compound **2-P1b** (CD_2Cl_2, 400 MHz).

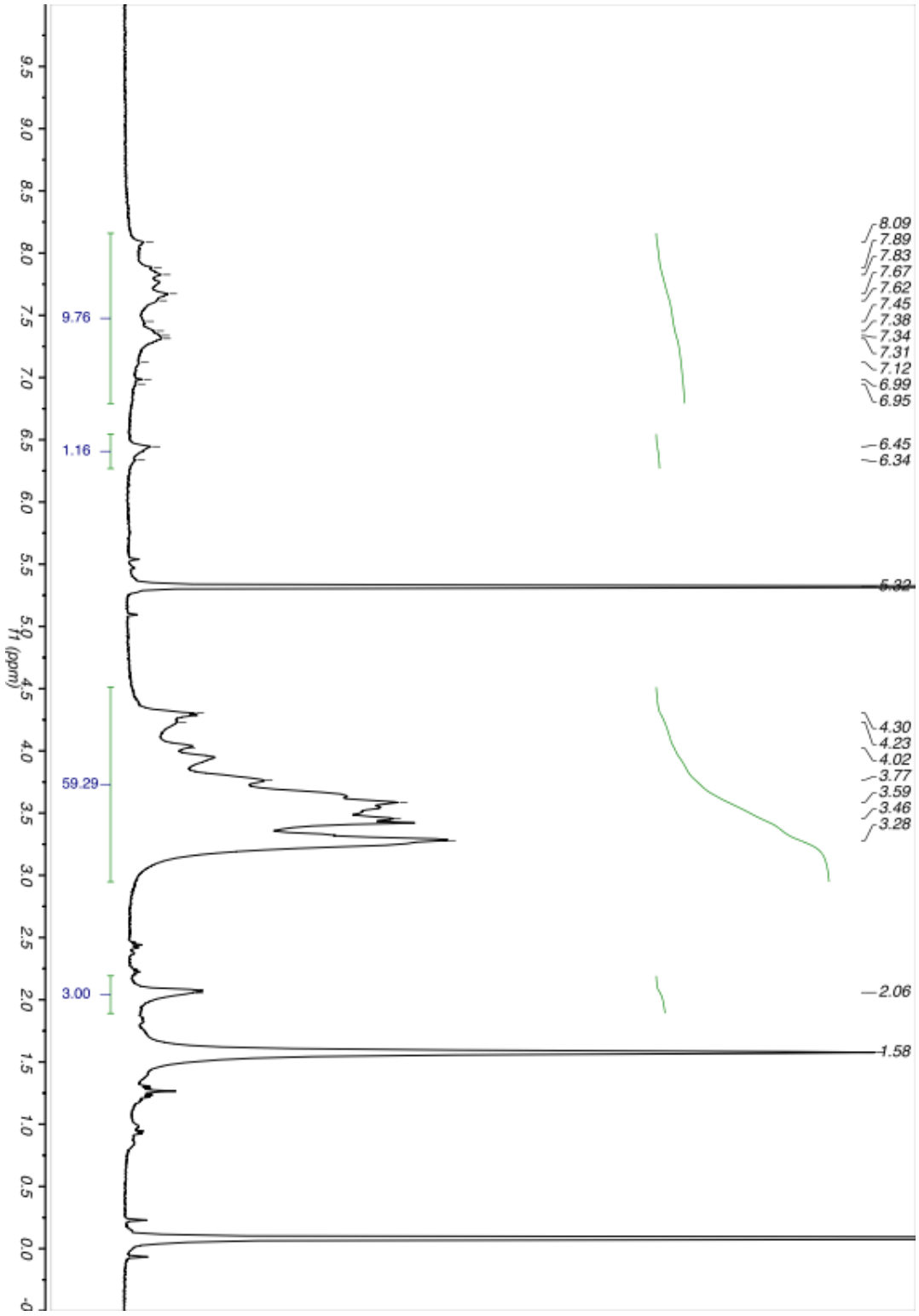

Figure Appendix B.13.^{1}H NMR spectrum of compound **2-P2** (CD_2Cl_2, 400 MHz).

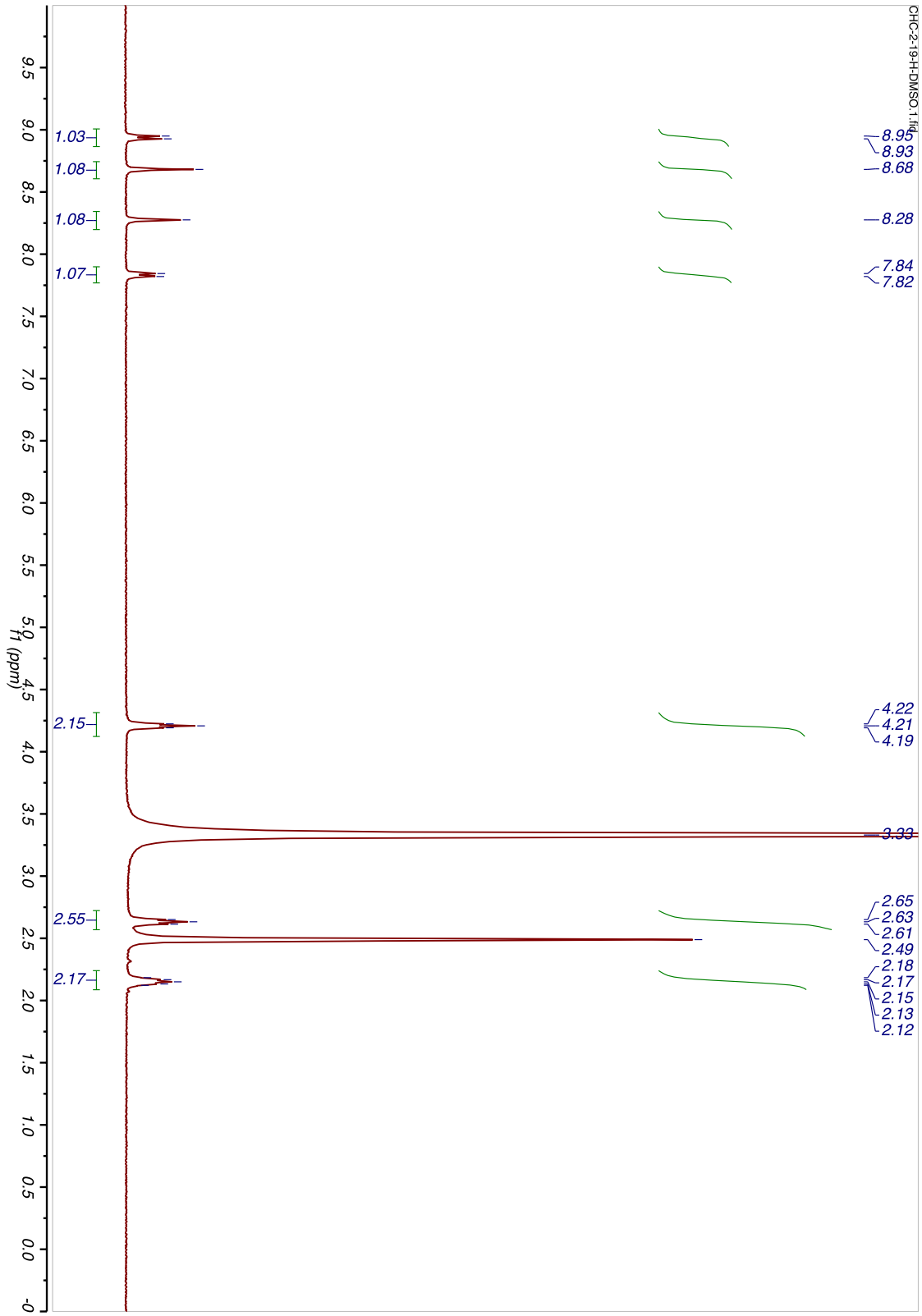

Figure Appendix B.14.[1]H NMR spectrum of compound **3-1** (d_6-DMSO, 400 MHz).

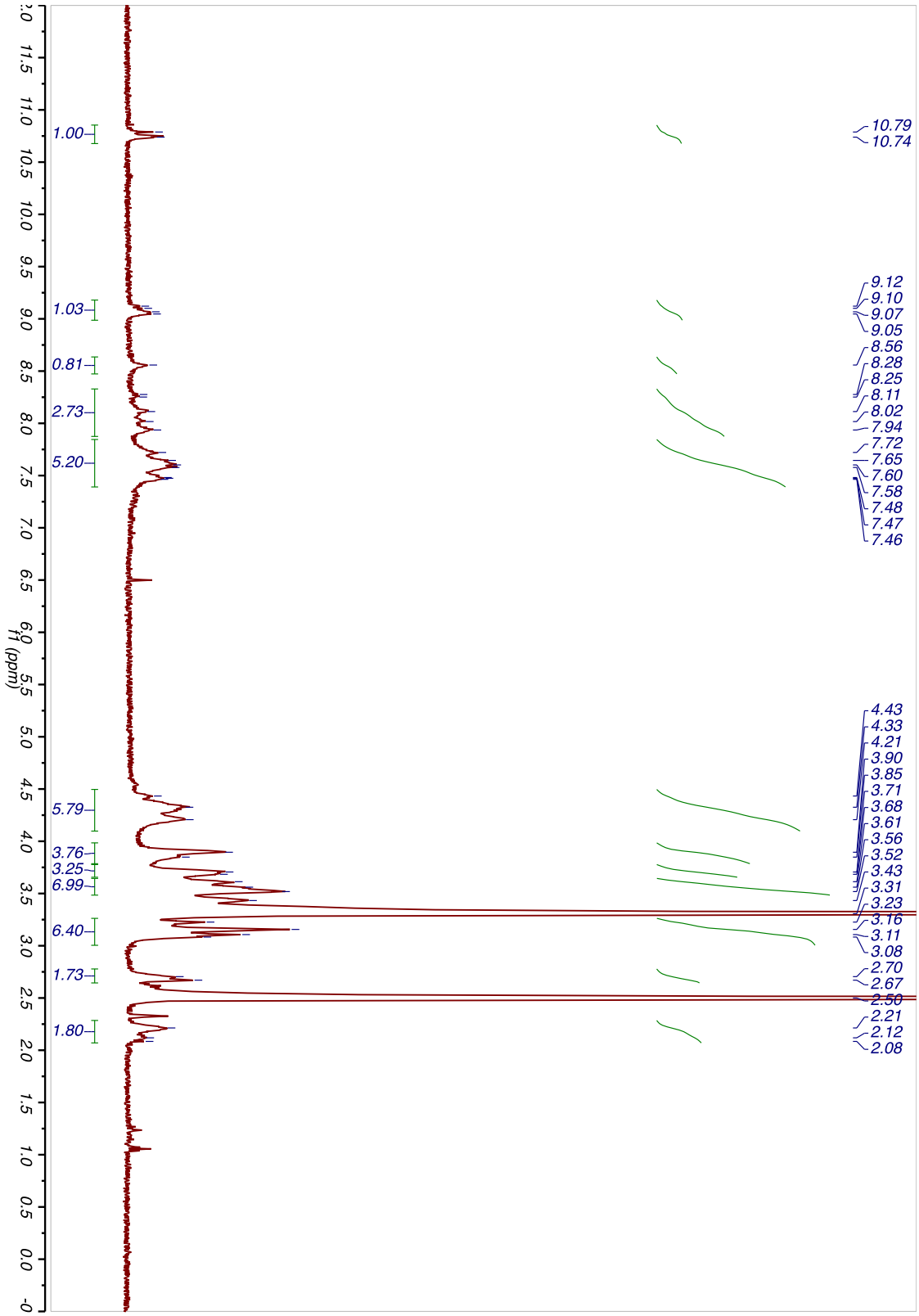

Figure Appendix B.15.[1]H NMR spectrum of compound **3-P1** (d_6-DMSO, 400 MHz).

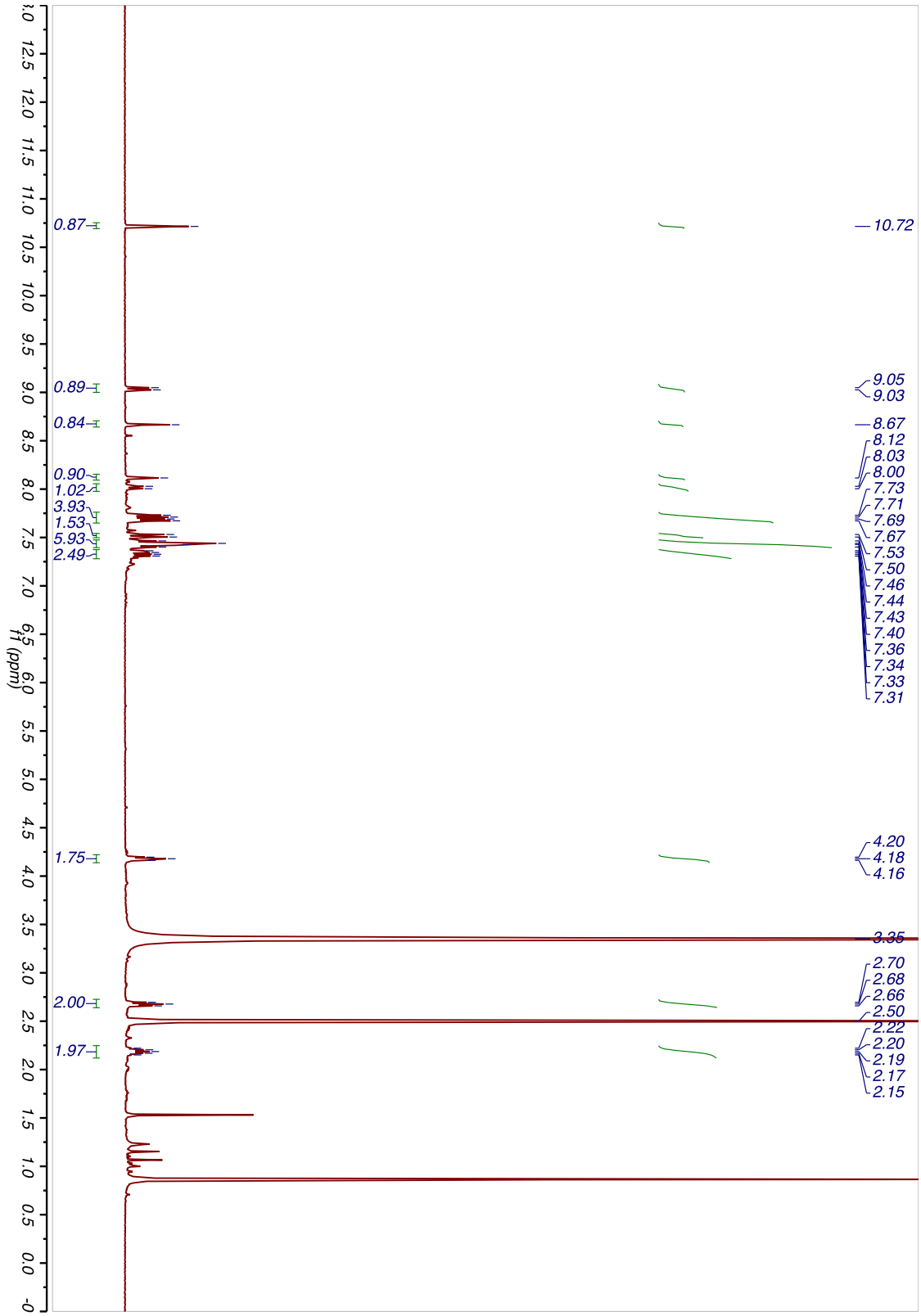

Figure Appendix B.16.[1]H NMR spectrum of compound **3-M1** (d_6-DMSO, 400 MHz).

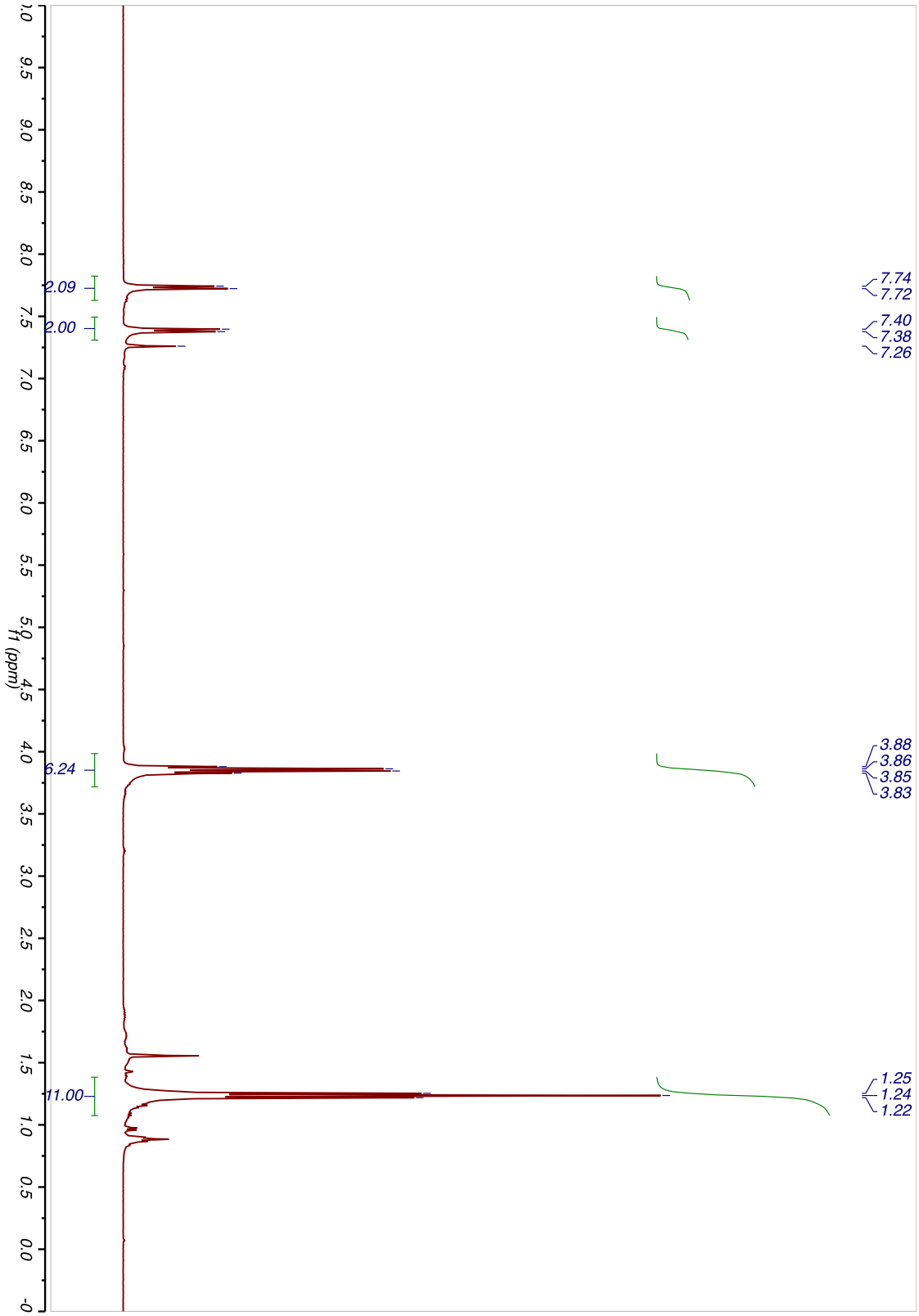

Figure Appendix B.17.^{1}H NMR spectrum of compound **4-1** ($CDCl_3$, 400 MHz).

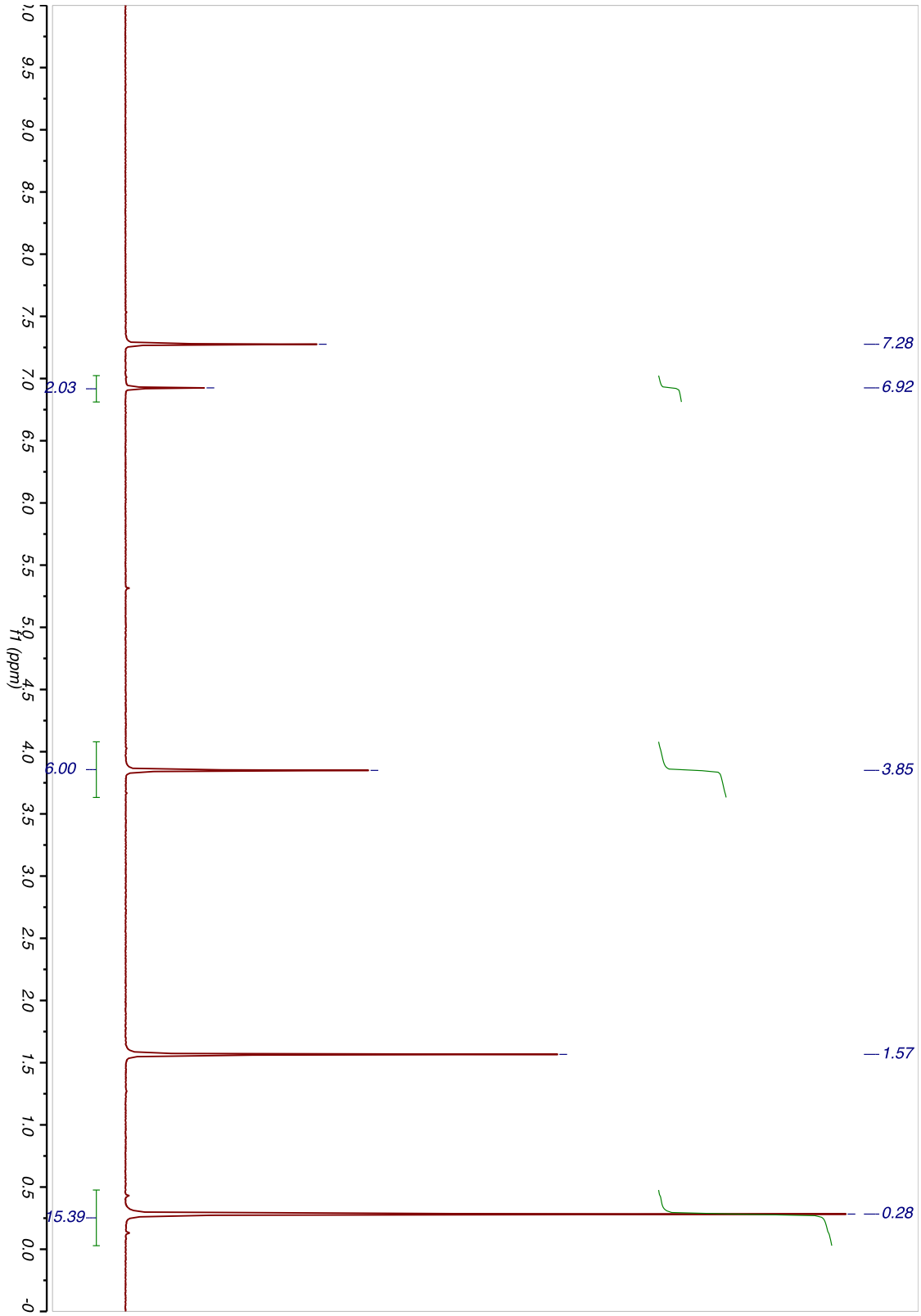

Figure Appendix B.18.[1]H NMR spectrum of compound **4-S1** ($CDCl_3$, 400 MHz).

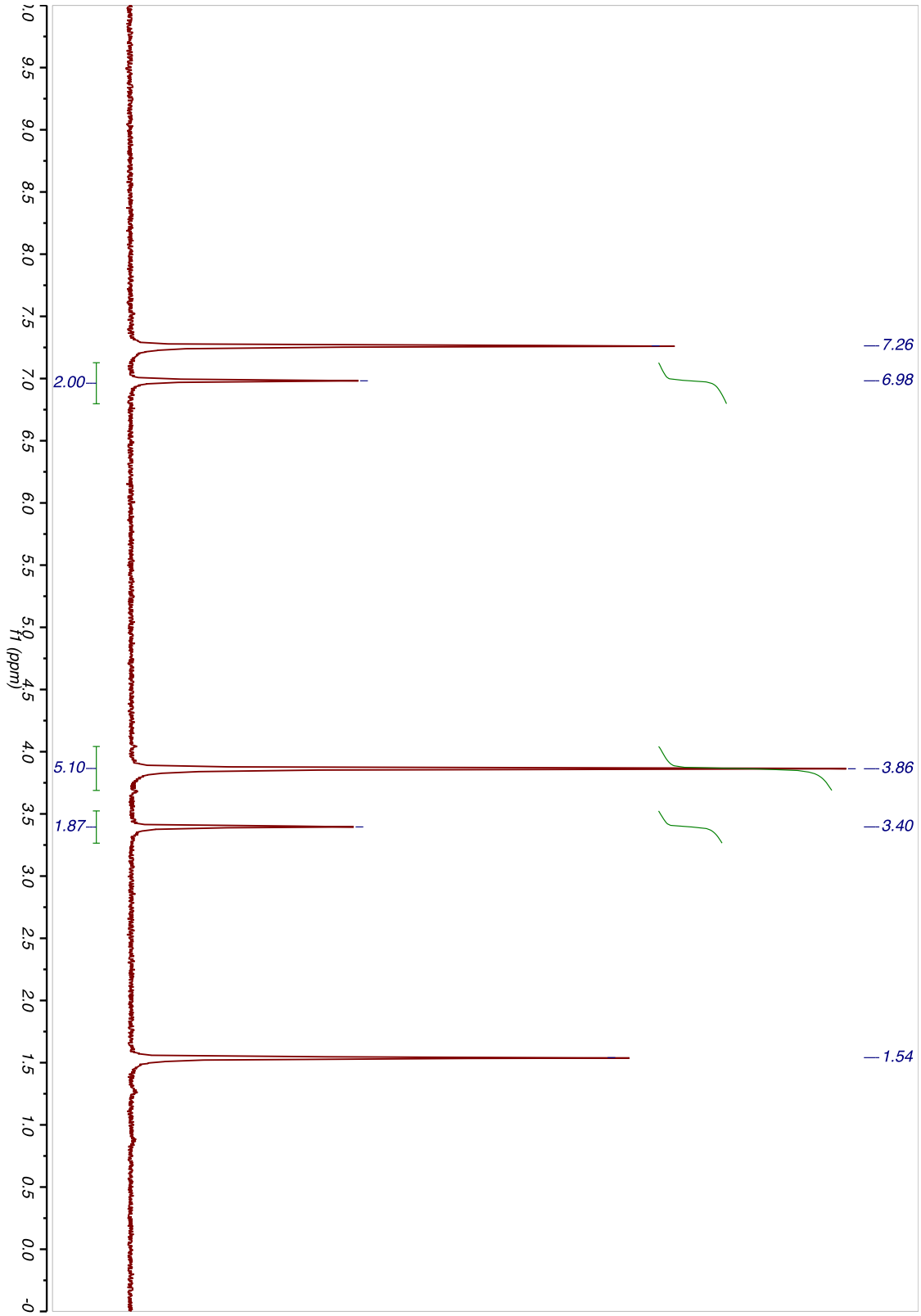

Figure Appendix B.19.^{1}H NMR spectrum of compound **4-2** ($CDCl_3$, 400 MHz).

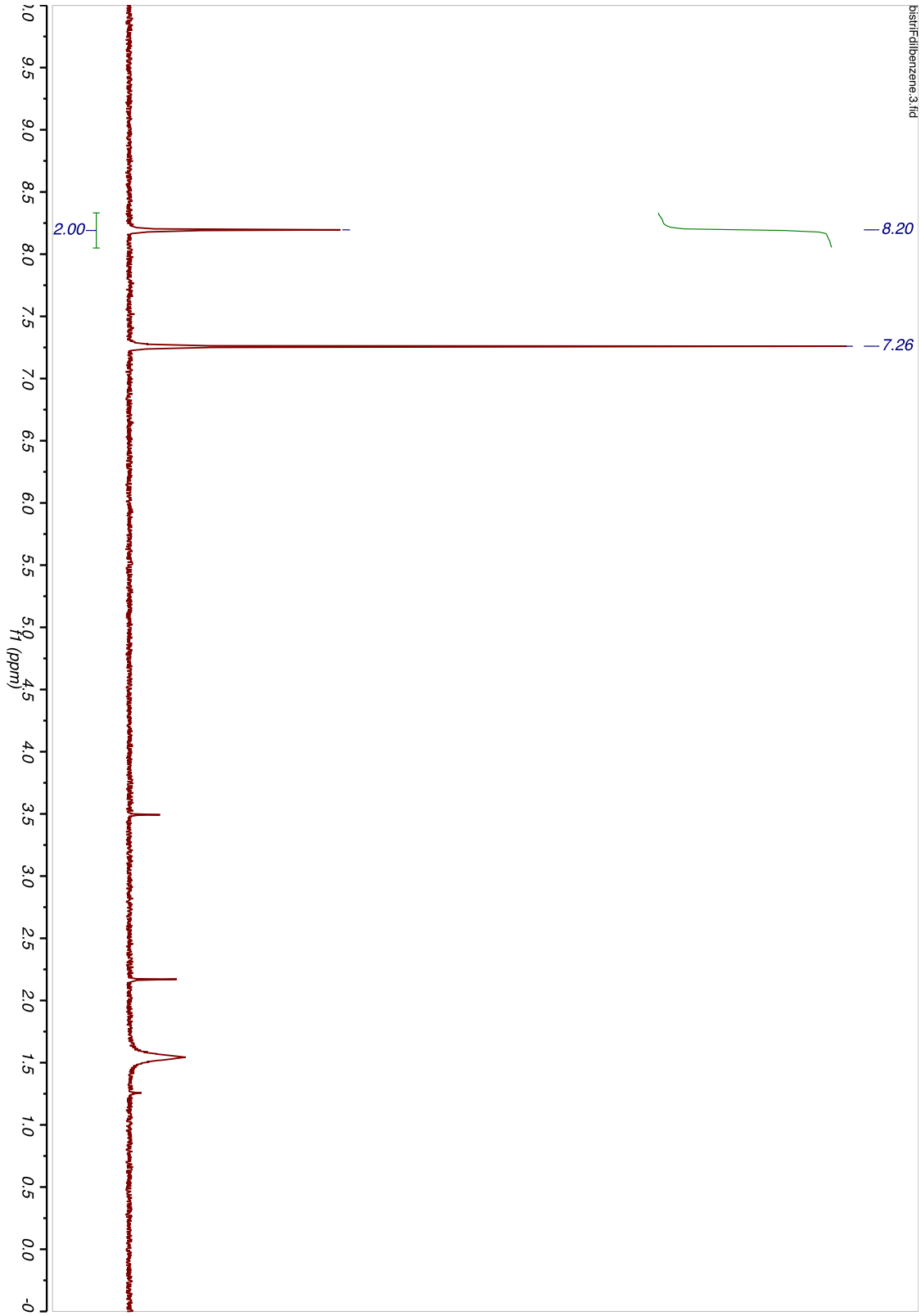

Figure Appendix B.20.^{1}H NMR spectrum of compound **4-6** ($CDCl_3$, 400 MHz).

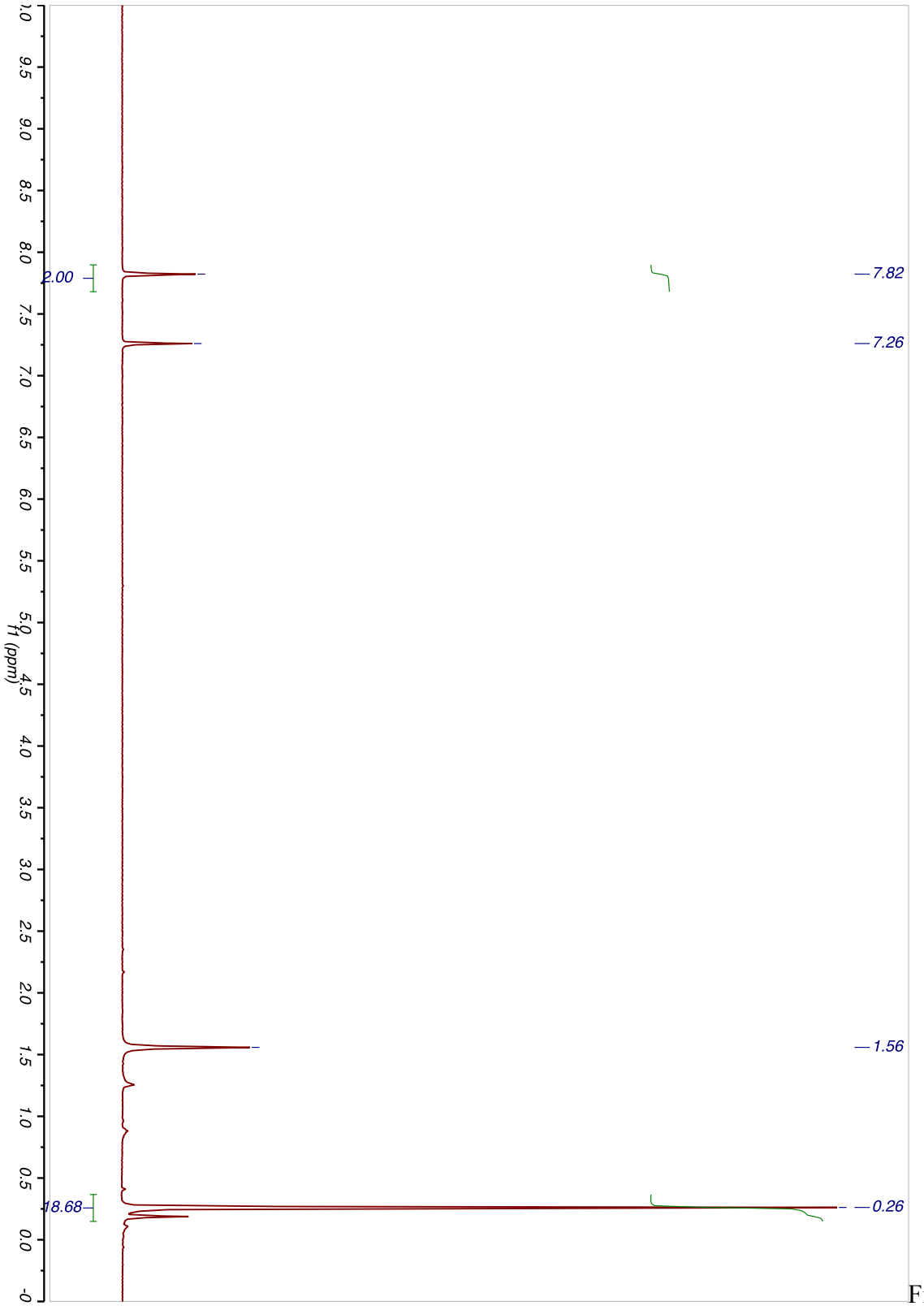

Figure Appendix B.21. ^{1}H NMR spectrum of compound **4-S3** ($CDCl_3$, 400 MHz).

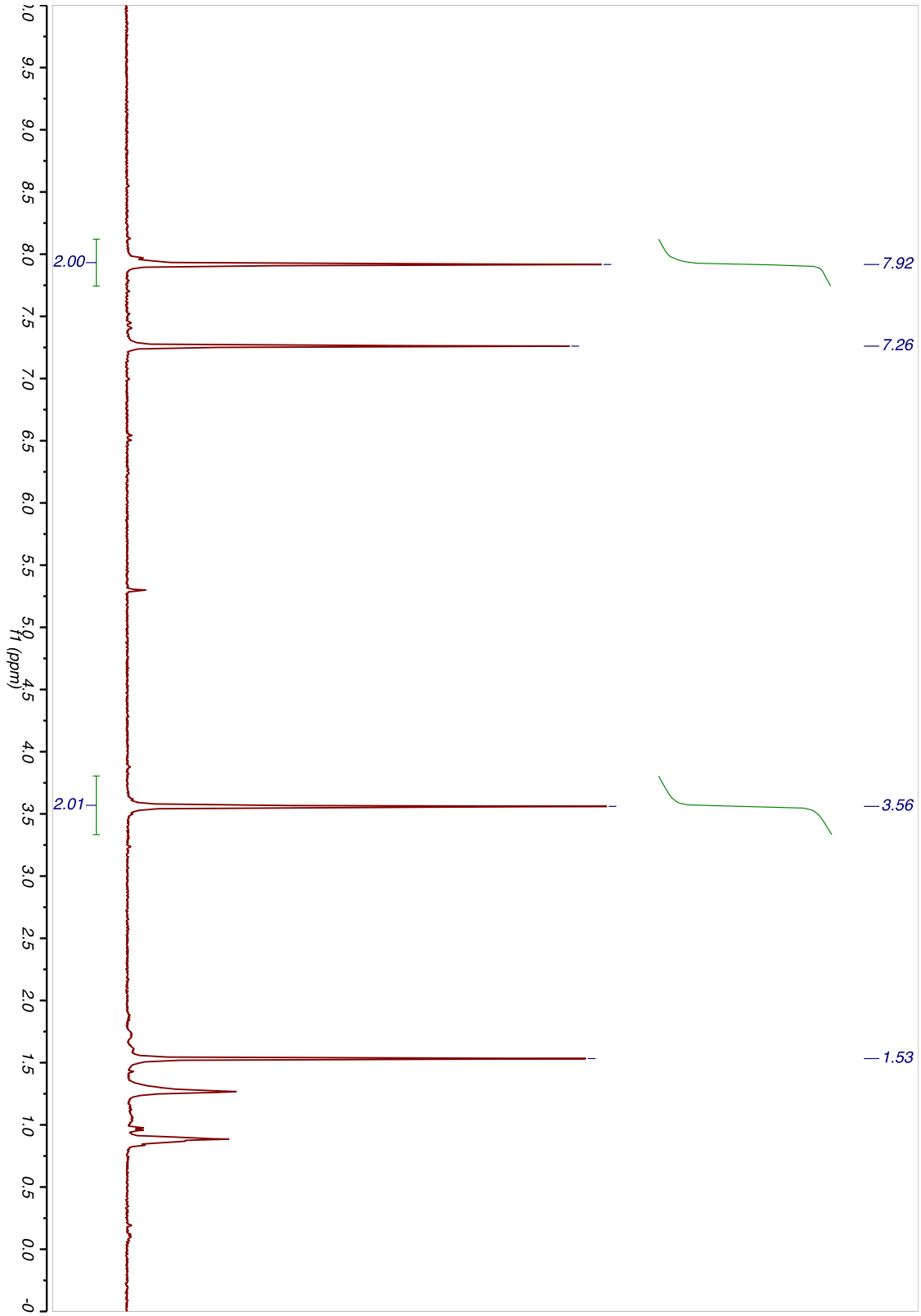

Figure Appendix B.22.^{1}H NMR spectrum of compound **4-3** ($CDCl_3$, 400 MHz).

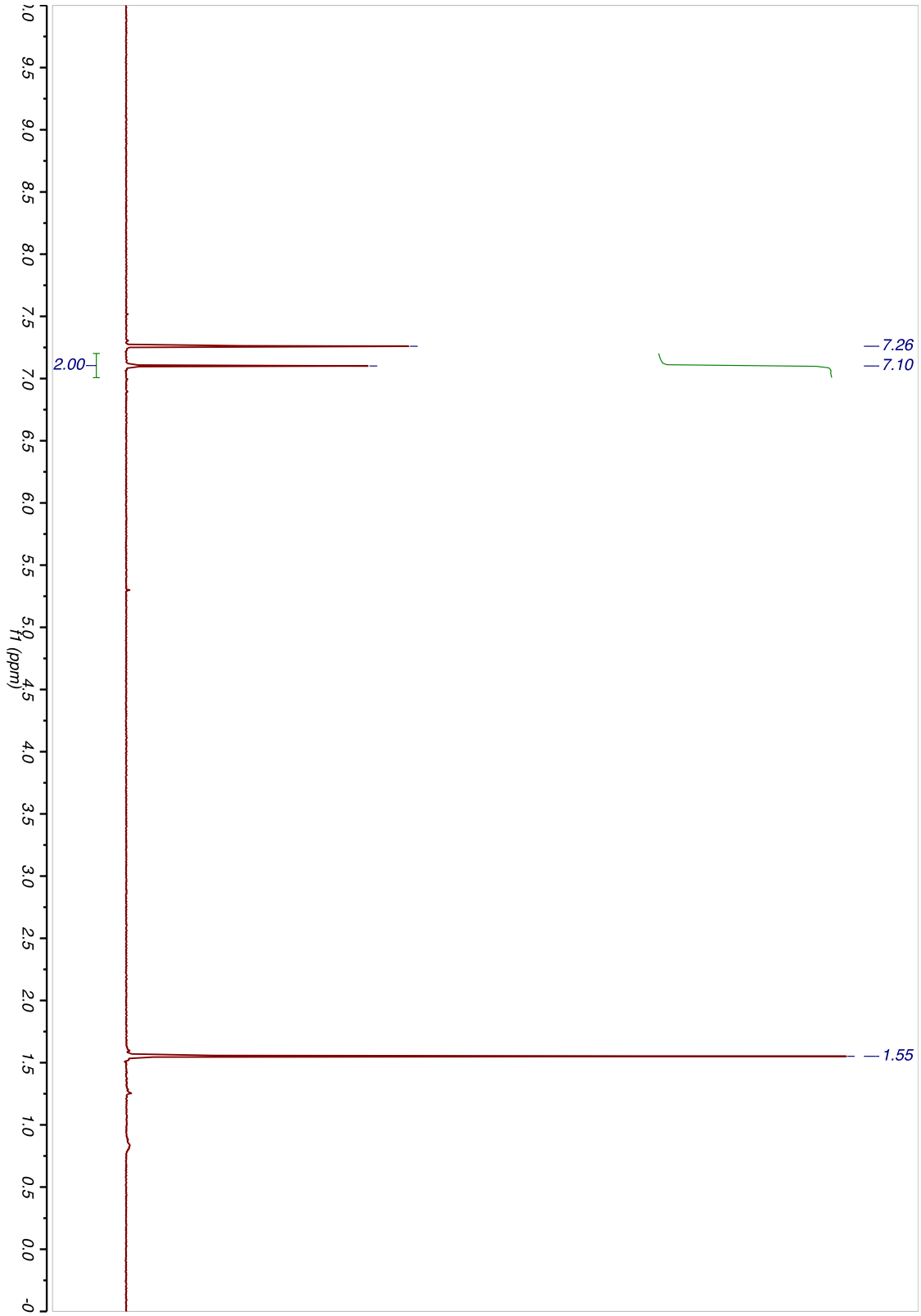

Figure Appendix B.23.^{1}H NMR spectrum of compound **4-S4** ($CDCl_3$, 400 MHz).

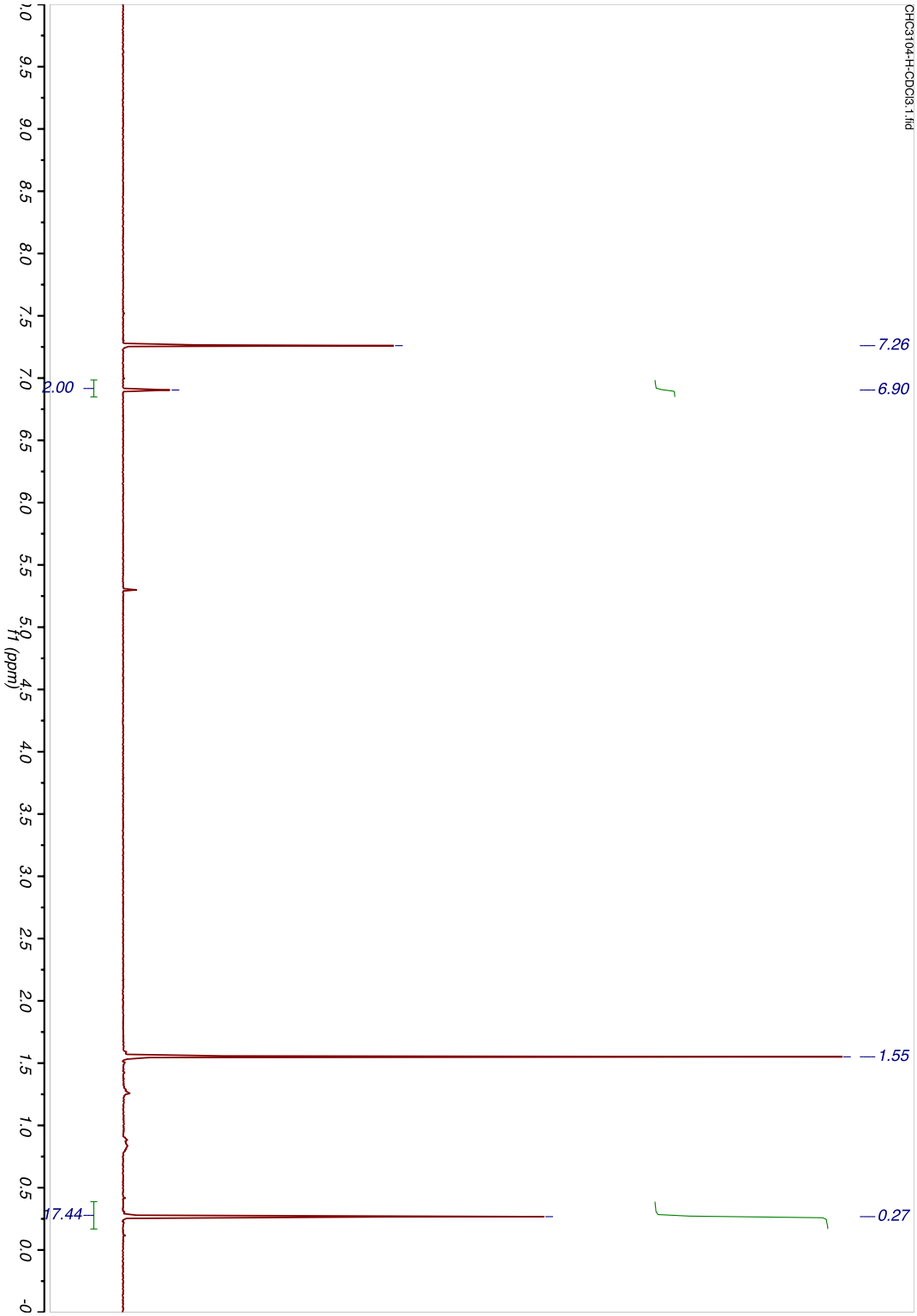

Figure Appendix B.24.^{1}H NMR spectrum of compound **4-S5** ($CDCl_3$, 400 MHz).

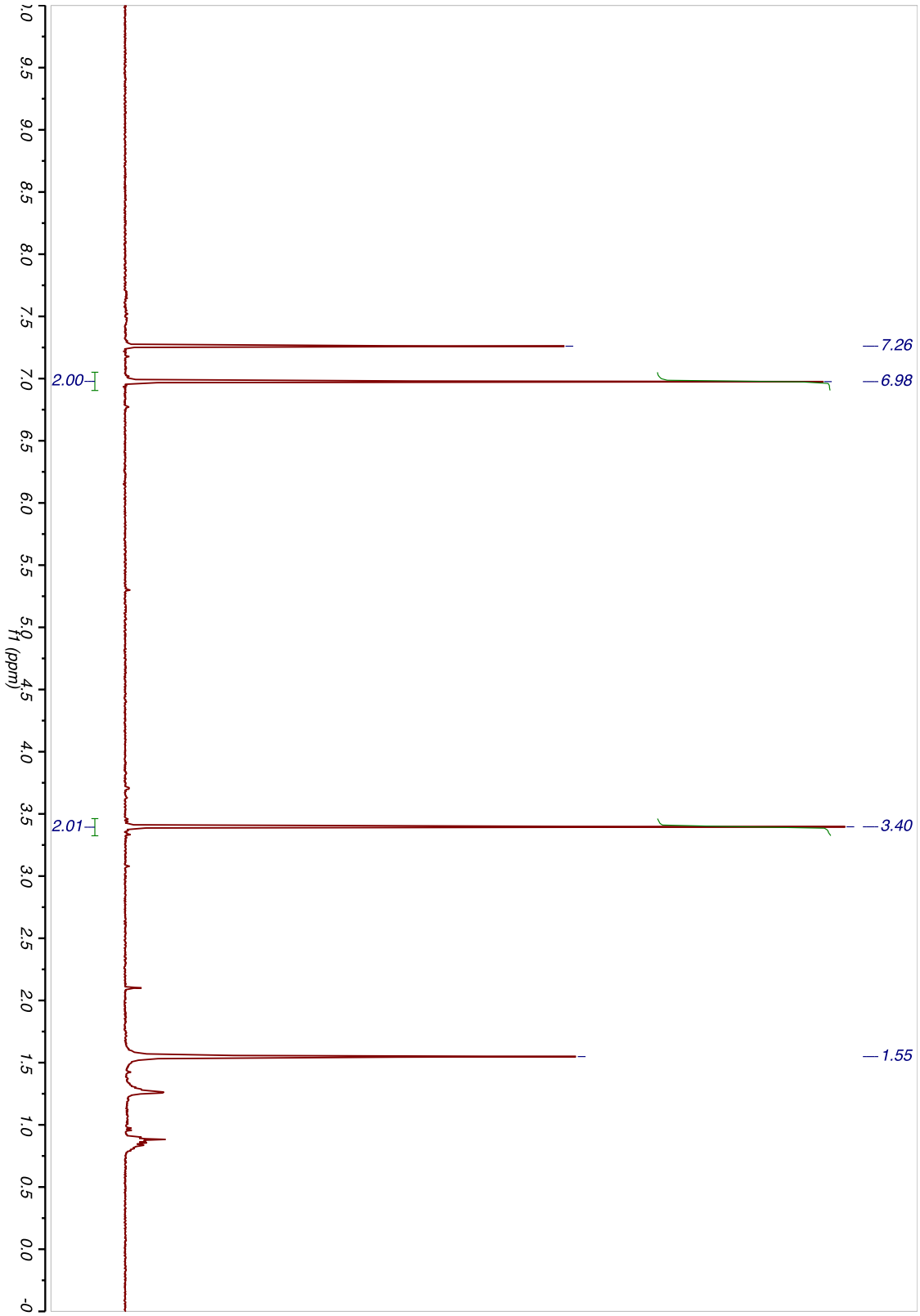

Figure Appendix B.25.^{1}H NMR spectrum of compound **4-4** ($CDCl_3$, 400 MHz).

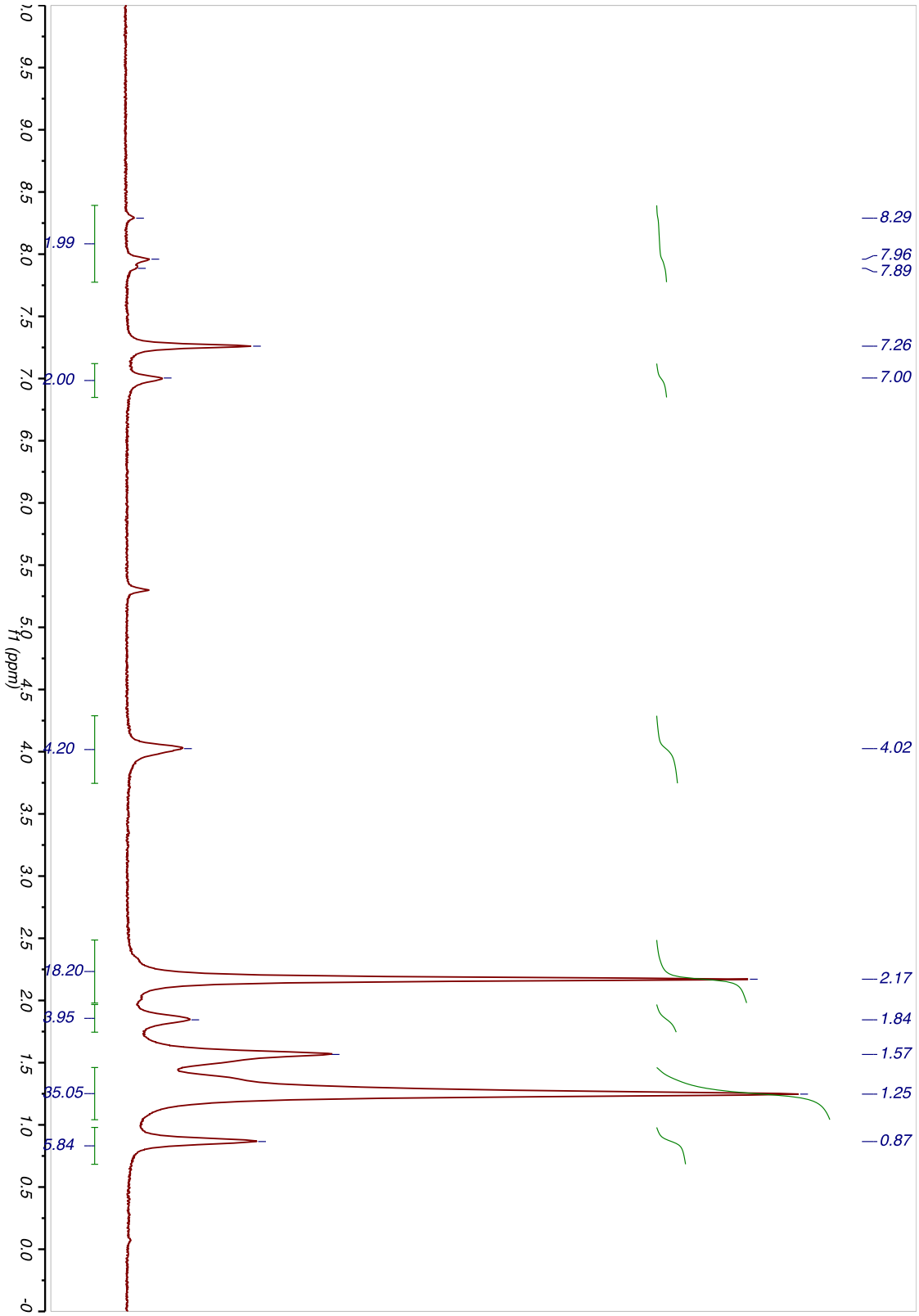

Figure Appendix B.26.[1]H NMR spectrum of compound **4-P1** ($CDCl_3$, 400 MHz).

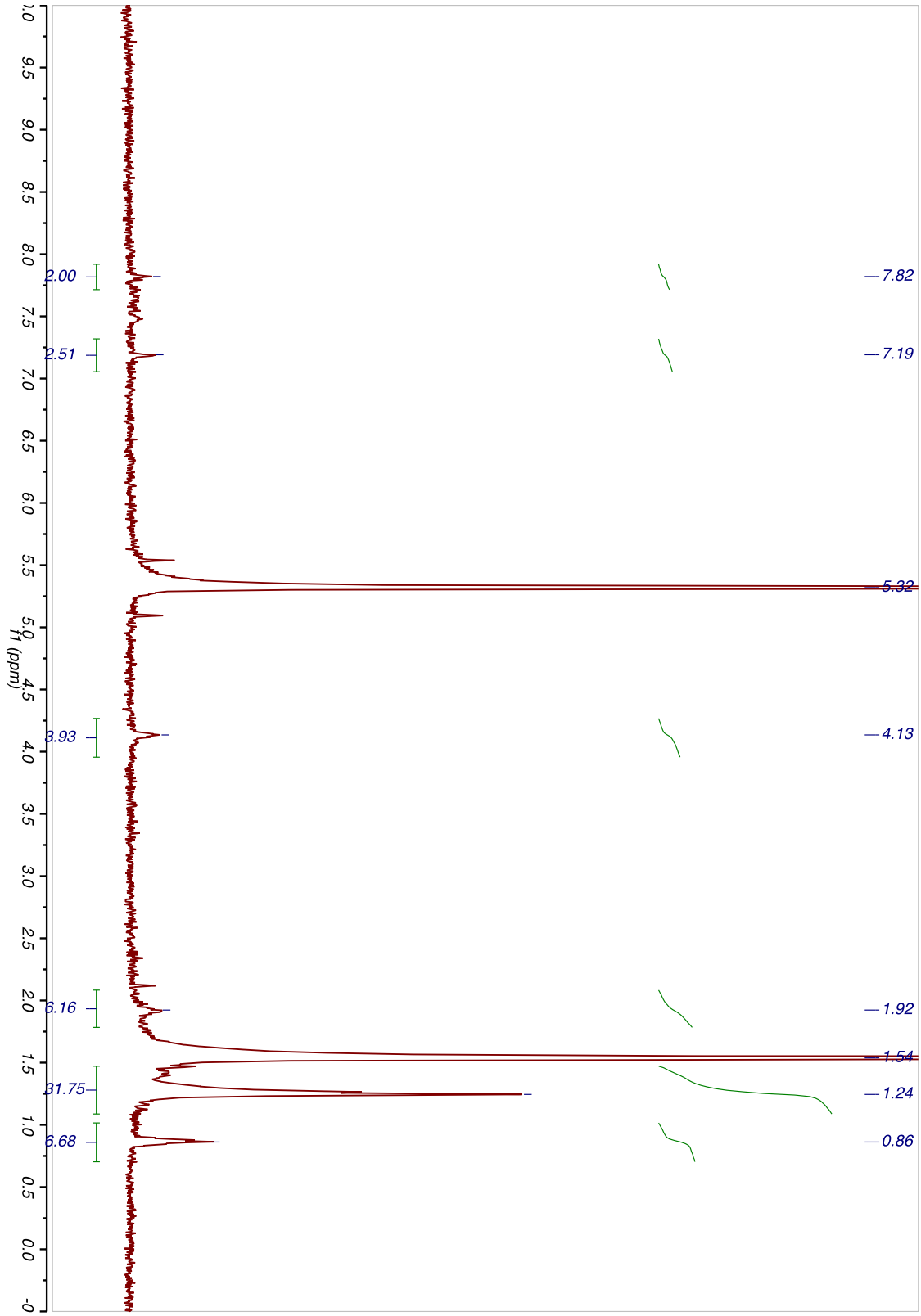

Figure Appendix B.27.[1]H NMR spectrum of compound **4-P2** (CD_2Cl_2, 400 MHz).

VITA

Chien-Hung Chiang was born in 1984 in Taichung, Taiwan. He received his Bachelor of Science in Chemistry in June 2007 from Tamkang University in New Taipei, Taiwan. He began his research career in the lab of Professor Hsiu-Fu Hsu. In June 2009, he graduated with a Master of Science in Chemistry with a thesis titled, "Manipulation of Molecular Alignments of Liquid Crystalline Molecules by Self-Assembled Monolayers of Thiol-functionalized Discogens." After serving for the R.O.C Air Force, he became a research assistant in the advanced organic materials laboratory in Tamkang University. His research interesting included supramolecular chemistry, organic photovoltaic, and amplification of chirality by sergeants and soldiers principle. In August 2012, he moved to Louisiana State University in Baton Rouge, Louisiana. He joined the laboratory of Professor Evgueni E. Nesterov and his major research contributed is the development of higher energy gap control of fluorescence in conjugated polymers and its application in sensing biomedical species, and surface-initiated stepwise polymerization. Chien-Hung is a candidate for the Doctor of Philosophy in Organic Chemistry which plan to be awarded in May 2018 with a dissertation entitled, "Higher Energy Gap Control of Fluorescence in Conjugated Polymers".